Use of Magnetic Nanoparticles for Wastewater Treatment

by

Asha Parekh

Bachelor of Technology in Chemical Engineering (2008)
Indian Institute of Technology Kharagpur, Kharagpur, India

Master of Science in Chemical Engineering Practice (2009)
Massachusetts Institute of Technology, Cambridge, MA

Submitted to the Department of Chemical Engineering
in partial fulfillment of the requirements for the degree of

Doctor of Philosophy in Chemical Engineering Practice
at the
Massachusetts Institute of Technology
June 2013

Signature of Author.....
Department of Chemical Engineering
June 2013

Certified by.....
T. Alan Hatton
Ralph Landau Professor of Chemical Engineering Practice
Thesis Supervisor

Accepted by.....
Patrick S. Doyle
Singapore Research Professor of Chemical Engineering
Chairman, Committee for Graduate Students

Use of Magnetic Nanoparticles for Wastewater Treatment

by

Asha Parekh

Submitted to the Department of Chemical Engineering on June, 2013,
in partial fulfillment of the requirements for the degree of
Doctor of Philosophy in Chemical Engineering Practice

Abstract

Contamination of marine sediments and water environments by urban runoffs, industrial and domestic effluents and oil spills is proving to be of critical concern as they affect aquatic organisms and can quickly disperse to large distances as highlighted by the recent Gulf oil spill disaster. Polycyclic aromatic hydrocarbons (PAHs), poly chlorinated biphenyls (PCBs), dichlorodiphenyltrichloroethane (DDT) and heavy metals like mercury, lead and manganese are among the ubiquitous trace contaminants of marine and freshwater systems. Presence of these contaminants raise concerns as small quantities of the organic chemicals have been shown to be carcinogenic to mammals and can pose a risk to both human health and the aquatic biota.

We have proposed a remediation technique based on a magnetically enhanced separation technology as an alternative to existing methods to separate the target contaminants from a sediment matrix or wastewater stream. This technology uses specifically tailored surface modified magnetic nanoparticles (MNP) that are capable of a high uptake of trace metals. These particles have a magnetic core that facilitates their recovery, a shell that provides stability, protection from oxidation and a surface to which contaminant specific ligands are attached.

The advantages of this alternative are that it involves low cost chemicals and magnets, can be implemented in continuous manner and is target specific. To evaluate the feasibility of this project, we have explored thermodynamics of adsorption of contaminants on particles and transport of these particles through their medium of application (water and porous media). This work focuses on treating effluents contaminated with heavy metals, in particular, mercury. For the treatment, dithiocarbamate functionalized magnetic nanoparticles were synthesized and their

adsorptive properties for mercury at different pH conditions, ionic strengths and in presence of salinity and competing ions were explored. A competitive adsorption model based on mercury speciation was developed to explain the experimental results. In addition to the adsorption experiments, theoretical models to determine binding constants of the functional group on these particles to the mercury species were evaluated using Gaussian.

Transport properties through porous (representing sediment like structures) and non-porous (representing effluents) media were studied using finite element models. The simulations provided a fundamental understanding of how magnetic nanoparticles would behave differently under magnetic field gradients and in porous media. In addition, parametric results of a continuous separation model that quantifies the trend in separation as a function of system parameters were also investigated.

Bench scale runs for treating wastewater-containing mercury with these particles were demonstrated. Apart from adsorption, this process uses a well-studied high gradient magnetic separation (HGMS) system to capture the magnetic nanoparticles. Breakthrough analysis of mercury and particles through the entire system, capture on particles by the HGMS system, recovering magnetic nanoparticles by stripping off the contaminant were studied in this work.

As part of the PhDCEP Capstone paper, commercialization prospects of this technology have been examined for industrial applications, particularly heavy metal removal. An in-depth market analysis of North America's water and wastewater treatment chemicals market was carried out to determine market attractiveness. This was followed by competitor analysis and evaluation of this technology's value proposition based on economics and technical applicability. A roadmap of strategies that need to be adopted based on key market insights was discussed. This chapter concludes with the verdict on magnetic nanoparticles' potential as a disruptive game changer in industrial wastewater treatment market.

Thesis Supervisor: T. Alan Hatton
Title: Ralph Landau Professor of Chemical Engineering Practice

Dedicated to Papa, Ma, Jitu and Rekha

Acknowledgements

I would like to sincerely thank my advisor Professor T. Alan Hatton for the constant support and guidance he provided me during the last few years. Completing a PhD is not always smooth sailing but your confidence in me has helped me tackle every challenge on the way.

My thesis committee members, Professor William H. Green, Professor Philip M. Gschwend and Dr. Lev Bromberg were more than just that. They were mentors who provided me helpful insights at every juncture of my work and I would like to thank them for their time and efforts. Lev, I would especially like to thank you for the particles you synthesized that were used in this work and all the useful discussions we've had on this project.

Hatton group is a relaxed and friendly group that I am both proud and lucky to be a part of. All its members have helped me in some way or the other and I would like to thank all of them for being an awesome second family. In particular, this lab would not have been the same without our lab safety nazi Michael C. Stern who is also one of my best friends. Mike, thank you for all the wonderful research and non-research related discussions we have had. Vaibhav Somani, Su Kyung Suh, Sanjoy Sircar, Kunshan Sun and Sa Wang, thank you for being great friends. It's because of you guys that I looked forward to coming to work every day. I would also like to thank Fei Chen for jump starting me on my project and introducing me to the wonder software COMSOL.

Life at MIT would have been dull without my Indian mafia and would like to especially thank Karthik Shekhar, Prithu Sharma, Mehul Jain,Amrit Jalan, Ankita Jain and Nidhi Shrivastav for being more than just a sounding board. The conversions over endless cups of chai, cookouts and workouts have been truly inspirational. Mukul Singhee and Srimoyee Bhattacharya thank you for the insightful discussions we have had on research, technology and much more. It has been a long journey from undergrad days but I am glad we are still thick as thieves.

This thesis would not have been possible without Saurabh Tejwani, who not only introduced me to my wonderful research group but also helped me even out my worries about

research every time things did not work. Thank you for your patience and 'don't stop believing' attitude for it has inspired me to achieve this work.

My family, papa, ma, Jitubhai, Rekhaben, Sunil jiju and Sonali bhabhi, thank you for your love and faith in me. Everything I am and have accomplished is because of you. Mummy and papa, this thesis is for you.

Table of Contents

List of Figures

List of Tables

Chapter 1. Introduction

1.1 Motivation and Approach

Contamination of fresh and marine sediments and water environments by oil spills, urban runoffs, industrial and domestic effluents is proving to be of critical concern as the presence of contaminants affects aquatic organisms and can quickly disperse to large distances as highlighted by the recent Gulf oil spill disaster.[1] Heavy metals like mercury (Hg), lead (Pb), manganese (Mn) and organic compounds like polycyclic aromatic hydrocarbons (PAHs), poly chlorinated biphenyls (PCBs), dichlorodiphenyltrichloroethane (DDT) are among the ubiquitous trace contaminants of marine and freshwater systems. The presence of these contaminants raise concerns as small quantities (ppb to ppm levels) of these chemicals have been shown to be carcinogenic to mammals and can pose a risk to both human health and the aquatic biota. In addition, these contaminants tend to accumulate in organisms and aquatic ecosystems owing to their resistance to biodegradation.[2]

Heavy metal contamination is a result of anthropogenic activities, with coal fired plants, mining, solid waste incinerators, paper and chloro-alkali industries being some of the common sources.[3] Contaminants present could exist either in dissolved forms as in the case of industrial effluents or in suspended forms as in sediments and surface and ground waters. Traditionally, dissolved contaminants have been removed from water sources by adsorption on activated carbon,[4, 5, 6] ion exchange[7, 8] and solvent extraction.[3, 9] While in the case of suspended contaminants, common techniques to remove them are pump and treat, in-situ adsorption on activated carbon, bioremediation and stabilization and solidification using.[10] Though these techniques have been widely implemented, they have several disadvantages associated with them as discussed in a later section. Most popular of these techniques is the adsorption of contaminants on activated carbon but this process suffers from mass transfer limitations, issues of bacterial growth, channeling and difficulty in regeneration. In case of sediment structures, carbon is often left behind in the matrix being treated which risks re-release of adsorbed contaminants and migration of contaminant-laden carbon to new areas. Given that the carbon is concentrated with contaminants, the risk of re-release is much higher than the risk posed by the initial contamination.

Application of nano materials for environmental remediation, though in its infancy, has great potential for remediating sites and effluents in a cost effective manner.[11] As an alternative to existing remediation techniques, we propose using functionalized magnetic nanoparticles (MNPs) to adsorb the contaminants of interest. Their superiority to activated carbon lies in the fact that they offer high surface area to volume ratio by being nano sized. It also does not introduce mass transfer limitations common to porous structures as it has all the surface area outside the particle. Secondly, under the external magnetic field gradients, complete removal of the particles from their medium of application is possible. Unlike activated carbon which is left behind in the environment, we can now isolate the contaminant rich adsorbents. These versatile magnetic nanoparticles can be applied to both treat effluents and remediate sediment matrices. The biggest advantage of this process is that we are reducing the net volume of disposal waste by concentrating the contaminants from a large dilute volume to a small concentrated volume.

Figure 1-1 illustrates the procedure of using functionalized magnetic particles in situ to remediate sediments. In case of remediating sediments or treating suspended contaminants, there are four main steps to using magnetic nanoparticles. The first is to inject particles into the sediment matrix or contaminated site. The second step is to allow it to mix and adsorb contaminants. Next, the particles must be separated from the contaminated site by high magnetic field gradients and lastly the contaminants can be stripped off to recycle the particles. For treating effluents or dissolved contaminants in waste streams, the process is similar. The particles can be injected inline and allowed to pick up contaminants from the fluid. A descriptive schematic showing the steps of using HGMS for capturing particles from a fluid stream is shown in Figure 1-2.

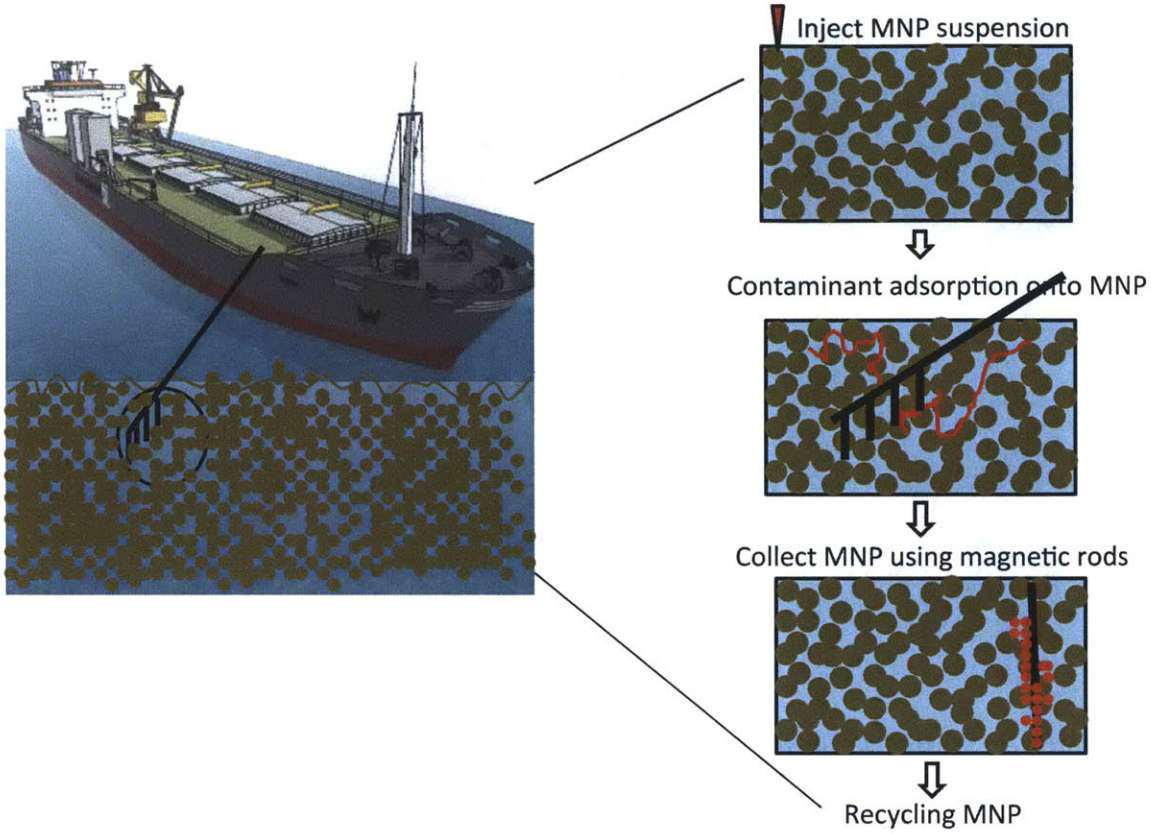

Figure 1-1: Schematic showing how to use magnetic nanoparticles (MNPs) in remediating sediments

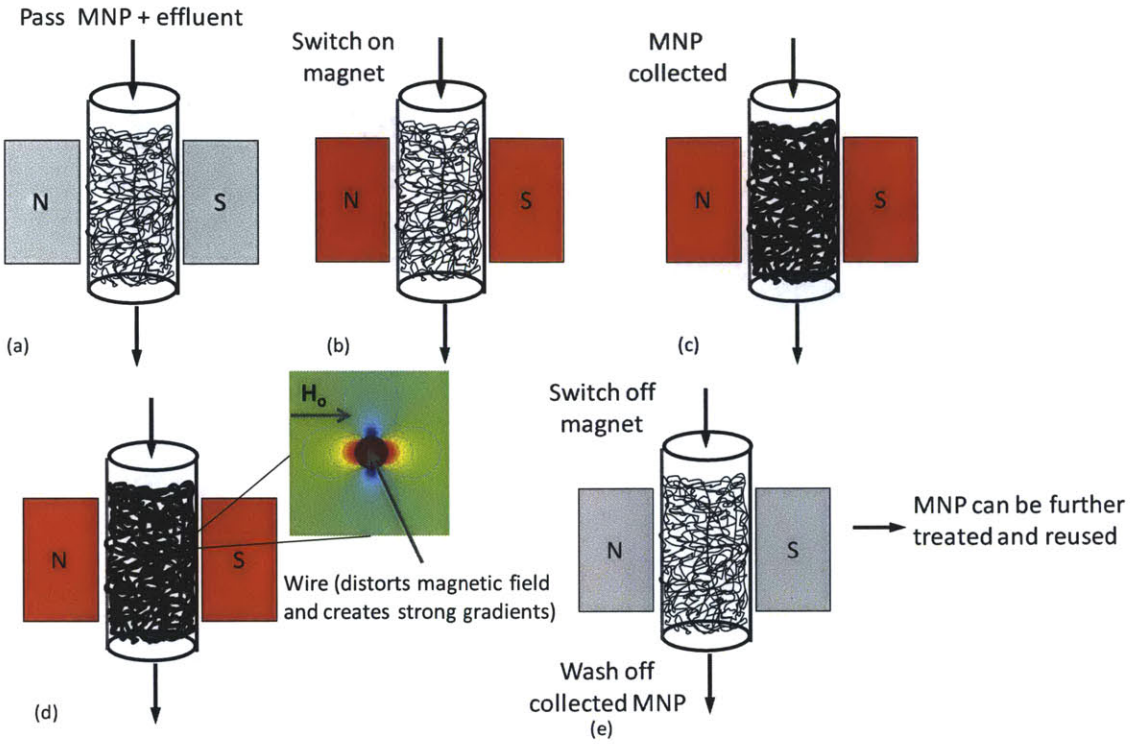

Figure 1-2: Schematic showing how magnetic nanoparticles (MNPs) can be used to treat effluents

The advantages of using this alternative nanotechnology compared to existing methods are that it involves low cost chemicals and magnets, can be implemented in a continuous manner for treating waste streams or can be an in situ technique for remediating sediments, almost complete recovery of adsorbents is possible owing to its magnetic properties and it can be target specific. Additionally, MNPs can be reused after the contaminant has been stripped off. Though the proposed magnetic nanotechnology is applicable to both sediments and waste streams, the focus of this thesis is on treating waste streams.

1.2 Background: Heavy Metal Contamination

1.2.1 Sources and Harmful Effects of Contamination

With the onset of the Industrial Revolution and increased anthropogenic activities such as mining, increased pollution of surface and groundwater by toxic metals have been observed.

'Heavy metals' is a loose definition based on density, atomic weight, and toxicity and applies to certain metals, metalloids, lanthanides and actinides (e.g. Ag, As, Be, Cd, Cr, Cu, Hg, Ni, Pb, Sb and Zn).[12] Disposal of these toxic metals in aquatic ecosystems constitutes a serious threat to human and animal health. Table 1-1 gives an overview of various sources of heavy metal contamination in waste streams. The table has been adapted from the information given in Dean et. al.[3]

Table 1-1: Industrial sources of heavy metal contamination

Industrial Source	Al	Ag	As	Cd	Cr	Cu	Fe	Hg	Mn	Pb	Ni	Sb	Sn	Zn
Pulp and paper mills					X	X		X		X	X			X
Organic chemicals/ Petrochemicals/ Alkali-chlorine/ Inorganic chemicals	X		X	X	X		X	X	X	X			X	X
Fertilizers	X		X	X	X	X	X	X	X	X			X	X
Cement/ Leather tanning/ Textile industries					X									
Steam generation/ power sources					X									X
Automotive/ Aircraft-finishing, plating	X	X		X	X	X		X			X			

There are several reasons for controlling heavy metal concentrations in the environment. Some of the heavy metals such as Hg, Cd, Pb and Cr are dangerous to human health and to the environment, while some are corrosive like Zn and Pb, and some pollute systems in which they are operated e.g., As pollutes catalysts.[3] However, the biggest problem lies in the tendency of some of them to bio-accumulate.[2] For example, mercury is a toxic element that impairs the

human nervous system.[10] Though less toxic in its inorganic form, it easily converts to its organic counterpart in presence of methyl groups, in particular methylmercury that is dangerous as it has a high bioavailability, is easily taken up by aquatic organisms and thus rapidly enters and accumulates in the food chain. The hazards of mercury poisoning were highlighted by the outbreak of Minanmata disease in Japan following an industrial release of mercury sulphate and methylmercury.[13, 14] Consequently a legal limit of 1ppm mercury in fish and less than 2ppb of mercury in drinking water was established by the US EPA.[15] Some of the important adverse effects of heavy metals on human health have been highlighted in Table 1-2. Most metals are harmful if adsorbed in high concentrations, however the metals mentioned in the table are especially harmful as they are already present in the atmosphere at elevated concentrations.[10]

Table 1-2: Harmful effects associated with some of the heavy metals

Metals	Toxicities	References
Antimony (Sb)	Antimony pneumoconiosis (respiratory effects due to inhalation), dermatitis, gastrointestinal disorders	10, 16
Arsenic (As)	Group 1 carcinogen, arsenicosis skin lesions, facial edema, vomiting, damage to liver, cardiovascular and nervous system	10, 17
Cadmium (Cd)	Pulmonary irritation, kidney damage, proteinuria, pneumonitis, Itai-Itai disease, prostate and lung cancers	10, 18
Cobalt (Co)	Respiratory problems, edema, hemorrhage of the lung	10, 19
Lead (Pb)	Memory and learning deficits, cardiovascular effects in adults, damage to neurologic, hematologic and renal systems, fertility damage, chronic nephropathy	10, 20
Manganese (Mn)	Coughing, bronchitis, increased susceptibility to lung diseases	10, 21
Mercury (Hg)	Memory loss, dementia, deficit in attention, ataxia, dysphasia, dizziness, irritability, blindness and deafness, gingivitis, gastrointestinal irritation, kidney dysfunction	10, 22
Nickel (Ni)	Dermatisis, headache, nausea, allergic dermatitis, chronic asthma, lung fibrosis, cardio-vascular and kidney diseases, lung and nasal cancer	10, 23
Zinc (Zn)	Depression, lethargy, neurologic signs such as seizures and ataxia, increased thirst, gastrointestinal irritation and vomiting	10, 23

1.2.2 Current Remediation Techniques

Brief descriptions of some of the methods of treating wastewater streams are given below.

1) Chemical precipitation: This process involves an oxidation-reduction reaction where contaminants are precipitated out as hydroxides, sulfides, carbonates or phosphates[10]

2) Bio-precipitation: This uses bacteria to reduce the contaminants to its sulfides form that precipitates out of the system.

3) Ion-exchange: This uses functionalized synthetic or natural resins/polymers to remove contaminants[7-8]

4) Adsorption: Physical surface adsorption onto natural or modified sorbents such as activated carbon, chitosan, coconut husk etc. is employed in this process. [5, 24, 25]

5) Bio-sorption: Similar to adsorption but involves use of biomass, yeast for sorbents.[26]

6) Solvent extraction: Uses solvents that has a higher affinity/solubility for contaminants to extract the target metals.[9]

7) Electrochemical separation: This uses electric fields to separate out contaminants.[3]

Though in use, these techniques suffer from certain disadvantages, which are highlighted below. Use of activated carbon, for example has issues such as requirements of long contact times as its highly porous structure introduces mass transfer limitations, high pressure drops if implemented in packed columns, dangers of bacterial growth, clogging and difficulties in regeneration without degrading the porous structure.[27] Solvent extraction too becomes infeasible for dilute waste streams and disadvantages such as high solvent costs and difficulty in regeneration often deter its implementation. Resin fouling and resin degradation are some of the common problems of ion-exchange processes. Stabilization and solidification (precipitation) of contaminants require accurate chemical injection and often let the contaminants remain behind in the sediment matrix, risking release of contaminants and migration of solidified complexes. Bioremediation on the other hand is a time consuming and difficult to control technique.[28, 29]

Since these remediation techniques are implemented on industrial scales, they need to be evaluated on the basis of their cost-effectiveness, performance, and simplicity. Our magnetic based technology is a promising alternative as it offers an effective and simple solution using inexpensive components and does not have any mass transfer limitations or risk of being left behind in the treatment matrix.

1.3 Background: Magnetic Nanoparticles

1.3.1 Structure and Synthesis Routes

Magnetic nanoparticles are particles in the size range of 1-200nm that respond to external magnetic fields. These are typically made of iron, nickel, cobalt and their chemical compounds.

A colloidally stable suspension of magnetic particles is called a magnetic fluid or a ferro-fluid. Particles in these fluids do not settle in presence of external gravitational fields or less intensive magnetic fields because of their small size and stabilizing coatings on their surfaces. The discussion in this section is limited to magnetic nanoparticles.

Magnetic nanoparticles structure has silica coated magnetic core (~10nm) and a polymer shell (structure is shown in Figure 1-3). The silica shell allows for protection from oxidation of the core, a longer shelf life of these particles and a platform for attaching contaminant-specific ligands. The synthesis process resulted in the formation of clusters of these particles in the size range of 50-100nm (more details on its synthesis are provided in the next section and Chapter 2). The magnetic force acting on a particle is directly proportional to the volume of the magnetic particle. The presence of multiple magnetic cores in a cluster thus aids in its removal by increasing the magnetic content in a particle. We also have the flexibility to tailor the chemistry of these ligands to remove specific classes of contaminants, for example, heavy metals and organic compounds.

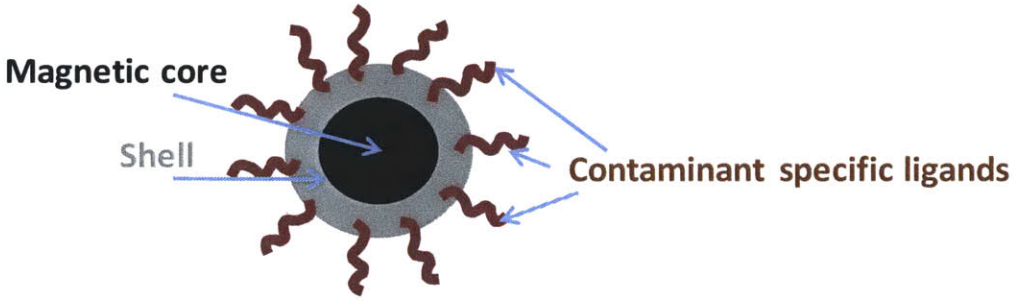

Figure 1-3: Image of a typical magnetic nanoparticle (MNP) structure

This section outlines the different chemical routes adopted for synthesis of super-paramagnetic nanoparticles. Superparamagnetism refers to particles that do not suffer hysteresis losses under different applied magnetic fields. One of the advantages of our technology is that we do not need a narrow size distribution. Therefore we use a fairly simple co-precipitation method to prepare 50-100nm clusters. The following methods have been reported in the literature as common procedures for preparing nanoparticles.

Precipitation from Solution (Hydrothermal Synthesis): Uniform particles are prepared via homogeneous precipitation reactions at high temperatures and high pressure where nucleation and growth of nuclei take place. In this process, a single short burst of nucleation occurs when the concentration of constituent species reaches critical super-saturation. The nuclei obtained are allowed to grow uniformly by diffusion of solutes to their surfaces until a definite size is attained. The strategy is based on general phase transfer and separation mechanism occurring at the interfaces of solid and liquid phases. A classical model proposed by LaMer and Dinegar was first used to explain the mechanism of formation of sulphur colloids.[30] This method rigorously controls size (based on temperature) and shape (based on starting material).[31] Sun et. al. proposed a size controlled synthesis to produce 4 nm Fe_3O_4 nanoparticles. Larger monodispersed particles can also be made using a seed-mediated growth method.[32]

Co-precipitation of ferrous hydroxide with different oxidizing agents can form spherical magnetite particles. A stoichiometric combination (2:1 molar ratio) of ferrous and ferric hydroxides in pH controlled aqueous media can also yield spherical particles.[33] It is a convenient, easily reproducible and simple to implement process. Size, shape and composition of the MNPs depend on the type of salts used (sulphates/chlorides etc), ratio of Fe^{2+}: Fe^{3+}, temperature, pH and ionic strength of the precipitating media. The biggest three disadvantages of this process are that particles produced are polydisperse, magnetite formed is unstable to oxidation and that particles have a tendency to agglomerate.

Thermal decomposition: Inspired by the synthesis of high quality semiconductor nanocrystals and oxides in non aqueous media by thermal decomposition, magnetite synthesis by the same approach has been developed.[34] Mono-disperse magnetic nanocrystals with small size (< 10nm) can be made through thermal decomposition of organometallic compounds like metal acetylacetonates, metal cupferronates and metal carbonyls in high boiling organic solvents containing stabilizing surfactants (oleic acid, hexadecylamine and various other fatty acids).[35] Reaction temperature, ratios of starting reagents, reaction times as well as aging period are crucial in control of size and morphology.

Micelle Synthesis/Micro-emulsion synthesis: A microemulsion is a thermodynamically stable isotropic dispersion of two immiscible liquids where the micro-domain of the dispersed liquid is stabilized by an interfacial film of surfactant molecules.[36] There are two types of emulsion: water-in-oil (w/o) and oil-in-water (o/w) emulsions. The aqueous phase is surrounded by a thin layer of surfactant dispersed in a continuous hydrocarbon layer in the first case. When two w/o micro-emulsions, each containing one of the two reactants are mixed, microdoplets collide, coalesce and break again with resulting precipitate formation. Solvent can be added to these micro-emulsions to facilitate precipitate separation by centrifuging or filtering. Although many types of MNPs have been synthesized by this technique, the yield of NP is low; particle size and shape vary substantially, and it is not amenable to scale up.

1.3.2 Applications

MNPs have a wide range of applications including use in therapy (drug delivery,[37] hyperthermia treatment[38]), diagnostics (contrast agents in Magnetic resonance imaging[37]), data storage and separations (protein separations,[39] organic extractions[40]) .

Therapeutic applications: Use of magnetic nano or micro particles as drug carriers to targeted tumor cells was first proposed in 1970s by Widder et. al.[41] The therapeutic drug can be either attached to or encapsulated within magnetic nanoparticles. These drug carriers are injected into the bloodstream close to the cancer site. Magnetic fields are used to move these magnetic nanoparticles. While this is effective for sites on the body's surface, it easily becomes difficult to target internal organs. Hyperthermia is an alternative approach to cancer treatment that involves heating the cancerous cells without damaging the nearby cells. Injecting magnetic nanoparticles near the tumor and heating them up by alternating magnetic fields achieve this. Alternating the direction of the magnetic fields results in changing particle magnetization that in turn results hysteresis or heating up of the particles.

Diagnostics: Magnetic nanoparticles are also used as contrast agents for magnetic resonance imaging and help in distinguishing cancerous cells from healthy cells.[37,42]

Separations: Magnetic particles and fluids have also been used for separating cells and proteins.[39,43,44] In biological applications, the particles have a ligand to which specific protein or cell can attach to and be separated from the solution by magnetic means.

Several environmental applications for magnetic nanoparticles also exist. Moeser et.al[40] have demonstrated effective removal of PAHs from aqueous systems using magnetic nanoparticles. Some of the other applications[45,46,47] involve using micro magnetite particles as a selective adsorbent for targeted solutes, such as radionuclides, heavy metal ions or organic dyes. Highly porous magnetic beads have also been used effectively for removing metal ions from water. It has also been demonstrated that nano scale bimetallic particles are effective in transformation of trichloroethene (TCE) into benign hydrocarbons like ethane.[48] NPs of bimetals of Fe-Ni shows an acceleration of reduction of chloroform.[49] Recently, iron NPs have been used for arsenic removal from drinking water.[50] In addition, field implementations of nanomaterials for environmental cleanup has also been gaining popularity.[11] However, despite the recent popularity of magnetic nanoparticles, it has been shown by Lecoanet et al.[51] that nanosized materials may not as valuable as thought of in environmental remediation as they do not migrate through sediments at rapid enough rates and can be toxic to the environment. This thesis addresses the feasibility of using functionalized magnetic nanoparticles for heavy metal removal from an aqueous stream.

1.4 Background: Common Magnetic Separation Processes and Equipment

Moffat et.al. comprehensively reviews the different types of magnetic separation processes that can be implemented for environmental and industrial applications.[52] They are magneto collection, magneto flocculation, magneto sedimentation, magneto floatation, magneto sorting, magneto stabilization, magneto transport, magneto tagging and magneto carrier technology, and are differentiated from each other on the basis of relative magnetic susceptibilities of the magnetic material and the medium around it and the magnetic field gradient that is applied. The magneto carrier technology is of particular interest to us, where colloidal particles that are not magnetically susceptible and are difficult to separate by traditional methods are separated from the stream by attaching them to magnetic carriers. The attachment to magnetic carriers enables the colloidal particles to be easily removed by magnetic means. The

proposed environmental cleanup technology utilizes this principle to remove contaminants that remain dissolved or suspended in the environment.

Magneto processing has been in use since early 1900s when it was first applied to mineral applications. Since then the technology has evolved and has been applied to newer mining and construction processes, bioprocesses and environmental separations. Today, there are several commercial companies like Metso,[53] Eclipse Magnetics[54] and Steinert[55] that build efficient magnetic separator which can be easily integrated to an existing process line. Of these products, High gradient magnetic separation (HGMS) based magnetic circuit based filters are the most convenient, easily integrable and efficient option available.

High gradient magnetic separation (HGMS): This is an effective process for separating small and weakly magnetic particles from an aqueous mixture. This uses a column packed with thin (μm) stainless steel magnetizable wires and placed in an external electromagnet. When the electromagnet is switched on, the wires distort the magnetic field lines generated by the electromagnet and generate strong gradients in their vicinity. The strong gradients result in a stronger force acting on the magnetic particles that will attract them to the wires. These particles remain attached or collected on the wires as long as the external magnetic field is switched on. Once the electromagnet is switched off, the particles lose their magnetic properties and fall off the wires. Some of the pros for using HGMS are that it is a low cost, highly selective unit process than can be easily applied to very small particles and a broad range of processes while some of the inherent cons are that it is a non-continuous process where channeling, dispersion effects and clogging can occur. An additional disadvantage is that the electromagnet is a bulky and expensive object that can put a strain on user's resources. The collection of these particles depends on the magnetic force acting on it which is given as

$$F = \mu_0 M_v V_p \nabla H \tag{1}$$

Here, μ_0 is the free space permeability ($\frac{N}{A^2}$), M_v is the saturation volume magnetization of the particle ($\frac{emu}{cm^3}$), V_p is the volume of the particle (cm^3), ∇H is the field gradient applied by the electromagnet. For successful collection of these particles, the magnetic force should be greater than any other force in the system, such as fluid drag force or gravitational force. A brief

schematic of the HGMS has been shown earlier Figure 1-4 show a commercially available cyclic HGMS with the magnetizable wire inserts..[53]

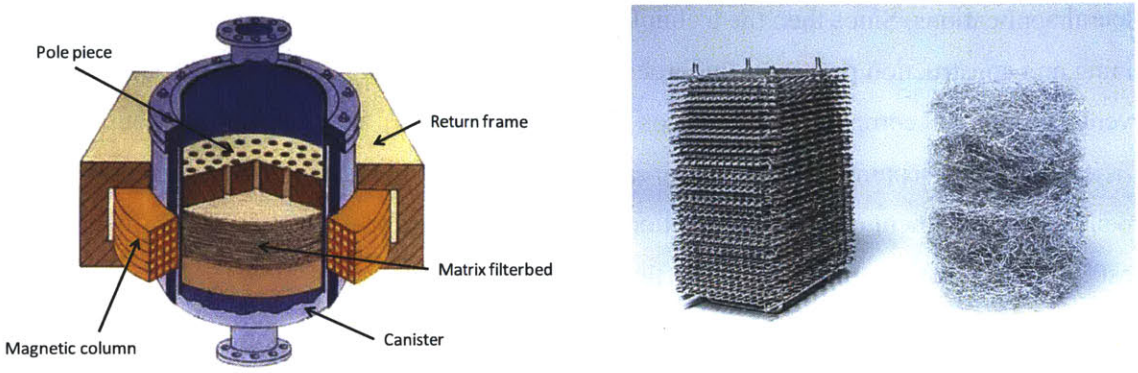

(a) (b)

Figure 1-4: (a) Commercially available cyclic HGMS system (b) Type of wires that can be used in commercially available HGMS systems

Magnetic switch based separators: These separators use the same principle of high magnetic gradients to separate out sub micron magnetic particles as HGMS. However the only difference is that they do not use a electromagnet but is equipped with a big rotor and rare earth iron boron magnets in a magnetic switch configuration. The switch can be either switched on or off depending on the configuration of the permanent magnet. The geometry of the magnetic flux circuit, similar to the previous type of separator, ensures a controlled buildup of magnetic material on the wires and that the material does not clog the wire matrix. A short purge cycle follows the switched on scenario when permanent magnets are pulled off from the flow system such that the collected magnetic material is removed from the separation chamber. Figure 1-5 shows the typical configuration of a commercially available magnetic filter from Eclipse Magnetics that that works on the principle of a magnetic switch.[54]

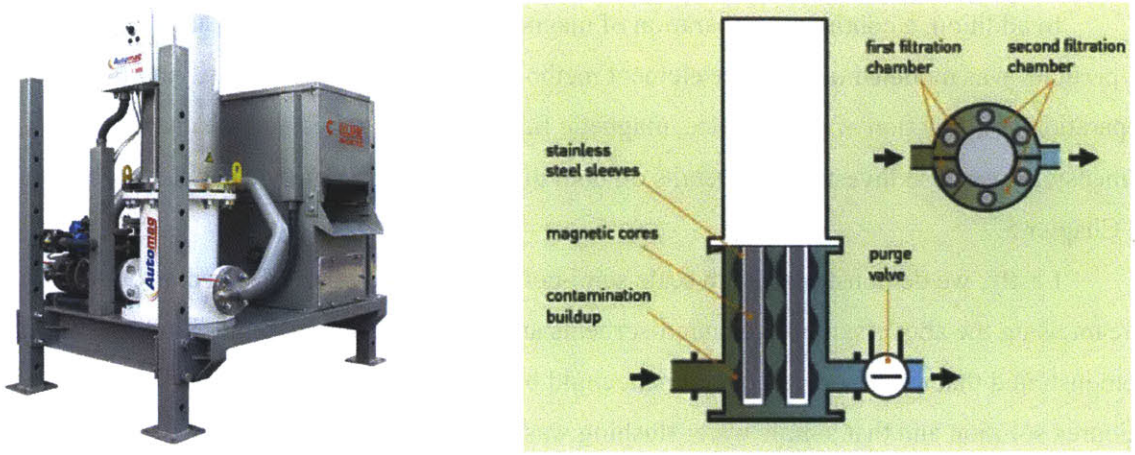

(a) (b)

Figure 1-5: (a) Commercially available magnetic switch based filter (b) Working principle of a magnetic switch based filter

1.5 Research Overview

The overall goal of this thesis is to evaluate the feasibility of using magnetic nanoparticles as nano sorbents to adsorb contaminants, in particular, heavy metals such as Hg, Pb and Mn from aqueous waste streams. To this end, we have tested dithiocarbamate functionalized silica coated magnetic nanoclusters in the size of 60-100nm and investigated their adsorption capacities for heavy metals (Hg, Pb and Mn) by carrying out adsorption experiments under different conditions of ionic strength, pH and presence of other metal salts (calcium and magnesium salts). Chapter 2 thus gives an overview of the synthesis and results of equilibrium adsorption experiments. It was found that mercury speciation impacts the overall adsorption behavior of mercury and was studied under different pH and in presence of chloride, calcium and magnesium ions. Results of mercury speciation model are discussed in Chapter 2.

To understand and map adsorption-binding capacities of different Hg species to the dithiocarbamate functional groups present on our nano sorbents, thermodynamic models using Gaussian were developed. Key findings from these models are discussed in Chapter 3.

In Chapter 4, simulation results on transport properties of these particles in a porous and non porous media using finite element models developed in COMSOL are discussed. The simulations provided a fundamental understanding of how magnetic nanoparticles would behave differently under magnetic field gradients and in porous media.

In addition, a continuous separation of magnetic nanoparticles from an aqueous mixture of particles was modeled using finite element method. Parametric results quantifying the trend in separation as a function of particle size, magnetic field gradient applied and the channel dimensions was also investigated. Details on both the model and parametric results can be found in Chapter 5.

Lastly, we demonstrated a lab scale semi-continuous removal of Hg from an aqueous stream using the above-synthesized nano-sorbents and a HGMS column. In addition, we demonstrated that the adsorbed contaminant could be easily stripped off the particles using thiourea solution and that simple water flushing was sufficient to remove the particles from the HGMS separation unit. Details of the experimental runs are given in Chapter 6. A brief discussion on scaling this technology is also included in this chapter with more details in the Capstone paper.

1.6 References

1. Goldenberg, S. Dispersant 'may make Deepwater Horizon oil spill more toxic' **2010**.

2. Zahir, F.; Rizwi, S. J.; Haq, S. K.; Khan, R. H., Low dose mercury toxicity and human health. *Environmental Toxicology and Pharmacology* **2005,** *20* (2), 351-360.

3. Dean, J. G.; Bosqui, F. L.; Lanouette, K. H., Removing heavy metals from waste water. *Environmental Science & Technology* **1972,** *6* (6), 518-522.

4. Padak, B.; Wilcox, J., Understanding mercury binding on activated carbon. *Carbon* **2009,** *47* (12), 2855-2864.

5. Rivera-Utrilla, J.; Sánchez-Polo, M.; Gómez-Serrano, V.; Álvarez, P. M.; Alvim-Ferraz, M. C. M.; Dias, J. M., Activated carbon modifications to enhance its water treatment applications. An overview. *Journal of Hazardous Materials* **2011,** *187* (1-3), 1-23.

6. Wang, J.; Deng, B.; Wang, X.; Zheng, J., Adsorption of Aqueous Hg(II) by Sulfur-Impregnated Activated Carbon. *Environmental Engineering Science* **2009,** *26* (12), 1693-1699.

7. Brower, J. B.; Ryan, R. L.; Pazirandeh, M., Comparison of Ion-Exchange Resins and Biosorbents for the Removal of Heavy Metals from Plating Factory Wastewater. *Environmental Science & Technology* **1997,** *31* (10), 2910-2914.

8. Curkovic, L.; Cerjan-Stefanovic, S.; Filipan, T., Metal ion exchange by natural and modified zeolites. *Water Research* **1997,** *31* (6), 1379-1382.

9. Silva, J. E.; Paiva, A. P.; Soares, D.; Labrincha, A.; Castro, F., Solvent extraction applied to the recovery of heavy metals from galvanic sludge. *Journal of Hazardous Materials* **2005,** *120* (1-3), 113-118.

10. Blais, J. F. D., Z.; Ben Cheikh, R.;Tyagi, R. D.; Mercier,G., Metals Precipitation from Effluents: Review *Journal of Hazardous, Toxic, and Radioactive Waste* **2008,** *12* (3).

11. Agency, U. S. E. P., Nanotechnology for site remediation fact sheet. 2009.

12. . http://en.wikipedia.org/wiki/Heavy_metal_(chemistry).

13. Harada, M., Congenital Minamata disease: Intrauterine methylmercury poisoning. *Teratology* **1978,** *18* (2), 285-288.

14. . http://en.wikipedia.org/wiki/Minamata_disease#cite_note-8.

15. . Pollution issues: Mercury (http://www.pollutionissues.com/Li-Na/Mercury.html).

16. . http://www.epa.gov/ttnatw01/hlthef/antimony.html.

17. . http://www.epa.gov/ttnatw01/hlthef/arsenic.html.

18. . http://www.epa.gov/ttnatw01/hlthef/cadmium.html.

19. . http://www.epa.gov/ttnatw01/hlthef/cobalt.html.

20. . http://www.epa.gov/oaqps001/lead/health.html.

21. . http://www.epa.gov/ttnatw01/hlthef/manganes.html.

22. . http://www.epa.gov/mercury/exposure.htm.

23. . http://www.epa.gov/ttnatw01/hlthef/nickel.html.

24. Zhou, L.; Wang, Y.; Liu, Z.; Huang, Q., Characteristics of equilibrium, kinetics studies for adsorption of Hg(II), Cu(II), and Ni(II) ions by thiourea-modified magnetic chitosan microspheres. *Journal of Hazardous Materials* **2009,** *161* (2-3), 995-1002.

25. Sreedhar, M. K.; Anirudhan, T. S., Preparation of an adsorbent by graft polymerization of acrylamide onto coconut husk for mercury(II) removal from aqueous solution and chloralkali industry wastewater. *Journal of Applied Polymer Science* **2000,** *75* (10), 1261-1269.

26. Das, S. K.; Das, A. R.; Guha, A. K., A Study on the Adsorption Mechanism of Mercury on Aspergillus versicolor Biomass. *Environmental Science & Technology* **2007,** *41* (24), 8281-8287.

27. Moeser, G. D. Colloidal magnetic fluids as extractants for chemical processing applications. Massachusetts Institute of Technology, Cambridge, **2003**.

28. Crannell, B. S.; Eighmy, T. T.; Krzanowski, J. E.; Eusden, J. D.; Shaw, E. L.; Francis, C. A., Heavy metal stabilization in municipal solid waste combustion bottom ash using soluble phosphate. *Waste Management* **2000,** *20* (2-3), 135-148.

29. Sediments, N. R. C. U. S. C. o. C. M., *Contaminated sediments in ports and waterways: Cleanup strategies and technologies*. 1997.

30. Lamer, V. K.; Dinegar, R. H., Theory, Production And Mechanism Of Formation Of Monodispersed Hydrosols. *Journal Of The American Chemical Society* **1950,** *72* (11), 4847-4854.

31. Tartaj, P., Superparamagnetic Composites: Magnetism with No Memory. *European Journal Of Inorganic Chemistry* **2009,** (3), 333-343.

32. Sun, X. H.; Zheng, C. M.; Zhang, F. X.; Yang, Y. L.; Wu, G. J.; Yu, A. M.; Guan, N. J., Size-Controlled Synthesis of Magnetite (Fe3O4) Nanoparticles Coated with Glucose and

Gluconic Acid from a Single Fe(III) Precursor by a Sucrose Bifunctional Hydrothermal Method. *Journal Of Physical Chemistry C* **2009,** *113* (36), 16002-16008.

33. Sasaki, N.; Murakami, Y.; Shindo, D.; Sugimoto, T., Computer simulations for the growth process of peanut-type hematite particles. *Journal Of Colloid And Interface Science* **1999,** *213* (1), 121-125.

34. Huang, L. M.; Chen, Z. Y.; Wilson, J. D.; Banerjee, S.; Robinson, R. D.; Herman, I. P.; Laibowitz, R.; O'Brien, S., Barium titanate nanocrystals and nanocrystal thin films: Synthesis, ferroelectricity, and dielectric properties. *Journal Of Applied Physics* **2006,** *100* (3).

35. Srouji, F.; Afzaal, M.; Waters, J.; O'Brien, P., Single-source routes to cobalt sulfide and manganese sulfide thin films. *Chemical Vapor Deposition* **2005,** *11* (2), 91-+.

36. Lu, A. H.; Salabas, E. L.; Schuth, F., Magnetic nanoparticles: Synthesis, protection, functionalization, and application. *Angewandte Chemie-International Edition* **2007,** *46* (8), 1222-1244.

37. Sun, C.; Lee, J. S. H.; Zhang, M., Magnetic nanoparticles in MR imaging and drug delivery. *Advanced Drug Delivery Reviews* **2008,** *60* (11), 1252-1265.

38. Ito, A.; Shinkai, M.; Honda, H.; Kobayashi, T., Medical application of functionalized magnetic nanoparticles. *Journal of Bioscience and Bioengineering* **2005,** *100* (1), 1-11.

39. Bucak, S.; Jones, D. A.; Laibinis, P. E.; Hatton, T. A., Protein Separations Using Colloidal Magnetic Nanoparticles. *Biotechnology Progress* **2003,** *19* (2), 477-484.

40. Moeser, G. D.; Roach, K. A.; Green, W. H.; Laibinis, P. E.; Hatton, T. A., Water-Based Magnetic Fluids as Extractants for Synthetic Organic Compounds. *Industrial & Engineering Chemistry Research* **2002,** *41* (19), 4739-4749.

41. Widder, K.; Flouret, G.; Senyei, A., Magnetic microspheres: Synthesis of a novel parenteral drug carrier. *Journal of Pharmaceutical Sciences* **1979,** *68* (1), 79-82.

42. Cunningham, C. H.; Arai, T.; Yang, P. C.; McConnell, M. V.; Pauly, J. M.; Conolly, S. M., Positive contrast magnetic resonance imaging of cells labeled with magnetic nanoparticles. *Magnetic Resonance in Medicine* **2005,** *53* (5), 999-1005.

43. Kuhara, M.; Takeyama, H.; Tanaka, T.; Matsunaga, T., Magnetic Cell Separation Using Antibody Binding with Protein A Expressed on Bacterial Magnetic Particles. *Analytical Chemistry* **2004,** *76* (21), 6207-6213.

44. Lee, I. S.; Lee, N.; Park, J.; Kim, B. H.; Yi, Y.-W.; Kim, T.; Kim, T. K.; Lee, I. H.; Paik, S. R.; Hyeon, T., Ni/NiO Core/Shell Nanoparticles for Selective Binding and Magnetic Separation of Histidine-Tagged Proteins. *Journal of the American Chemical Society* **2006,** *128* (33), 10658-10659.

45. Buchholz, B. A.; Nuñez, L.; Vandegrift, G. F., Radiolysis and Hydrolysis of Magnetically Assisted Chemical Separation Particles. *Separation Science and Technology* **1996,** *31* (14), 1933-1952.

46. Leun, D.; SenGupta, A. K., Preparation and Characterization of Magnetically Active Polymeric Particles (MAPPs) for Complex Environmental Separations. *Environmental Science & Technology* **2000,** *34* (15), 3276-3282.

47. Safarík, I., Removal of organic polycyclic compounds from water solutions with a magnetic chitosan based sorbent bearing copper phthalocyanine dye. *Water Research* **1995,** *29* (1), 101-105.

48. Elliott, D. W.; Zhang, W. X., Field assessment of nanoscale biometallic particles for groundwater treatment. *Environmental Science & Technology* **2001,** *35* (24), 4922-4926.

49. Horng, S.-H. H. a. J.-J. *The Reaction mechanism of decomposing chloroform by bi-metal nano-metallic particles of Fe/Ni*; Anaheim, CA, 2004.

50. Yavuz, C. T.; Mayo, J. T.; Yu, W. W.; Prakash, A.; Falkner, J. C.; Yean, S.; Cong, L. L.; Shipley, H. J.; Kan, A.; Tomson, M.; Natelson, D.; Colvin, V. L., Low-field magnetic separation of monodisperse Fe3O4 nanocrystals. *Science* **2006,** *314* (5801), 964-967.

51. Lecoanet, H. F.; Bottero, J. Y.; Wiesner, M. R., Laboratory assessment of the mobility of nanomaterials in porous media. *Environmental Science & Technology* **2004,** *38* (19), 5164-5169.

52. Moffat, G.; Williams, R. A.; Webb, C.; Stirling, R., Selective separations in environmental and industrial processes using magnetic carrier technology. *Minerals Engineering* **1994,** *7* (8), 1039-1056.

53. . Magnetic separators: http://www.metso.com/miningandconstruction/mm_sepa.nsf/WebWID/WTB-041102-2256F-551B9.

54. . Magnetic filtration: http://www.eclipse-magnetics.co.uk/product-categories/magneticfiltration.

55. . High gradient magnetic filter: http://www.steinert.de/home/products/high-gradient-magnetic-filter-hgf/.

Chapter 2. Adsorption of Heavy Metals from Aqueous Media by Dithiocarbamate-modified Core-shell Magnetic Nanoparticles

2.1 Introduction

Contamination of aquatic media by heavy metals is of serious environmental concern because their presence is toxic even in trace amounts.[1,2] Contaminants also accumulate in tissues of living organisms which in turn leads to various disorders and diseases. For example, mercury is introduced to these aquatic systems through waste streams of various industries including pharmaceutical, paper and pulp, battery production and mining. Mercury poisoning has far reaching health implications especially on the renal and nervous systems.[3,4,5] Thus to maintain safe water quality standards, it becomes essential to remove mercury and other toxic metals from these waste streams. In this chapter, the synthesis of novel dithiocarbamate-modified core-shell magnetic nanoparticles to adsorb heavy metals is discussed.The dithiocarbamate functional group has been widely reported to have high affinities ($\sim 10^8$) for heavy metals and in particular for mercury.[6,7,8,9] Thus magnetic nanoparticles have been modified to contain this functional group for removal of aqueous heavy metals. Dithiocarbamate-modified polyethyleneimine-silica coated magnetic nanoparticles have the unique properties of high surface area, a magnetic core that can be used for recovery of these magnetic sorbents, long term stability provided by the silica shell and high adsorption affinity to the mercury and other heavy metals. Also, these particles were used in a semi continuous manner to remove heavy metals from waste streams and can be effectively applied in the remediation of the toxic metals contaminated sediments. An additional unique characteristic of these particles is that one can reuse these particles by stripping off the contaminant using organic compounds such as thiourea.

The objective of this work is to evaluate the potential of these modified magnetic nanoparticles as adsorbents of mercury under different conditions of pH and salt concentrations, and in presence of other metals such as calcium and magnesium. Lead and manganese can also be removed from aqueous systems by adsorption to these particles that highlight the wide range of metals that can be targeted.

In this chapter, the adsorption characteristics of metals under different conditions of pH and salt concentration were studied. It was observed that pH and the presence of salts affected the adsorption equilibrium as it altered both mercury and dithiocarbamate ligand speciation. A chemical equilibrium software package MINEQL+, was used to determine the mercury speciation under different pH conditions and salt concentrations. With the focus of characterizing these particles for metal removal, a competitive adsorption model based on mercury speciation data was developed to determine the binding constants for various mercury species.

2.2 Experimental Section

2.2.1 Materials

Iron (II) chloride tetrahydrate, iron (III) chloride hexahydrate, ammonium hydroxide (28 wt%), tetramethylammonium hydroxide (TMAOH), epoxy-functional 3-glycidoxypropyl trimethoxysilane (GPTMS), methanol, acetone, carbon disulphide, mercuric nitrate monohydrate and dimethyl sulfoxide (DMSO) were purchased from Sigma Aldrich. Lupasol G-20 (polyethylenimine) was purchased from BASF. All chemicals were used in the form in which they were received.

2.2.2 Particle Synthesis

Magnetite-silica core-shell particles functionalized with dithiocarbamate (DTC-M/SiO_2) were synthesized in four consecutive steps (Figure 2-1). First, magnetite particles were prepared; they were well dispersed in water with the aid of TMAOH. In the second step, the magnetic particles were encapsulated by a shell comprising tetraethyl orthosilicate (TEOS) and GPTMS. The third step was the attachment of PEI to the core-shell particle (PEI-M/SiO_2). Lastly, the fourth step was to modify PEI-M/SiO_2 with carbon disulphide to yield the dithiocarbamate modified magnetic nanoparticles. Dr. Bromberg (research scientist in our lab) carried out this four-step synthesis of dithiocarbamate modified core-shell magnetic nanoparticles.

$FeCl_3.6H_2O$ (7.58, 28 mmol) and $FeCl_2.4H_2O$ (2.78 g, 14 mmol) were dissolved in 25 ml deionized water and the solution was brought to 80°C under nitrogen purge within 30 min. The solution was poured into 25 ml of 28wt% NH_4OH and the resulting black precipitate was stirred and kept at 80°C for 1 h. The resulting particle suspension was sonicated for 1 min and separated

from the supernatant by magneto-collection (magnetic field, ~1.2 T). The particles were then placed into a tube containing 30 ml of 0.33 M aqueous solution of TMAOH. The suspension was observed to be stable for more than couple of hours. The particles were separated by magneto-collection and washed twice by 50 ml of deionized water each time. The above steps were repeated three times and the resulting TMAOH-stabilized magnetite suspension fractions were combined (100 ml total, magnetite content, ~30.5 g) and diluted by 100 ml ethanol. Then, 10 ml of TEOS were added and the suspension was sonicated for 5 min, followed by addition of 10 ml of GPTMS. The suspension was kept under vigorous shaking at room temperature for two days, after which fractions of the suspension were conjugated with PEI as follows. Particles were synthesized using 190 ml of the above suspension (magnetite content, 30 g), to which a 20 % solution of Lupasol (15 g PEI in 75 ml water) was added. The mixture was kept at 80°C for 1 h followed by shaking at 250 rpm at room temperature for two days. Then the product was dialyzed against an excess of deionized water (MWCO 12-14 kDa), snap-frozen and lyophilized.

Modification with carbon disulphide was conducted using dry (lyophilized) PEI-M/SiO2 particles. Namely, 2.7 g particles were suspended in 10 ml DMSO and 12 ml of carbon disulfide was added to the above suspension. The resulting mixture was shaken for 48 h and 45 gms of particles were recovered by centrifugation (9,500 rpm, 15 min), washed by water, methanol and acetone and dried on air.

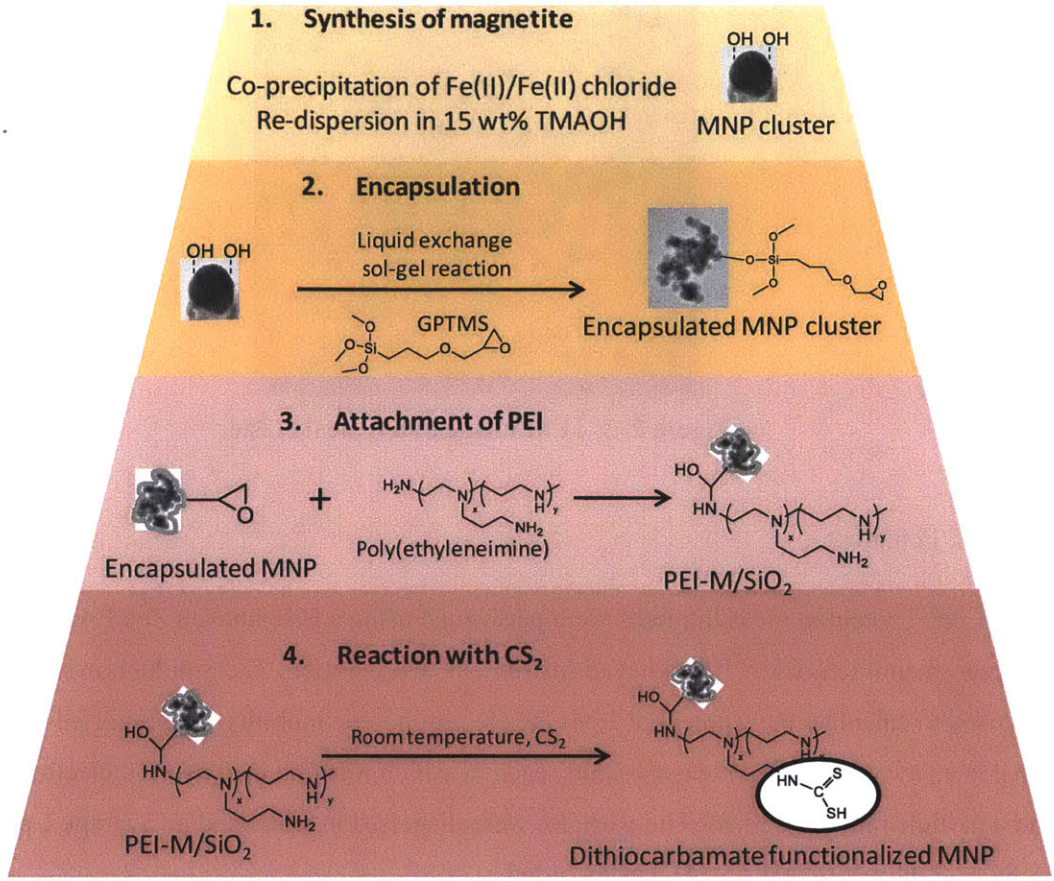

Figure 2-1: Steps involved in synthesis of dithiocarbamate modified magnetic nanoparticles

2.2.3 Particle Characterization

2.2.3.1 Transmission Electron Microscopy (TEM):

Images of the synthesized magnetic nanoparticles were taken using a JEOL 200CX TEM microscope. Figure 2-2 shows a transmission electron microscope image of one typical particle cluster. As seen from the image, the magnetite particles are coated by a silica shell and are connected to each other by polyethylenimine polymer to form clusters. Here the darker spots or beads represent the magnetite, the silver lines represent the silica shell and the grey region represents the polymer. The approximate size of the cluster was 70nm. All of the synthesized dithiocarbamate-modified core shell particle clusters were in the size range of 60-100nm.

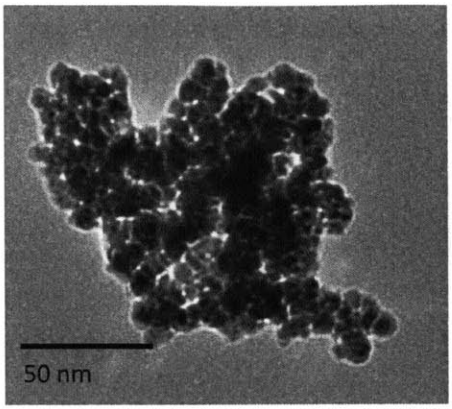

Figure 2-2: TEM image of a typical cluster

2.2.3.2 ζ Potential:

All ζ potential measurements were performed using a Brookhaven ZetaPALS ζ potential analyzer, manufactured by Brookhaven Instruments Corporation. The Smoluchowski equation was used to calculate the ζ potential from the electrophoretic mobility. The reported ζ potential value is an average of five measurements, each of which was obtained over 10 electrode cycles and a particle radius of 50nm. The particles were dispersed in water and an average ζ potential of 18.89 +/-2.44 mV (@pH =5.54) was recorded.

2.2.3.3 Thermo Gravimetric Analysis (TGA):

TGA was conducted using a Q5000IR thermogravimetric analyzer manufactured by TA Instruments, Inc., New Castle, DE. The sample was subjected to heating scans (20 ^{O}C/min) in a temperature ramp mode. As the sample is heated in air, it continues to lose polymer weight till it reaches the magnetite weight in the sample. The derivative weight curve suggests that temperature range where weight loss is maximum further collaborating with the fact that the sample has lost all of its polymer weight when heated to 800^{o}C. The TGA results (Figure 2-3) show that the particles contain about 63% of magnetite per gram of particle.

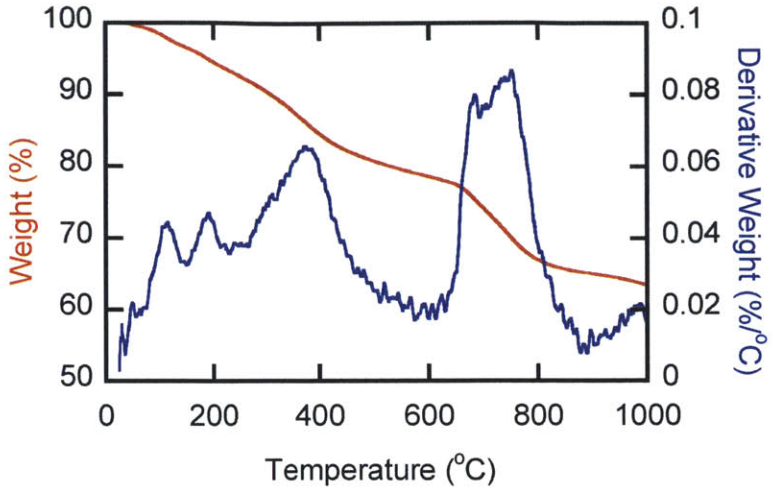

Figure 2-3: TGA results indicating magnetite content in particle is ~63%

2.2.3.4 Superconducting Quantum Interference Device (SQUID):

The magnetization of particles under applied fields was determined using a Magnetic Property Measurement System model MPMS-5S (Quantum Design). The SQUID measurements were performed at 300 K over a 0-2 T range. SQUID measurements (Figure 2-4) confirm strong super paramagnetic behavior. The saturation magnetization of these particles was determined to be 38.43 emu/g of particle or 61 emu/g of magnetite.

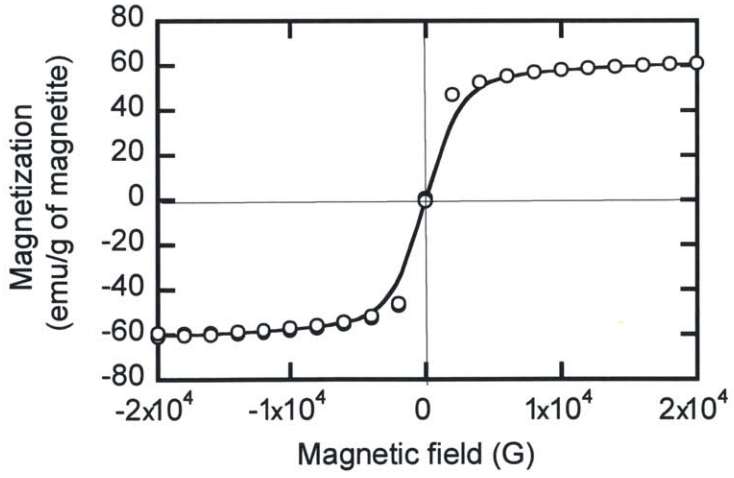

Figure 2-4: Magnetization curve obtained for the synthesized particles

2.2.3.5 Elemental Analysis

Elemental analysis was done to determine the ratio of iron to sulfur content in the particles. It was found that the concentration of the functional group 'HS-C=S' responsible for the mercury adsorption was approximately 0.91mmol/gm particles.

2.2.3.6 Fourier Transform Infrared Spectrometer (FTIR)

FTIR was used to analyze the nature of the functional groups on these particles. FTIR spectra (Figure 2-5) indicate the presence of 'C=S' and 'S-C=S' bonds on the particles confirming the presence of the dithiocarbamate group.

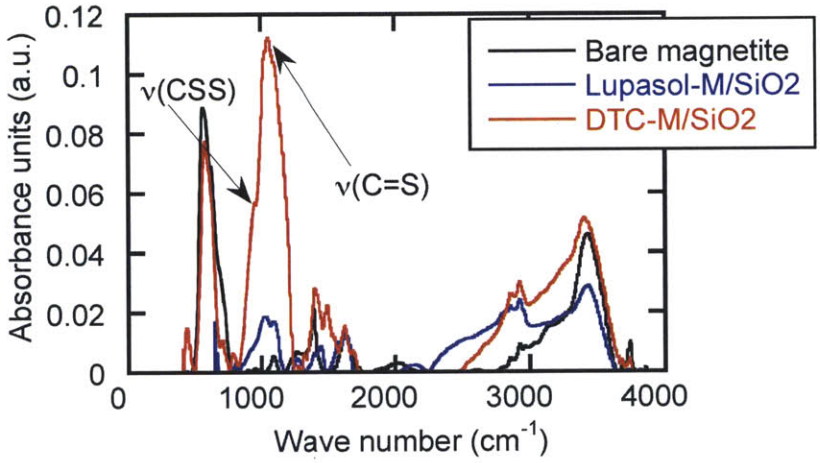

Figure 2-5: FTIR spectrum of the particle indicating C=S and S-C=S bonds

2.3 Adsorption Experiments

To determine the adsorption capacity of the synthesized particles, equilibrium adsorption isotherms were determined under varying conditions of pH, salt concentrations and presence of other metals. These experiments were performed at room temperature in batches where 20 ml of aqueous solution containing the same concentration of magnetic nanoparticles (1.5mg/ml) were taken. To these vials mercury at a concentration of 0-30ppm or 0-150 μM was added. These vials were then shaken continuously at 200 rpm for one day to allow equilibrium to be achieved,

following which, the particles in the solution were removed using magnets (magnetic field ~1.2T) and the supernatant analyzed by inductively coupled plasma - optical emission spectroscopy (ICP-OES) for remaining metal ions. All experiments were performed in duplicate (Figure 2-6).

The mass of mercury adsorbed per unit mass of nanoparticles was determined via the equation

$$Q_{eq} = \frac{(C_o - C_{eq})V}{m} \tag{2-1}$$

Where, C_o and C_{eq} are the initial and equilibrium concentrations (mg/ml) of mercury respectively in the aqueous phase, V is the volume (ml) of the aqueous phase and m is the mass weight (g) of the nanoparticles used.

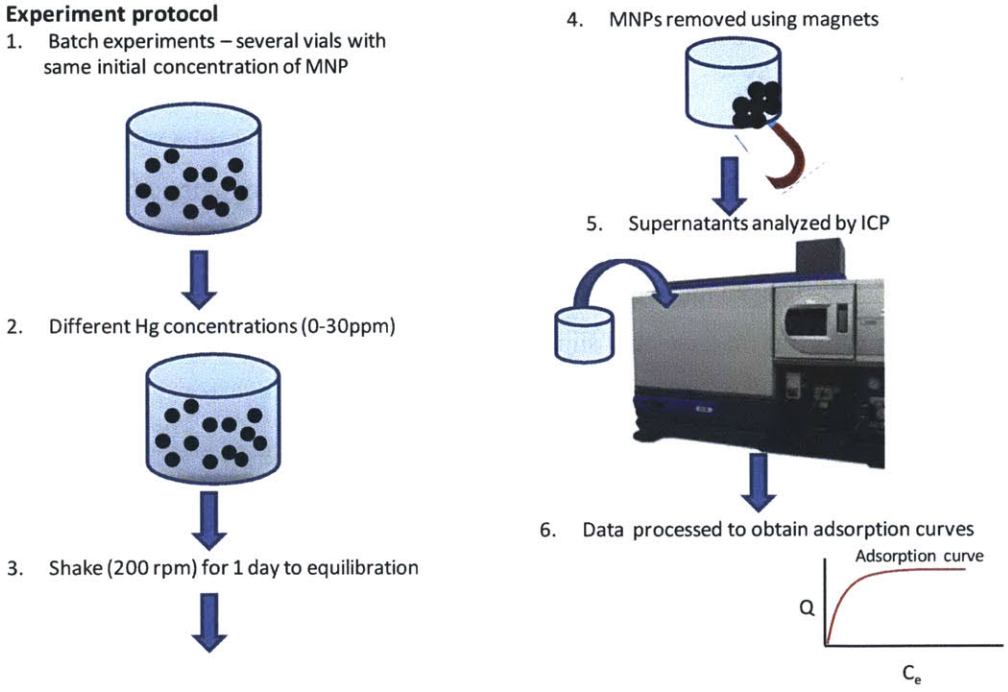

Figure 2-6: Protocol followed for equilibrium adsorption experiments

2.3.1 Effect of pH and Salinity on Mercury Adsorption

Mercury uptake experiments were performed at four different pHs (3.7, 5.2,6.7 and 8.9 where ionic strengths ~ 0) where pHs were adjusted using 0.1M solutions of HNO_3 and NaOH. Addition of buffer to control the pH of the solution was not used because of the possibility that the ionic components of the buffer would interfere with the metal speciation and its adsorption process. Mercury uptake experiments were performed at different salt concentrations ([NaCl] = 0.1, 1, 2 M) while keeping the pH constant at 6.7. Note all pH measurements were taken after the solution had come to equilibrium.

2.3.2 Competitive Adsorption with Ca^{2+} and Mg^{2+} ions

In addition to the uptake measurements mentioned above, the competitive adsorption of Hg and Ca salts and competitive adsorption of a ternary mixture of Hg, Ca and Mg salts to the particles was evaluated at pH = 6.7 and [NaCl] = 0. Different vials with the same initial concentration of particles (1.5mg/ml) were taken. To these vials, Hg and Ca salts were added such that the resultant [Hg] and [Ca] were in the 0-30ppm or 0-150 μM range. In another batch, similar addition of Hg, Ca and Mg salts was done to get resultant [Hg], [Ca] and [Mg] in the 0-30ppm or 0-300 μM range. These vials were shaken at 200 rpm for one day. After which the particles are removed using bar magnets and supernatants were analyzed by ICP-OES for equilibrium concentration of metal ions.

2.3.3 Adsorption of Lead and Manganese

These particles were also used to adsorb other metals such as lead and manganese. Experimental procedure similar to those used in the mercury adsorption experiments was performed. Instead of mercury, lead and manganese salts in the same concentration range of 0-30ppm (or 0-300 μM) were used. Note the concentrations of lead and manganese ions are twice as high as the mercury ion concentrations.

2.4 Results and Discussions

2.4.1 Equilibrium Adsorption Curves for Mercury

A typical adsorption isotherm, obtained for mercury adsorption at pH = 6.7 and in the absence of salt, is shown in Figure 2-7. The experiment was performed in duplicates to determine the error bars in the adsorption pattern. The adsorption follows Langmuir type behavior, with a linear increase in adsorption at lower equilibrium concentrations of the metal and a plateau level of adsorption at higher concentrations. In all the isotherm plots, the x-axis is the amount of Hg measured to remain in solution phase after equilibrium is established while the y-axis is determined by difference between amount added and amount measured to remain in solution. A Langmuir model (Equation 2) was applied to the experimental data and the fit (Equation 3) is shown in Figure 2-8.

$$Q_{eqm} = \frac{Q_{max} b C_{eqm}}{1 + b C_{eqm}} \tag{2-2}$$

$$\frac{1}{Q_{eqm}} = \frac{1}{bQ_{max}} + \frac{1}{Q_{max}} \frac{1}{C_{eqm}} \tag{2-3}$$

The Langmuir constants obtained were Q_{max} (or the maximum adsorption) = 434mg/g and b (or the affinity of the adsorbate to the adsorbent) = 0.21 l/mg while the fit had a R^2 value of 0.95. A positive value of 'b' indicates adsorption of the adsorbent while the R^2 value also indicates a good fit. However, the maximum adsorption predicted by the fit is higher than the experimentally determined functional groups present and on careful examination it was found that most data had a curvature effect. These discrepancies in expected and experimental data (over prediction and curvature effect) along with obtaining different adsorption isotherms at different pHs (Figure 2-9) and salinity conditions (Figure 2-10) was explained on the basis of metal speciation. In addition, the base case suggests that every dithiocarbamate ligand is active towards Hg adsorption as the maximum adsorption hovers around 180mg/g of magnetic nanoparticle or 0.91mmoles/g of magnetic nanoparticles.

Under different conditions of pH and salt concentrations, there are different mercury species present that in turn have a different adsorption affinity towards the dithiocarbamate group present on the nanoparticles. We observe little difference in adsorption curves under different pHs as there is little difference in Hg speciation in the studied pH range.

Theoretical binding of various mercury species to a model dithiocarbamate group is discussed in the next chapter while this chapter focuses on the experimental results.

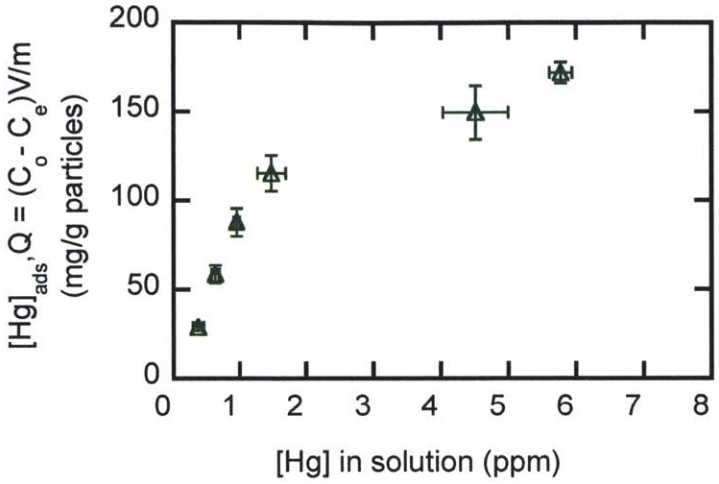

Figure 2-7: Mercury adsorption isotherm for pH=6.7 and [NaCl] =0

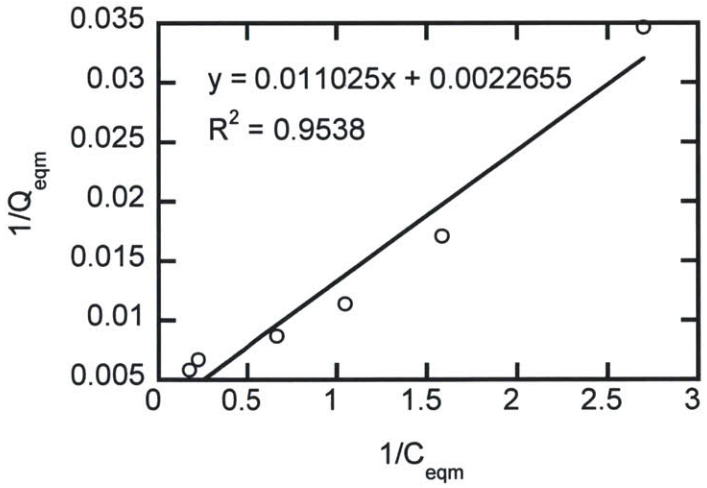

Figure 2-8: Langmuir fit to mercury adsorption isotherm data obtained at pH 6.7

Solution pH has little impact on the adsorption capacity of the particles even though it controls the speciation of Hg and ligands in water. As seen from Figure 2-9, increasing the pH, results in very little variation in the equilibrium adsorption curves. The little variations in the results can be explained on mercury speciation as a function of pH and the basis of hard soft acid

base theory (HSAB theory). At higher pHs (pH > 6), the majority of mercury complexes exist as $Hg(OH)_2$ (Figure 2-11) that in turn has a softer characteristic and a greater affinity for the dithiocarbamate group (soft base) compared to naked mercury ions. It has been reported[7, 10, 11] that at lower pHs, the relatively smaller size of Hg^{2+} has lower affinity to -CSSH binding sites because of the hard characteristics of Hg^{2+}, and that H^+ competes with mercury complexes for the sorbent resulting in lower adsorption.

In addition to the solution pH, the sorption capacity of the particles is also impacted by the presence and concentration of competing ligands such as chloride ions. In presence of NaCl, Hg(II) will partition between several different forms (e.g. HgClx, Hg-sorbent, HgClx-sorbent) which results in lower adsorption onto the magnetic nanoparticle. It is observed in Figure 2-10, that as the salt concentration increases, the equilibrium condition shifts to the right of the plot or higher equilibrium concentration of mercury and lower adsorption capacity. Increasing salinity results in higher concentrations of chloro complexes of mercury such as $HgCl_3^-$ and $HgCl_4^{2}$. The measurements suggests that the binding of Hg(II) to the sorbent is much stronger than the binding of Hg(II) to chloride ions, since you have a lot more Cl^- present than sorbent binding sites. There will be additional salt effects like changes in dielectric constant, stabilization of charged species but further experiments under different salts were not carried out. Similar phenomena have been reported for the impact of Cl^- on mercury removal by polyaniline[12].

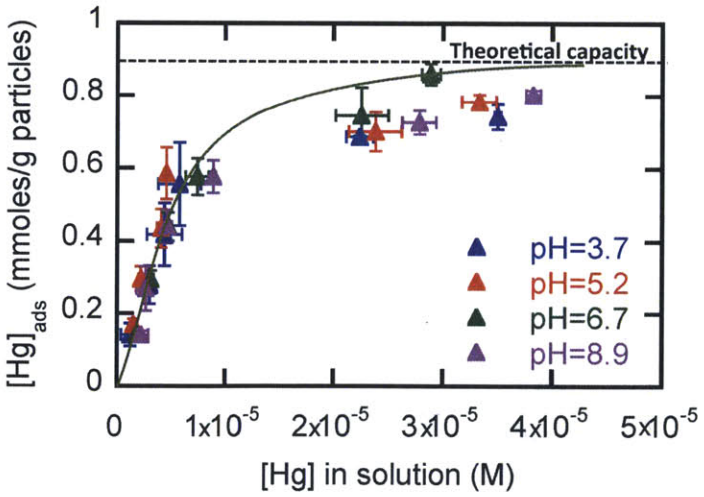

Figure 2-9: Increasing pH results in very little variation in adsorption curves

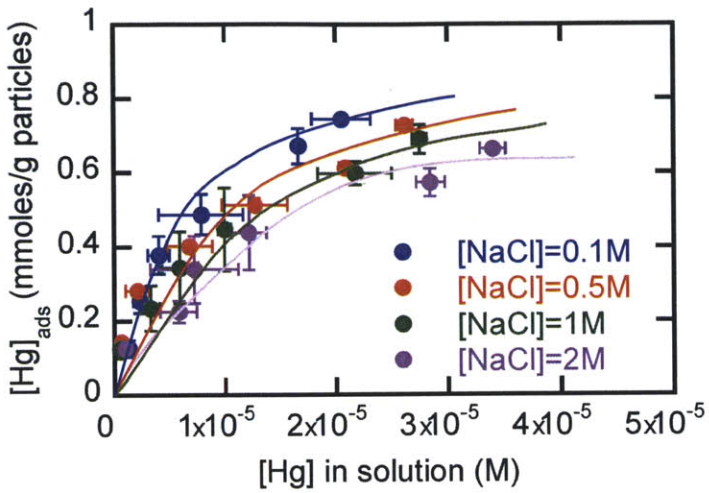

Figure 2-10: Increasing salt concentration results in decreased adsorption of mercury ions

2.4.2 Mercury Speciation using MINEQL+

The differences in adsorption curves under different experimental conditions can be explained on the basis of the existence of different mercury species present in different concentrations. Metals such as Hg^{2+} can form inner or outer sphere complexes with inorganic ligands such as OH^- and Cl^- to form different species.[13] To understand the impact of speciation phenomena on adsorption, aqueous phase concentrations of mercury species at different pHs and ionic strengths of salt were evaluated using MINEQL+, a chemical equilibrium modeling software.[14] The stability constants (units for K = L/moles) for mercury complexes with counter ions used in the speciation calculations are reported in Table 2-1.

Table 2-1: Stability constants for mercury species[15] as used by MINEQL+

Reaction	Log10K
$Hg^{2+} + Cl^- = HgCl^+$	13.5
$Hg^{2+} + 2Cl^- = HgCl_2$	20.2
$Hg^{2+} + 3Cl^- = HgCl_3^-$	21.2
$Hg^{2+} + 4Cl^- = HgCl_4^{2-}$	21.8
$Hg^{2+} + OH^- + Cl^- = HgCl(OH)$	10.4
$Hg^{2+} + OH^- = Hg(OH)^+$	2.79

$Hg^{2+} + 3OH^- = Hg(OH)_3^-$	-14.9
$Hg^{2+} + NO_3^- = HgNO_3^+$	5.76
$Hg^{2+} + 2NO_3^- = Hg(NO_3)_2$	5.38

Speciation of mercury as a function of pH and salinity conditions is shown in Figure 2-11 and Figure 2-12. As seen from the speciation data, for pH > 4, $HgOH_2$ is the dominant species while in the presence of salt, chloro complexes of Hg such as $HgCl_4^{2-}$ become predominant.

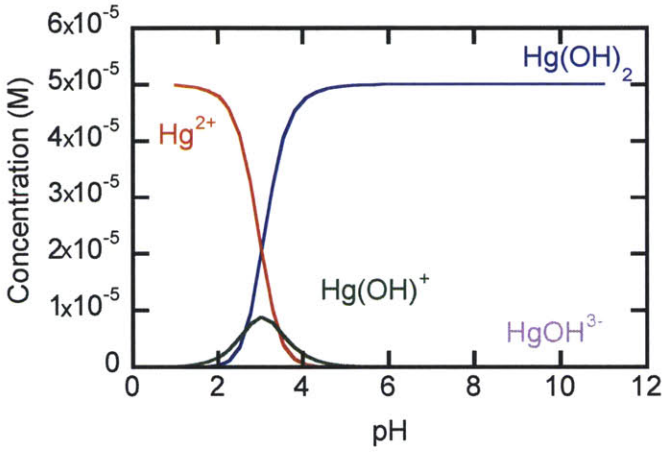

(a)

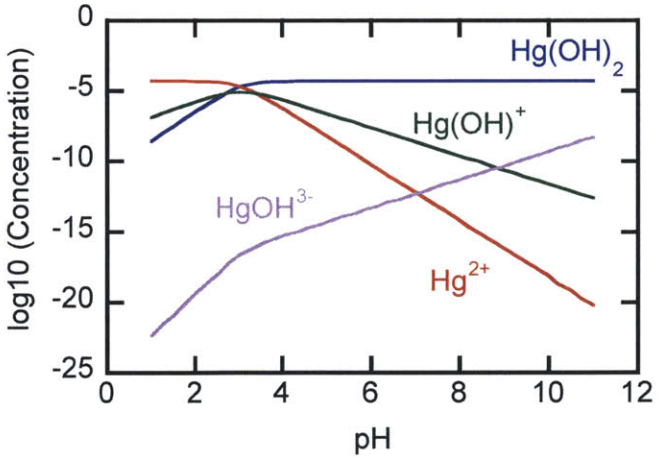

(b)

Figure 2-11: Aqueous mercury speciation as a function of pH (Initial concentration of Hg salt = 10ppm or 50 μM) (a) Speciation in terms of absolute concentration (b) Speciation in terms of log10 of concentrations

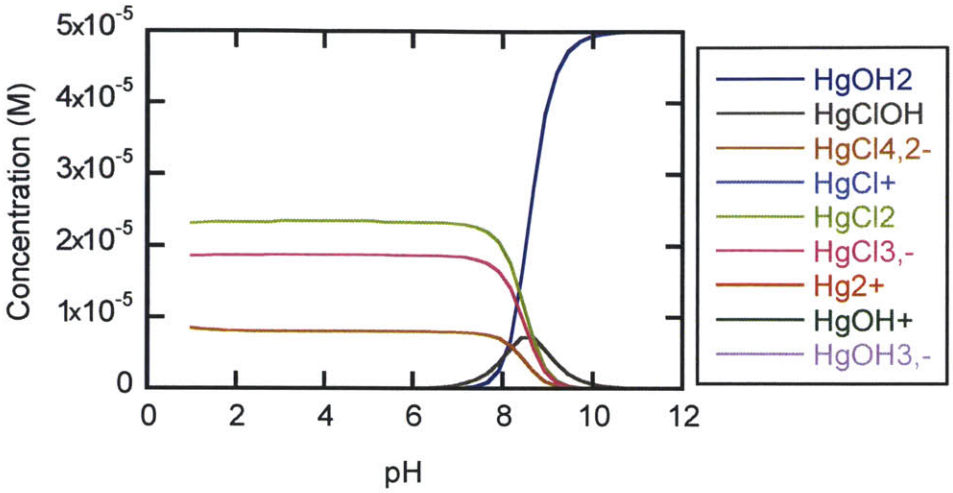

(a)

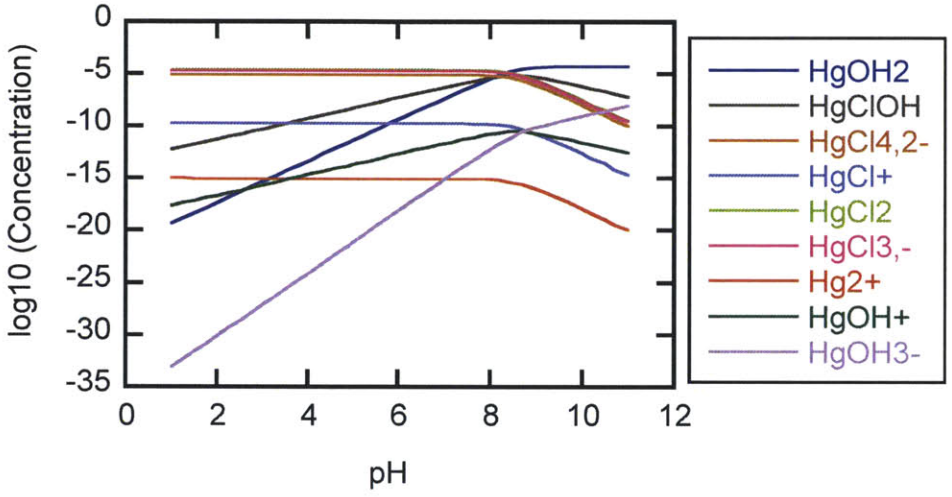

(b)

Figure 2-12: Aqueous mercury speciation as a function of pH (Initial concentration of Hg^{2+} = 10ppm or 50 μM, [NaCl] = 0.1M) (a) Speciation in terms of absolute concentration (b) Speciation in terms of log10 of concentrations

Mercury speciation shows a higher concentration of $HgOH_2$ under most pH conditions of interest (except pH=3.7). However, the dominant species is $HgCl_4^{2-}$ when the experiments are conducted in the presence of excess chlorides. The chloro mercury complexes have a lower affinity for the dithiocarbamate group that will result in lower adsorption. Its possible that a tiny bit of chloride contamination might have resulted in similar adsorption curves for experiments

with NaCl = 0 and NaCl =0.1M. This is possible since the stability constant of $HgCl_2$ is so large (LogK=20) that tiny [Cl^-] will react with most of the Hg(II) present to form $HgCl_2$. The other possible explanation is that $Hg(OH)_2$ and $HgCl_2$ have similar binding affinities to carbamate zwitterion which eventually result in similar adsorption curves.

2.4.3 Effect of Salts of Divalent Cations (Ca, Mg) on Mercury Adsorption

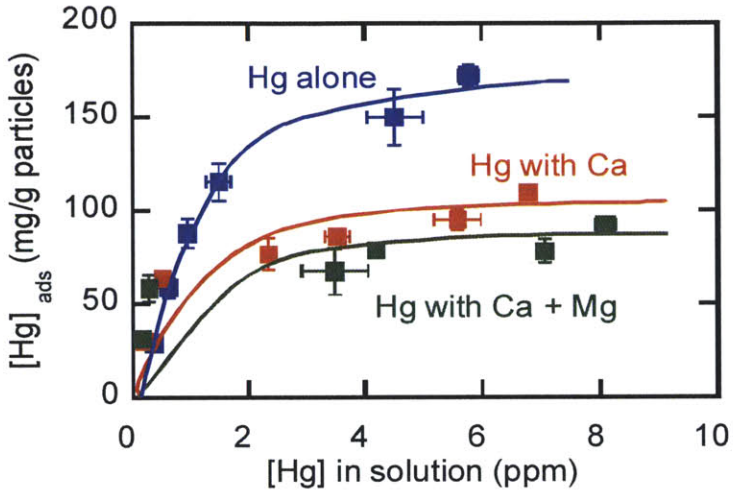

Figure 2-13: Mercury adsorption is reduced in presence of Ca and Mg salts

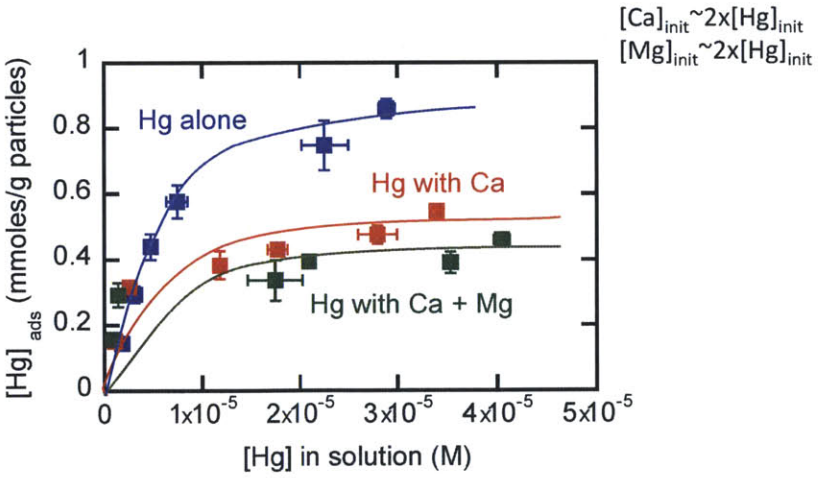

Figure 2-14: Mercury adsorption (mmole basis) is reduced in presence of Ca and Mg salts.

Figure 2-13 and Figure 2-14 shows experimental data on mercury adsorbed in the presence of calcium salt and from a ternary mixture of mercury, calcium and magnesium ions. Note that both calcium and magnesium salt concentrations were twice as high as mercury salt concentrations. Hg adsorption curve in mmole basis tends towards the maximum adsorption limit as defined by the number of functional groups on the particles.

It was observed that there is a reduction in mercury adsorbed from the binary mixture of mercury and calcium ions and further reduction if magnesium ions are present. However despite the competition from Ca^{2+} and Mg^{2+}, Hg ions are still adsorbed on the -CSSH group.

2.4.4 Adsorption of Lead and Manganese

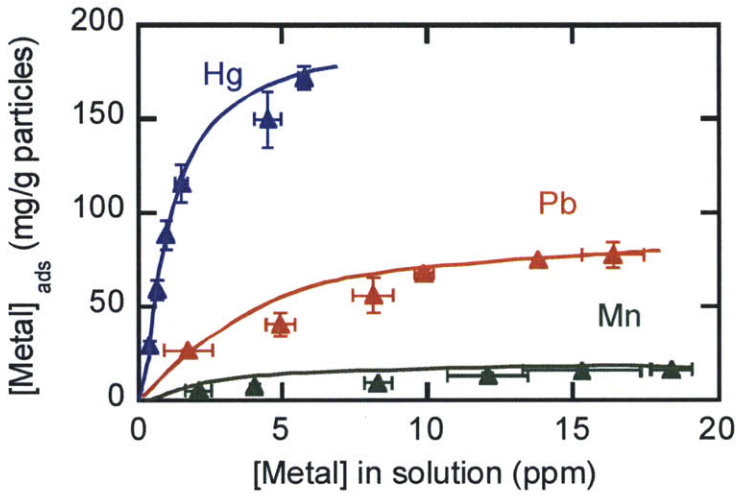

Figure 2-15: Dithiocarbamate modified MNP also adsorb lead and manganese

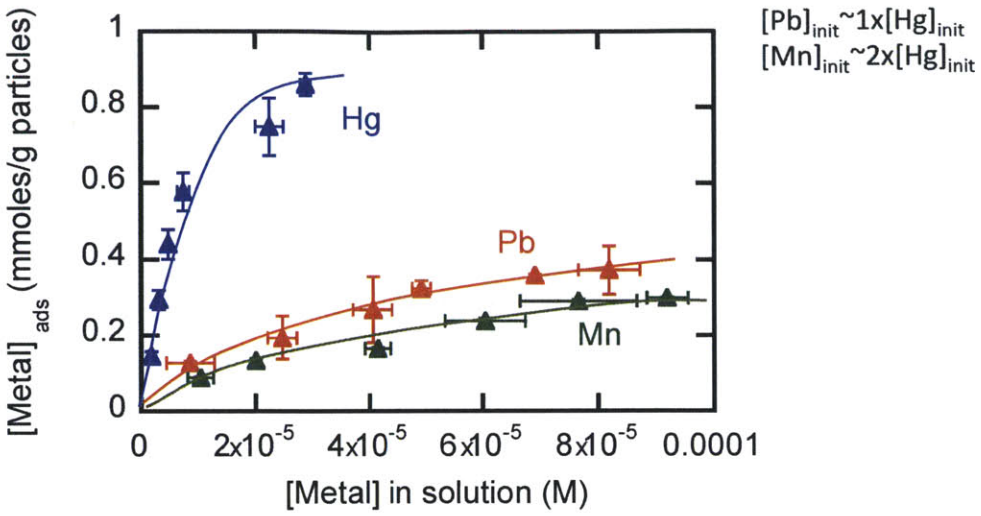

Figure 2-16: Dithiocarbamate modified MNP also adsorb lead and manganese (mmole basis)

In addition to being used in mercury adsorption experiments, these particles were also challenged with adsorbing Pb and Mn metal ions. These particles adsorbed less lead than mercury and less manganese than lead (Figure 2-15 and Figure 2-16). Note that lead and manganese salt concentrations were respectively same or twice as high as mercury salt concentrations. Hg adsorption curve in mmole basis reaches the maximum adsorption limit as defined by the number of functional groups on the particles. When compared on mmole basis, Mn adsorption curve is closer to Pb's but distinctly lower than Pb adsorption curve. Since Hg and Pb have almost the same atomic weight and the curves look about the same, dihiocarbamate binds Hg(II) about 10x more tightly than it binds the Pb ion (the stability constant K of Hg-DTC is about 10x as large as that for Pb-DTC) and since Mn is about ¼ the molecular weight of the others, to achieve 15 ppm of Mn we would actually put about 4x as many moles of Mn in the solution as we did for Hg or Pb. So the binding constant of Mn-DTC is about 6x smaller than that for Pb-DTC, and around 60x smaller than that for Hg-DTC.

Based on the HSAB theory, there is a decreasing trend in "softness" from Hg to Pb to Mn that results in decreasing binding with the dithiocarbamate group (which is a soft base). According to this theory the expected trend of softness for various metals is Hg>Cu>Pb>Cd~Zn>Fe>Ni>Co>Mn.[16] The observed trend in adsorption affinity is also supported by Denizli et. al[7] and McClain et. al.[8] Based on the results obtained for Pb and Mn, we can extend the use of these particles to remove other metals from the waste stream.

2.5 Summary

In this chapter, we discuss the synthesis of functionalized magnetic nanoparticles. The choice of functionality, the dithiocarbamate group, was based on its reported high adsorption affinity for heavy metals. The particles were characterized for size, magnetic properties and the presence and quantity of functional groups present on their surfaces. Characterization shows that 60-100nm superparamagnetic nanoparticle clusters with dithiocarbamate groups were synthesized. These particles were subsequently used in adsorption experiments to determine their adsorption capacity for mercury. Eight mercury adsorption experiments, pH=3.7,5.2,6.7 and 8.9 with no salt and with [NaCl] = 0.1,0.5,1 and 2M at pH=6.7 were performed. Varying pHs over the range 3.7 to 8.9 did not affect the measured Hg isotherms too much. The little variation in adsorption was attributed to the increased concentration of the $HgOH_2$ species that has a higher binding affinity for dithiocarbamate than does Hg^{2+}. In the presence of salts, adsorption equilibrium was reduced with increasing salt concentration. This was explained by the competing effect of chloride ions for mercury and the lower affinity of chloro mercury complexes for the dithiocarbamate group.

Differences in adsorption curves at different pHs and salt concentrations prompted the investigation of mercury speciation and the relative abundances of the different species under varying experimental conditions. MINEQL+ was used to determine the mercury speciation. It was shown that $HgOH_2$ was dominant above pH = 4 while $HgCl_4^{2-}$ was dominant in the presence of chlorides. In addition, mercury adsorption experiments in the presence of calcium ions and calcium and magnesium ions were performed. Amount of mercury adsorbed decreased with increasing competition from calcium and magnesium ions. The particles were also used for adsorbing lead and manganese ions. The experiments showed a lower adsorption affinity (both on mass and mole basis) for lead compared to mercury and manganese compared to lead. The trend of adsorption affinity is in good agreement with the prediction from HSAB theory.

These results indicate the feasibility of using these particles to remove heavy metals but depending on the target contaminant, we can optimize the design of these particles by exploring other chemistries for the functional group on the magnetic nanoparticles. This offers interesting opportunities of particle design and synthesis that can target organic compounds, metals or a mix

of both. The existing structure of magnetic nanoparticles in terms of magnetite content (which affects the particle recovery) and the polymer content (which affects the attachment of the functional groups responsible for removing target species) can also be optimized for maximum target contaminant removal while ensuring particle recovery. In addition to the particle design optimization, determining the toxicity of these particles with and without the contaminant adsorbed to it is an essential next step[17] in implementation of this technology as it determines the efficiency of recovering magnetic nanoparticles and the time invested to recover a very high percent of the particles.

2.6 References

1. Rapsomanikis, S.; Craig, P. J., Speciation of mercury and methylmercury compounds in aqueous samples by chromatography-atomic absorption spectrometry after ethylation with sodium tetraethylborate. *Analytica Chimica Acta* 1991, *248* (2), 563-567.

2. Zhou, L.; Wang, Y.; Liu, Z.; Huang, Q., Characteristics of equilibrium, kinetics studies for adsorption of Hg(II), Cu(II), and Ni(II) ions by thiourea-modified magnetic chitosan microspheres. *Journal of Hazardous Materials* 2009, *161* (2-3), 995-1002.

3. Zahir, F.; Rizwi, S. J.; Haq, S. K.; Khan, R. H., Low dose mercury toxicity and human health. *Environmental Toxicology and Pharmacology* 2005, *20* (2), 351-360.

4. Clarkson, T. W., Human toxicology of Mercury. *The Journal of Trace Elements in Experimental Medicine* 1998, *11* (2-3), 303-317.

5. Caussy, D.; Gochfeld, M.; Gurzau, E.; Neagu, C.; Ruedel, H., Lessons from case studies of metals: investigating exposure, bioavailability, and risk. *Ecotoxicology and Environmental Safety* 2003, *56* (1), 45-51.

6. Say, R.; Birlik, E.; Erdemgil, Z.; Denizli, A.; Ersöz, A., Removal of mercury species with dithiocarbamate-anchored polymer/organosmectite composites. *Journal of Hazardous Materials* 2008, *150* (3), 560-564.

7. Denizli, A.; Kesenci, K.; Arica, Y.; Piskin, E., Dithiocarbamate-incorporated monosize polystyrene microspheres for selective removal of mercury ions. *Reactive and Functional Polymers* 2000, *44* (3), 235-243.

8. McClain, A.; Hsieh, Y.-L., Synthesis of polystyrene-supported dithiocarbamates and their complexation with metal ions. *Journal of Applied Polymer Science* 2004, *92* (1), 218-225.

9. Venkatesan, K.; Srinivasan, T.; Vasudeva Rao, P., Removal of complexed mercury by dithiocarbamate grafted on mesoporous silica. *Journal of Radioanalytical and Nuclear Chemistry* 2003, *256* (2), 213-218.

10. Manohar, D. M.; Anoop Krishnan, K.; Anirudhan, T. S., Removal of mercury(II) from aqueous solutions and chlor-alkali industry wastewater using 2-mercaptobenzimidazole-clay. *Water Research* 2002, *36* (6), 1609-1619.

11. Das, S. K.; Das, A. R.; Guha, A. K., A Study on the Adsorption Mechanism of Mercury on Aspergillus versicolor Biomass. *Environmental Science & Technology* 2007, *41* (24), 8281-8287.

12. Wang, J.; Deng, B.; Chen, H.; Wang, X.; Zheng, J., Removal of Aqueous Hg(II) by Polyaniline: Sorption Characteristics and Mechanisms. *Environmental Science & Technology* 2009, *43* (14), 5223-5228.

13. Allen, H. E., The significance of trace metal speciation for water, sediment and soil quality criteria and standards. *Science of The Total Environment* 1993, *134* (Supplement 1), 23-45.

14. Schecher, W. D.; McAvoy, D. C., MINEQL+: A software environment for chemical equilibrium modeling. *Computers, Environment and Urban Systems* 1992, *16* (1), 65-76.

15. Allison, J. D. B., D. S.; Novo-Gradac, K. J. , MINTEQA2/PRODEFA2, A Geochemical Assessment Model for Environmental Systems: Version 3.0 Users Manual. U.S. Environmental Protection Agency Athens, GA, 1991.

16. Pearson, R. G., Hard and soft acids and bases, HSAB, part II: Underlying theories. *Journal of Chemical Education* 1968, *45* (10), 643-null.

17. Goho, A. M. Testing the Toxicity of Nanomaterials *Technology review* [Online], 2008.

Chapter 3. Theoretical Predictions on Binding Constants of Functional Ligands and Mercury Species

3.1 Introduction

In Chapter 2, we saw the importance of solution conditions and the impact they had on mercury speciation. In addition, it is also important to understand what role the pH plays as it determines when the protons ions become freely accessible to bind with the functional ligand. Here, the functional ligand refers to the unit with both secondary amine (-NH-) and dithiocarbamate groups (-CSSH) i.e. it refers to -NHCSSH. Thus, protonation and deprotonation of the functional ligand is possible resulting in different forms of the functional group, the zwitterionic, protonated and deprotonated forms. These forms have a role to play in the resultant binding to various mercury species and are an important consideration when predicting equilibrium adsorption behavior and the feasibility of using these particles for treating systems with different environments.

The aim of this work was to use a thermodynamic model to predict the binding energies and hence, the binding constants for various forms of the functional ligand with the different mercury species. Models in Gaussian, an electronic structure program, were developed to gain an insight into the above interactions. These models thus help in mapping the various binding constants and placing the associated mercury species in a spectrum of least favorable to most favorable binding to our synthesized particles. This information is useful in understanding the impact of speciation and environmental conditions that might result in unfavorable binding to our synthesized particles. Binding constants to mercury species in conjunction with the mercury speciation model developed in Chapter 2, were used to predict adsorption curves for some of the experimental conditions. Comparison of energy predictions using two methods, HF and B3LYP, was also included. Given the limitations of the Gaussian models, the feasibility of this approach has also been discussed.

3.2 Computational Methodology

Electronic structure optimization and energy calculations were performed using the Gaussian 03 (g03)[1] program with the inbuilt method of Hartree Fock (HF). HF method was chosen as it had been reported to work for aqueous solutions of mercury sulphide.[2] There are two basis sets that can be applied for theoretical calculations of transitional metal complexes such as that of Hg, SDD (Stuttgart/Dresden) and LanL2DZ basis sets.[3,4,5] Since, both these basis set were reported to work well, SDD was chosen to be used as the basis set for all atoms, i.e., C, H, O, N, S and Hg in the g03 calculations. Radii of the atoms were taken from the United Atom Hartree Fock (UAHF) set. We first solved for an optimized gaseous electronic structure for each molecule. Thereafter, the free energy of the solvated optimized gas-phase geometries of molecules were evaluated using the conductor-like polarizable continuum model (CPCM)[6] in the g03 software package. In CPCM, the program assumes uniform dielectric properties of the solvent around the structure of the molecules and is an approximation to the solute-solvent interactions. The solvent corrected free energy for each of the molecules was then used to calculate the binding constant of mercury species to different forms of functional group by using the equations provided below.[7]

Equation 1 relates the free energy of reaction to the binding constant while Equation 2 gives the relation between free energies of the products and reactants to free energy of reaction.

$$\Delta G_{rxn} = -RT\ln K \quad (1)$$

where, ΔG_{rxn} is the free energy of the reaction, given as free energy of products minus the free energy of the reactants (includes both binding and electrostatic energy), R is the universal gas constant, T is the temperature and K is the binding or complexation constant

$$\Delta G_{rxn} = \Delta G_{products} - \Delta G_{reactants} \quad (2)$$

3.2.1 Different Forms of Dithiocarbamate Functional Group

Functionalized magnetic nanoparticles are complex particles to model, so we assumed the functional form of the ligand on the particle to be $CH_3NHCSSH$ as it was the simplest representation of an organic compound having both the secondary amine and the dithiocarbamate group. However similar to amino acids, we found that this ligand in its zwitterionic form had a

lower energy compared to its non-zwitterionic uncharged form and hence was assumed to be the most dominant form of the ligand. With a change in pH, it is possible to protonate and deprotonate the ligand. Possible forms of the ligand with pH changes are shown in Figure 3-1. Electronic surface potential plots of the molecules, where the colors are proportional to the electronic potential, red representing the most electronegative part and blue, most electropositive part are shown in this figure. All other colors fall in the spectrum between them.

The pKa value for the -CSSH group has been reported[8] to be around 3 while that of the amine or PEI (in case of the actual particles) has been reported[9] to be around 9. Since most of the experiments were conducted at pH=6.7, we believe that the majority of our particles in the experiments had the functional ligand in the zwitterionic form along with very small concentrations of protonated and deprotonated forms. Figure 3-2 illustrates the dominance of different ligand forms as a function of pH.

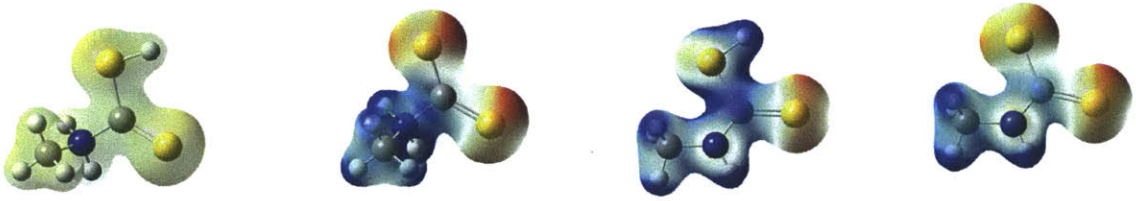

CH_3-NH_2(+)-CSSH (+1) (a)

CH_3-NH_2(+)-CSS(-) (0) (b)

CH_3-NH-CSSH (0) (c)

CH_3-NH-CSS- (-1) (d)

Figure 3-1: Various forms of functional ligand that can exist (a) protonated form (Lp) (b) zwitterionic form (Lz) (c) neutral form (d) deprotonated form (Lm) of the ligand

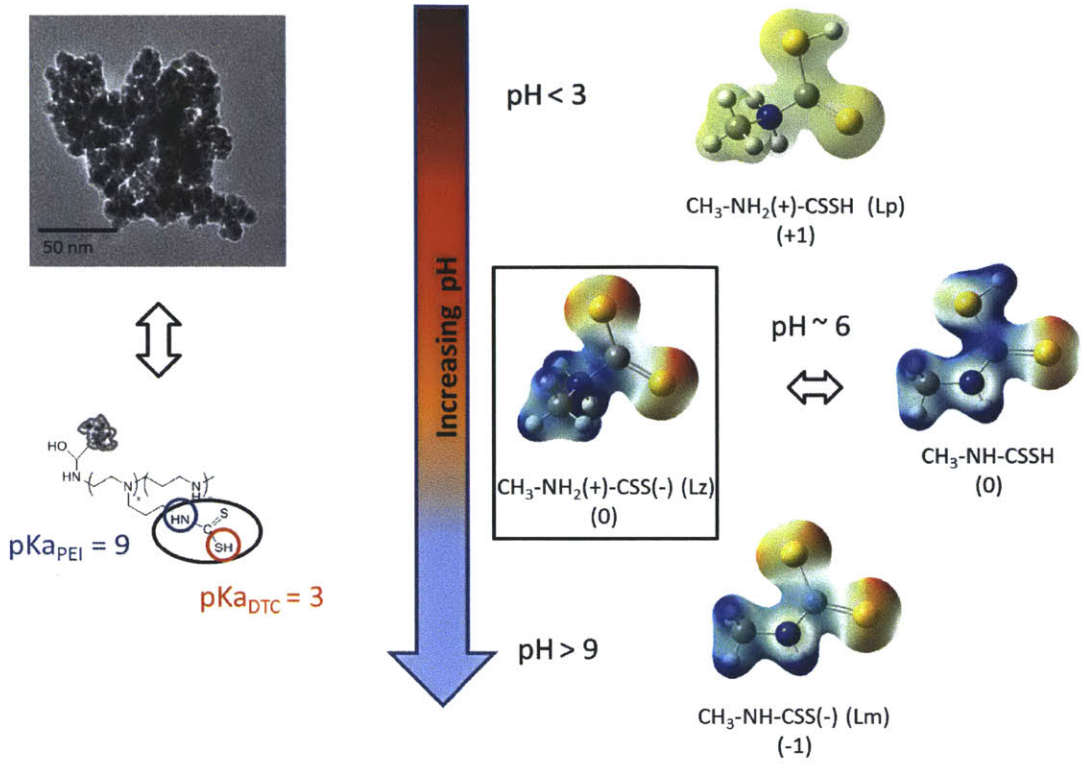

Figure 3-2: Dithiocarbamate functional group on the nanoparticle gets protonated or deprotonated with change in pH

Figure 3-3 illustrates the electronic surface potential images of different mercury species considered for binding to the nanoparticles. These were all the species that are predicted to exist in the system based on mercury speciation models developed in MINEQL+ (see chapter 2 for more details). Using these mercury species and ligand forms, binding constants were evaluated for each combination of species and ligand form using Gaussian.

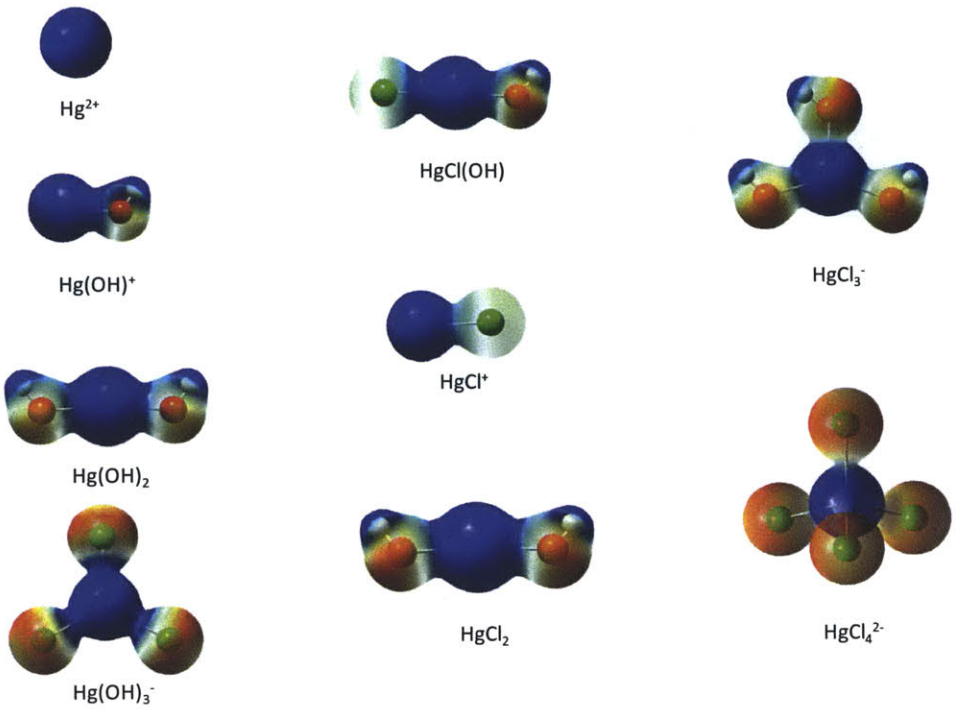

Figure 3-3: Various mercury species that were considered to bind with the different forms of ligand on the nanoparticles

3.3 Results

Based on the energy calculations performed by Gaussian, binding constants of ligand to hydroxo species of mercury show that both $HgOH^+$ and $HgOH_2$ have very high binding to the zwitterionic form of the ligand as compared to Hg^{2+} (Table 3-1 and Table 3-2). When the theoretical binding constants were used in conjunction with the relative proportion of species obtained from the speciation model to predict the overall equilibrium adsorption curve, we find an excellent fit to the experimental data (Figure 3-4).

Table 3-1: Binding constants of the zwitterionic form of the ligand to hydroxo mercury species

Species	**logK**
Hg2+	0.05
Hg(OH)+	4.64
Hg(OH)2	4.25

Table 3-2: Binding constants of all the ligand forms to hydroxo mercury species

	CH3-NH2(+)-CSSH (+1)	**CH3-NH2(+)-CSS(-) (0)**	**CH3-NH-CSSH (0)**	**CH3-NH-CSS- (-1)**
Hg^{2+}	-2.8	0.05	-0.08	17.8
$Hg(OH)^{+}$	-14.3	4.64	0.8	16.1
$Hg(OH)_2$	7.2	4.25	0.4	1.1

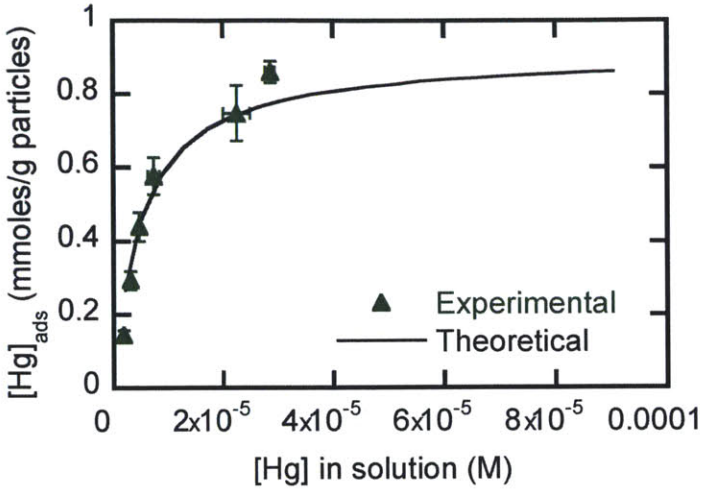

Figure 3-4: Predicted theoretical equilibrium adsorption curve using binding constants for zwitterionic form of ligand from Gaussian matches well with the experimental data

Binding values reported in Table 3-2 show that under acidic condition (which promotes the protonation of the ligand form), binding of mercury species is unfavorable while under basic conditions (when the ligand is deprotonated or CH_3NHCSS^- form) binding is favorable for all mercury species especially Hg^{2+}.

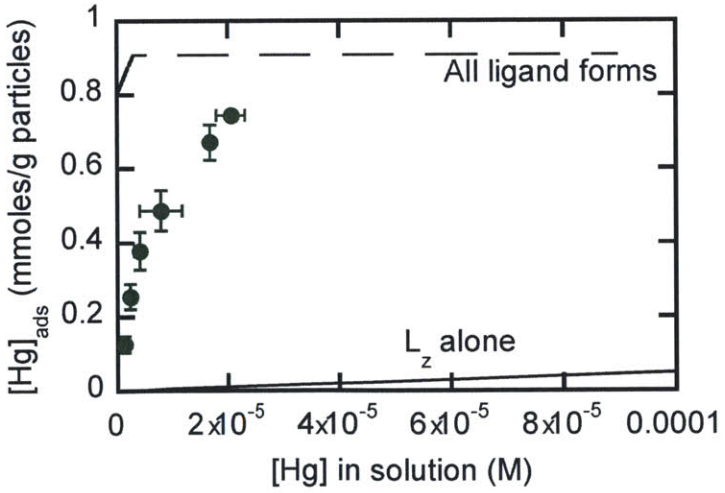

Figure 3-5: Predicted theoretical equilibrium adsorption curve using binding constants for all ligand forms from Gaussian is much higher than experimental data

If equilibrium of all ligand forms and hydroxo mercury species is taken into account to predict the overall equilibrium adsorption curve, the binding of Hg^{2+} to the deprotonated ligand (which has the highest binding constant or 'K' value) dictates the overall adsorption. This consideration results in the adsorption curve plateau-ing off even at lower equilibrium concentrations of Hg. There is an over prediction in [Hg] adsorption capacity as shown in Figure 3 5.

A similar computational procedure was followed for the chloro complexes of mercury. Values in Figure 3-3 show that the binding of the functional group to almost all species of Hg chloro complexes are unfavorable (except $HgCl^+$ which has some binding to the zwitterionic form of ligand). Based on these values the overall adsorption curve predicted (Figure 3-6) is inconsistent with the experimental data. In fact, the theoretical prediction is much lower than the experimental data. The reason for this difference is that all species are in equilibrium and as small concentrations of the deprotonated form of the ligand binds strongly with $HgCl^+$, other mercury chloro complexes dissociate to form $HgCl^+$ to maintain equilibrium between various mercury chloro complexes.

Table 3-4 lists the values of the binding constant of mercury chloro complexes to different ligand forms. Based on these values, it can be seen that protonated ligand form has little affinity for the chloro complexes of mercury. Deprotonated ligand forms have little binding affinities for mercury chloro complexes except for $HgCl^+$ with which it shows very high binding. As mentioned earlier, in a real system, it is this strong binding that will dictate the overall binding to the particles. Even if $HgCl^+$ is present in very small concentrations, almost all will react to deprotonated ligand form; this in turn will drive more $HgCl_2$ to form $HgCl^+$ to keep it in equilibrium. As more binding occurs, more of $HgCl_4^{2-}$ will be converted to $HgCl_3^-$ which will be converted to $HgCl_2$ and $HgCl^+$ to maintain equilibrium in the system (Equation 3). Using the values reported in Table 3-4 and assuming equilibrium of all species, we once again see the best-case scenario where complete and immediate binding to the ligands takes place (Figure 3-6).

$$HgCl_4^{2-} = HgCl_3^- + Cl^- = HgCl_2 + 2Cl^- = HgCl^+ + 3Cl^- \quad (3)$$

Table 3-3: Binding constants of the zwitterionic form of the ligand to the chloro mercury species

Species	logK
HgCl+	6.1
HgCl(OH)	-1.7
$HgCl_2$	-2.2
$HgCl_3^-$	-0.7
$HgCl_4^{2-}$	0.8

Table 3-4: Binding constants of all the ligand forms to chloro mercury species

	CH_3-NH_2(+)-CSSH (+1)	**CH_3-NH_2(+)-CSS(-) (0)**	**CH_3-NH-CSSH (0)**	**CH_3-NH-CSS- (-1)**
$HgCl^+$	-12.4	6.1	4.4	19.8
HgCl(OH)	-2.5	-1.7	-2.2	5.2
$HgCl_2$	-4.0	-2.2	-2.1	10.1
HgCl3	-2.0	-0.7	-4.8	3.7
HgCl4	-2.4	0.8	-	-

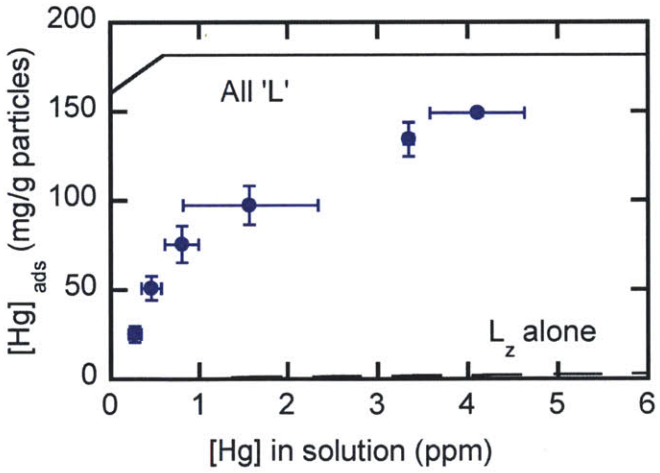

Figure 3-6: Predicted theoretical equilibrium adsorption curve in presence of chlorides using binding constants for the zwitterionic form and all ligand forms obtained from Gaussian does not match with the experimental data

These binding predictions show that the presence of Cl^- ions inhibits the binding of mercury with the functional ligand by forming chloro complexes of mercury that have lower affinity for the ligand. It can also be concluded that these particles would fail to work in acidic conditions as little to no binding is predicted for the dominant forms of both the ligand (i.e. $CH_3NH_2^+CSSH$) and mercury species (Hg^{2+}).

In addition to calculations reported above, Gaussian calculations using density functional theory was employed to check on the stability of predictions to the choice of method. B3LYP is a popular method known for its accuracy in predicting bond energies.[10] Comparison of ΔG values from both HF and B3LYP methods for neutral Hg species mentioned above (i.e. $HgOH_2$, $HgCl_2$ and HgClOH) are shown in the following table (Table 3-5). Neutral species were chosen as energy predictions for both ions have other errors associated with it.[11] ΔG predictions from both these methods are within 6-7 kcals/mole. This difference in energy values can be partially attributed to the electron correlation effect that is included in B3LYP method but not in HF method. Structure and bond lengths of the complexes formed in this case are also shown below (Figure 3-7).

Table 3-5: Comparison of ΔG values and average 'S-Hg' bond lengths from B3LYP and HF methods

Species binding to Lz form of the MNP	**ΔG predictions using HF method**	**Avg. bond length (Hg-S) by HF method (Angstroms)**	**ΔG predictions using DFT-B3LYP method**	**Avg. bond length (Hg-S) by DFT-B3LYP method (Angstroms)**
$HgOH_2$	-5.828182734	4.19	-1.82404	3.92
$HgCl_2$	3.067078183	3.25	-3.48851	3.16
HgClOH	2.357992448	3.46	-	-

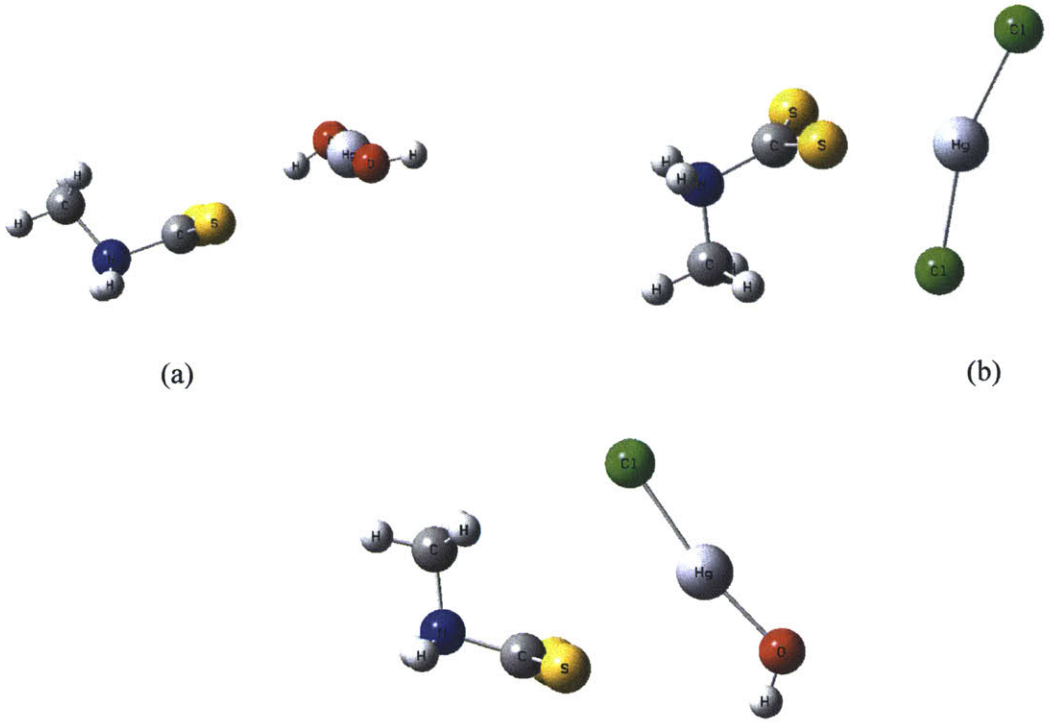

Figure 3-7: Binding structures of (a) $HgOH_2$, (b) $HgCl_2$ and (c) HgClOH with Lz form of the functional ligand on MNP by B3LYP/SDD, B3LYP/SDD and HF/SDD methods respectively

Gaussian provides an approximate solution to structure energies because of the assumptions inherent in the solvent continuum model. Solvation energy predictions for binding of metal species and organic compounds using CPCM calculations are complicated models and have often been inconsistent with experimental results.[12] In addition, as we see from the results, different methods predict differently for the solvation models. Thus the choice of method to be used is an important one and needs to be optimized for the system at hand. Therefore the values given in this chapter should not be taken in an absolute sense but relative to each other.

We would not expect to predict exact K's from this level of theory (as suggested by the scale of uncertainties in calculations by Hartree-Fock and DFT). It is especially more unreliable for cation + anion energetics as compared to neutral + neutral or ion + neutral energetics. However, these results do provide benchmark indications as to how binding takes place and is useful in discriminating species binding favorably from those that do not.

3.4 Summary

This chapter employs a theoretical approach to understand binding between a simplified functional ligand on our particles to mercury species. Based on the pKa values of both the imine and dithiocarbamate groups that are present on the particles, and the energy values predicted by Gaussian, it was seen that the zwitterionic form of the ligand is the most dominant form at pH = 6.7 and that hydroxo mercury species bind favorably with this ligand form. Additionally, a good agreement of adsorption curve predicted using these binding constants with experimental data was obtained. However, this was not so when one also included the chloro mercury species in the system. The zwitterionic form exhibits little to no binding to the chloro mercury species and given they are the dominant species, very little adsorption was seen. Equilibrium of various ligand forms (protonated, zwitterioninc, uncharged and negatively charged froms) and mercury species possibly explain the experimentally observed adsorption. When all these ligand forms were taken into account, immediate adsorption of mercury species was indeed predicted.

Gaussian predictions are good first step values and are useful in indicating species that bind favorably or unfavorably. However, there are some limitations in the solvation models and the energy predictions are at best good metrics for relative comparison and determining favorable binding. It is recommended to focus on finding and using the most optimal method for solution phase chemistry of mercury and organic compounds for higher accuracy in binding constant predictions.

3.5 References

1. Frisch, M. J. et. al. *Gaussian 03; Gaussian, Inc.* , Wallingford, CT, 2003.

2. Tossell, J. A., Calculation of the Structures, Stabilities, and Properties of Mercury Sulfide Species in Aqueous Solution. *The Journal of Physical Chemistry A* 2001, *105* (5), 935-941.

3. Dunning Jr, T. H.; Hay, P. J.; Schaefer Iii, H. F., *Modern Theoretical Chemistry* 1976, 1.

4. Asaduzzaman, A. M.; Schreckenbach, G., Degradation Mechanism of Methyl Mercury Selenoamino Acid Complexes: A Computational Study. *Inorganic Chemistry* 2011, *50* (6), 2366-2372.

5. Yang, G.; Jin, C.; Hong, J.; Guo, Z.; Zhu, L., Ab initio and density functional theory studies on vibrational spectra of palladium (II) and platinum (II) complexes of methionine and histidine: effect of theoretical methods and basis sets. *Spectrochimica Acta Part A: Molecular and Biomolecular Spectroscopy* 2004, *60* (13), 3187-3195.

6. Cossi, M.; Rega, N.; Scalmani, G.; Barone, V., Energies, structures, and electronic properties of molecules in solution with the C-PCM solvation model. *Journal of Computational Chemistry* 2003, *24* (6), 669-681.

7. Modell, M. T., J.W., *Thermodynamics and its applications*. 1996.

8. Humeres, E.; Debacher, N. A.; Sierra, M. M. d. S., Mechanisms of Acid Decomposition of Dithiocarbamates. 2. Efficiency of the Intramolecular General Acid Catalysis. *The Journal of Organic Chemistry* 1999, *64* (6), 1807-1813.

9. Ford, J.; Yang, S., Directed Synthesis of Silica Nanoparticles on Micropatterned Hydrogel Templates Tethered with Poly(ethyleneimine). *Chemistry of Materials* 2007, *19* (23), 5570-5575.

10. Padak, B.; Wilcox, J., Understanding mercury binding on activated carbon. *Carbon* 2009, *47* (12), 2855-2864.

11. Camaioni, D. M.; Dupuis, M.; Bentley, J., Theoretical Characterization of Oxoanion, XOmn-, Solvation. *The Journal of Physical Chemistry A* 2003, *107* (30), 5778-5788.

12. Takano, Y.; Houk, K. N., Benchmarking the Conductor-like Polarizable Continuum Model (CPCM) for Aqueous Solvation Free Energies of Neutral and Ionic Organic Molecules. *Journal of Chemical Theory and Computation* 2004, *1* (1), 70-77.

Chapter 4. Transport Properties of Magnetic Nanoparticles under Magnetic Field Gradients

4.1 Introduction

In this chapter we have considered the transport properties of magnetic fluids when used in both porous and non porous media. Special attention to properties such as velocity and dispersion of magnetic nanoparticles in the presence of external magnetic fields is given. A magnetic fluid is a colloidally stable suspension of surface modified magnetic nanoparticles (MNPs) in organic solvents or water. When it is injected in porous media, it spreads due to the tortuous path of the porous medium, variation in velocities and molecular diffusion. External forces, chemical interactions between solute and medium, medium and fluid properties affect this diffusion process. This phenomenon was first observed by Slichter in 1905.[1] For a particle diffusing in a porous medium, there exist three dispersion components: Molecular or Brownian diffusion, Mechanical dispersion and Hydrodynamic Chromatographic effect. Molecular or Brownian diffusion is caused by thermal fluctuations and is especially relevant for small particles that are on the order of 100 nm. Mechanical diffusion is caused by velocity variations between pores which result in greater movement of particles in the center of channels and less at the walls. The hydrodynamic chromatographic effect is a result of velocity variations of different sized particles. This effect can be neglected if the sizes of particles are a few orders of magnitudes smaller than channel size.

Magnetic dispersion occurs as a result of both the existing velocity field and magnetic field gradient field. Figure 4-1 shows the magnetic gradient induced magnetic velocity and the pressure gradient induced velocity fields in a porous medium. It is seen that pull due to an external magnetic field gradient (represented by red arrows) do not necessarily align with existing velocity field (represented by blue arrows) in porous media resulting in altered dispersion. In the presence of external magnetic fields, an additional effect of field dependent dispersion will be observed too. This work addresses the importance of magnetic dispersion in evaluating overall dispersion.

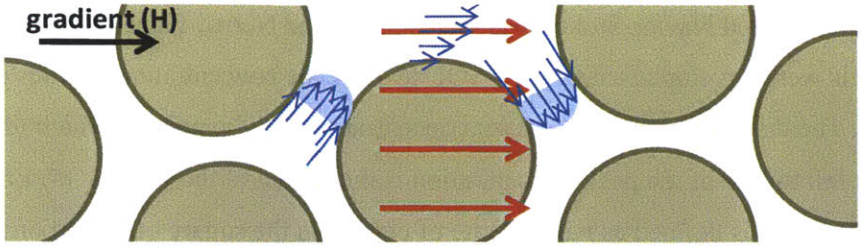

Figure 4-1: Velocity and magnetic field gradient induced velocity field lines in a porous medium

Modeling and simulation of transport of nanoparticles in porous media is difficult because of the complex interactions between particles and sediment structure and heterogeneity in the sediment structure. Modeling of mechanical dispersion in porous media has been addressed in two ways; treating the microstructures as a system of multiple capillary tubes, which has the distinct disadvantage of neglecting lateral diffusion amongst these tubes or using stochastic models[2,3,4] and volume averaging models.[5,6] An alternative to these two methods is to apply generalized Taylor Aris dispersion theory to two and three dimensional spatially periodic deterministic models of porous media.[7,8] The present work thus uses a simple approach to relate 'spreading' or diffusion concepts to dispersion both in presence and the absence of external magnetic field gradients and in a variety of unit porous cells.

4.2 Geometry and Modeling Approach

We consider two different geometries, 2D thin channel geometries with varying porosity and a 2D cross section of a porous medium (Figure 4-1 and Figure 4-2). The first system was used to obtain information on longitudinal dispersion alone while the second was used to study both longitudinal and lateral dispersion.

For any given geometry, a pulse input (line input for thin channel geometries and point input for cross sectional geometry) of soluble magnetic fluid is injected into the medium and observed for its transport through the medium over time. Figure 4-3 and Figure 4-4 illustrate the movement of magnetic fluid in the two model geometries used. In the first figure, a line source in a two dimensional thin porous channel spreads as it moves along the channel while in Figure 4-4 we observe a similar spreading for a point source in a two dimensional porous medium.

To solve coupled Navier-Stokes, Magnetostatcics and Nernst-Planck equations, finite element models were developed using COMSOL to calculate concentration profiles of the injected fluid. The distance between the peak concentration and the point at which the concentration fell to $1/e$ of the peak concentration is the spread of the fluid or 'σ'. Effective dispersion coefficient is defined as half the rate of change in the square of spread or, Dispersion $= \frac{1}{2}\frac{d\sigma^2}{dt}$. This work considers molecular diffusion, hydrodynamic dispersion and the chromatographic effect on dispersion as one mechanical dispersion effect and focuses on determining the dispersion in presence of magnetic field gradients.

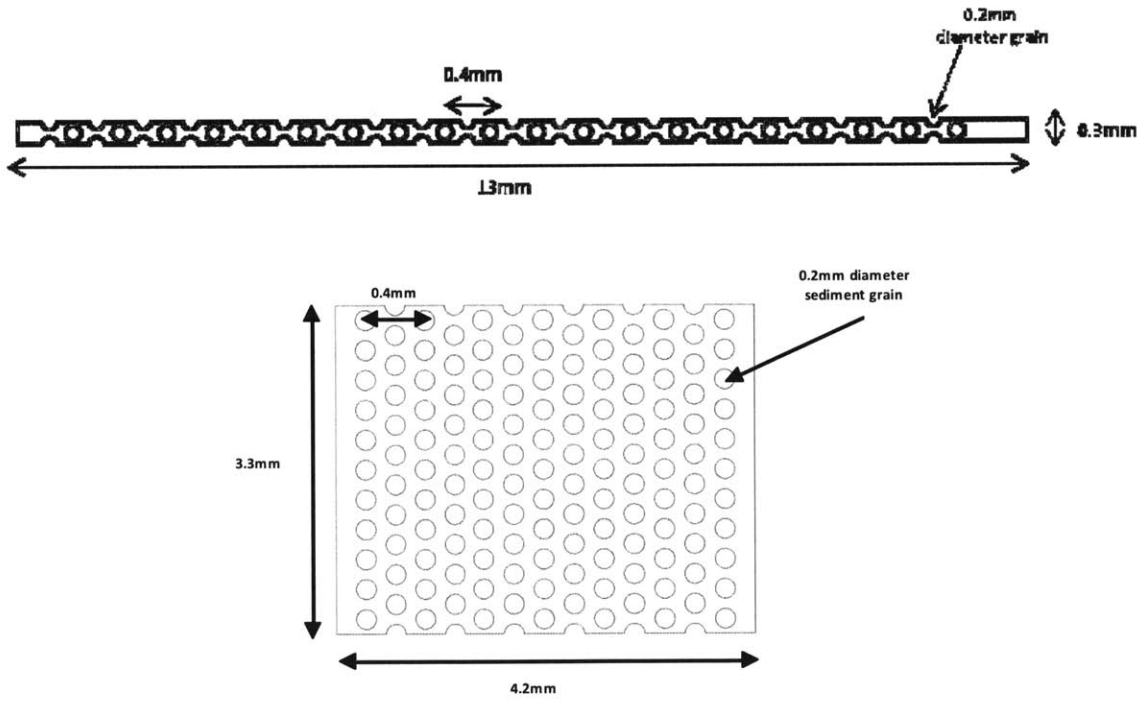

Figure 4-2: Example of the thin porous channel geometry and the porous cross sectional geometry

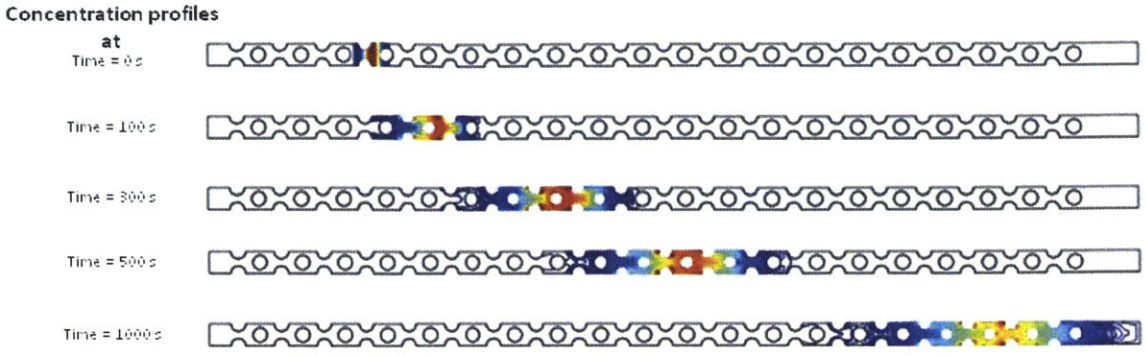

Figure 4-3: Example of concentration profiles in thin channel geometry at a Peclet number of 42

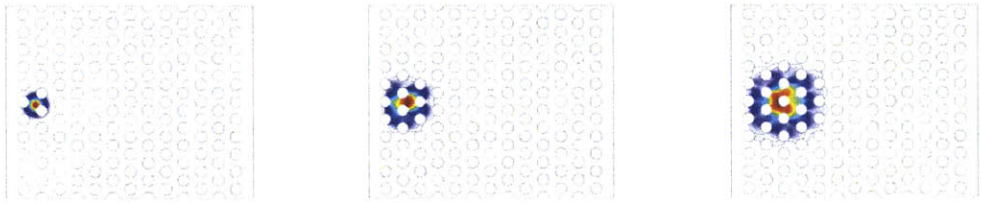

t = 0 t = 200s t = 500s

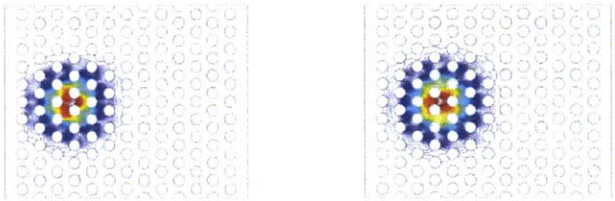

t = 800s t = 1000s

Figure 4-4: Example of concentration profiles in cross sectional porous geometry at a Peclet number of 3.4

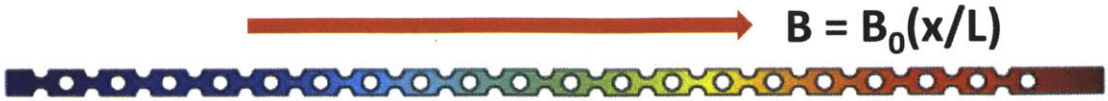

Figure 4-5: Magnetic field varies linearly in thin channel geometry

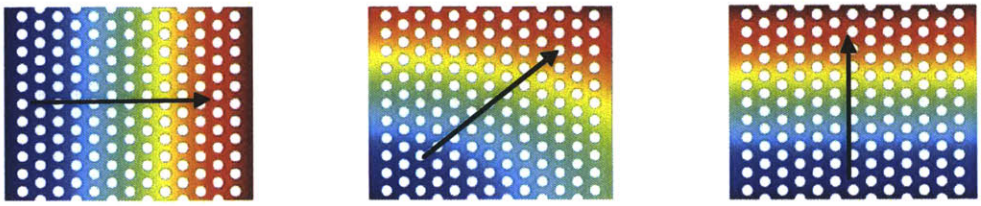

θ = 0° θ = 60° θ = 90°

Figure 4-6: Magnetic field varies linearly at different orientations in the cross sectional porous geometry (arrows represent the direction of magnetic field gradient)

For determining dispersion in presence of magnetic field gradient, linear field gradients are applied along the thin channel geometry as shown in Figure 4-5 or at various orientations as shown in Figure 4-6 and the above mentioned equations are solved once again. Figure 4-5 shows the linear magnetic field gradient applied in the channel with maximum field strength at the end of the channel while Figure 4-6 shows the magnetic field gradient in the porous medium at 0^o, 60^o and 90^o to the flow field. Color red refers to higher field strengths while blue refers to lower magnetic field strengths. The presence of the magnetic field gradients results in an additional magnetic flux term in the mass transport equation that alters the net dispersion coefficient.

The dispersion coefficient calculated in this case is a sum of both mechanical and magnetic dispersion coefficients. Magnetic dispersion coefficient is obtained by subtracting the dispersion coefficient evaluated in the absence of an external magnetic field from the value obtained in the presence of an external magnetic field.

Unless otherwise specified, parameter values kept constant in all simulations were ρ = density of the fluid = 1000 Kg/m^3, M_v = magnetization of the particle per unit volume =

2.83×10^5 A/m, a = particle size = 10nm, n_0 = number of particles introduced in the domain = 1.77×10^{12}

4.3 Governing Equations and Boundary Conditions

Navier-Stokes equation (Equation 1) and continuity equation (Equation 2) were used to determine the fluid flow through the channel.

$$\rho(u.\nabla)u = \nabla.[\rho + \eta(\nabla u + \nabla u^T)] \quad (1)$$

$$\nabla.u = 0 \quad (2)$$

Here, u is the velocity vector and ρ is the density of the medium. Boundary conditions used are as follows, inlet boundary: $U_0 = v_0$, walls or grains and channels: $u_T = 0$ (no slip) and outlet boundary: p_0 (normal stress) = 0

A convective diffusive equation (Equation 3) was used to determine the concentration profiles of magnetic fluid in the channel. This equation was modified with an additional term (given in red) that takes into account the presence of external magnetic field. The additional magnetic flux term (highlighted in red) is present only when external magnetic field gradients exist.

$$\frac{\partial c}{\partial t} + u.\nabla c = \nabla.(D_{mol}\nabla c) - \nabla(u_{mag}c) \quad (3)$$

$$u_{mag} = \frac{\mu_o M_v V_p \nabla H}{6\pi\eta a} \quad (4)$$

Here, c is the concentration of the magnetic fluid, t is the time, D_{mol} stands for molecular diffusion, μ_o is the free space permeability, M_v is magnetization per unit volume of the particles, V_p is the volume of each particle, H is the magnetic field, η is the viscosity of the fluid and a is the particle radius. Following boundary conditions were used: inlet boundary: $u\frac{\partial c}{\partial x}|_{in} = u_0\frac{\partial c_0}{\partial x}$, walls of the grains $u\frac{\partial c}{\partial x} + D\frac{\partial^2 c}{\partial x^2}|_{Total\ flux} = 0$, and outlet boundary: $u\frac{\partial c}{\partial x}|_{out} = u\frac{\partial c_0}{\partial x}$ (continuity of flux).

Last set of equation to be solved for was that of the magnetic field in the channel. Following equation from the magnetostatics module of COMSOL (Equation 5) was used to determine the magnetic field.

$$\nabla\times(\mu_0^{-1}\nabla\times A - M) = 0; A = A_z e_z \quad (5)$$

Here, A is the magnetic potential, M is the magnetization. For boundary conditions, $H_x = H_0\left(\frac{x}{L}\right)$ and $H_y = H_0\left(\frac{y}{L}\right)$ on the entire geometry and its boundaries, were used.

4.4 Comparison with Theoretical Relations and Porous Medium Literature

In this section, the theoretical Taylor Aris relation[9] on dispersion coefficient, a modified Taylor Aris relation to account for the presence of magnetic field (see Appendix 1 for details on the derivation) and two porous medium literature relations were used to evaluate dispersion coefficients. These theoretically determined dispersion coefficients were then compared with the results from our model. Figure 4-7 shows the comparison of dispersion coefficient in a non-porous medium to the predictions made by Taylor Aris equation. A theoretical derivation of magnetic field modified Taylor Aris equation was performed (details can be found in Appendix 1) and the dispersion coefficients evaluated from the relation obtained were compared to our simulation results (Figure 4-8). This was followed by comparison of dispersion coefficients of porous medium in absence of magnetic field gradients with porous medium literature results (Figure 4-9 and Figure 4-10). We observed good agreement in value of the dispersion coefficients obtained from our model and various theoretical sources. After confirming the accuracy of predictions, the method was extended to obtain magnetic dispersion coefficients in a porous medium. These predictions are discussed in the following section.

4.4.1 Test for Non-porous Medium Limits

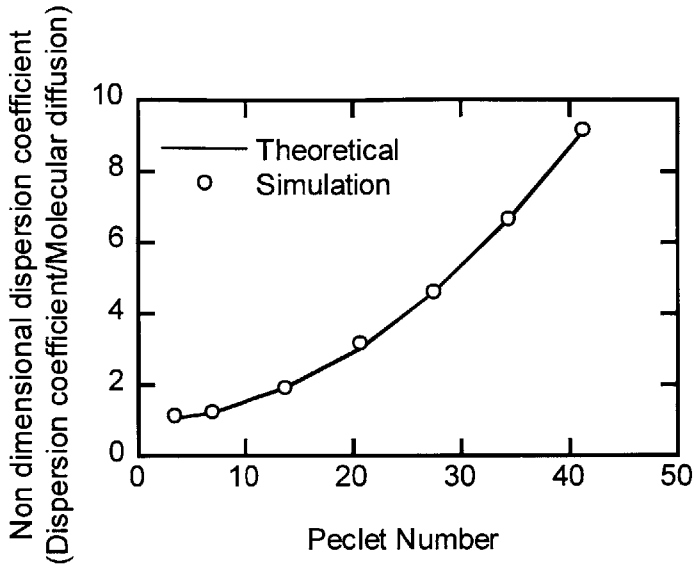

Figure 4-7: Comparison of dispersion coefficient in a non-porous medium with classic Taylor Aris dispersion coefficient

Results of simulations were performed on a non-porous geometry of 13mmx0.3mm size and compared to the results from the classic non-porous medium Taylor-Aris relation for dispersion (Figure 4-7). The Taylor- Aris model predicts that the effective dispersion coefficient for a thin channel to follow $\frac{Disp}{D_{mol}} = 1 + \frac{h^2u^2}{210D_{mol}^2}$, where h is the channel height, u is the channel averaged velocity, D_{mol} is the molecular diffusion value that can be determined by the Stokes-Einstein relation mentioned above. The Peclet number used in this figure and following figures are thus dependent on the cross sectional averaged velocity through the channel. As seen from the figure, the model and the methodology developed is robust for predictions in a non-porous medium as there is a good match between theoretical and model predictions.

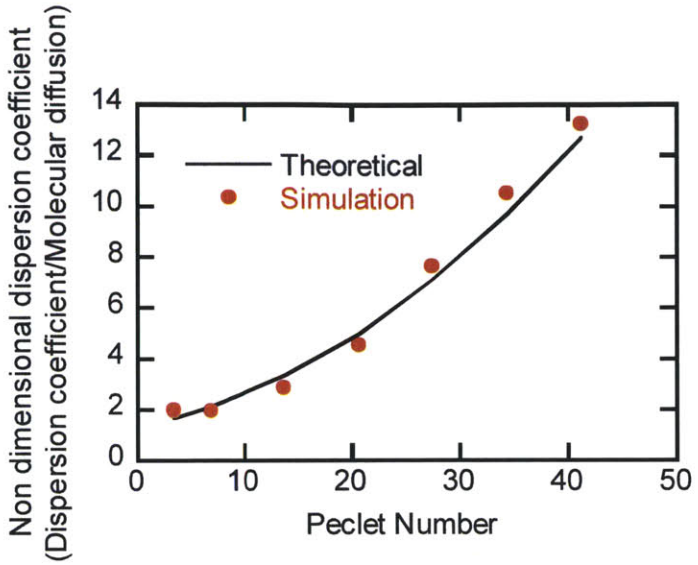

Figure 4-8: Prediction of combined hydrodynamic and magnetic dispersion coefficient in a non-porous medium and comparison with the coefficients obtained from the analytical Taylor Aris expression

To check the consistency of model predictions under magnetic field gradients, an additional test was designed in a non-porous medium. Dispersion coefficient values for the non-porous medium model with a magnetic field gradient (parallel to the flow field) were evaluated and compared with theoretically derived Taylor-Aris dispersion coefficients with an external magnetic flux term (for full derivation refer to Appendix 1). Effective dispersion coefficient in presence of an external magnetic field was derived as

$$\frac{\mathrm{Disp}}{\mathrm{D_{mol}}} = 1 + \frac{\mathrm{h^2}\left(\mathrm{u}+\frac{\mu_0 \mathrm{M_v V_p \nabla H}}{6\pi\eta \mathrm{a}}\right)^2}{210\mathrm{D_{mol}^2}} \tag{6}$$

Here h is the channel height, u is the channel averaged velocity, D_{mol} is the molecular diffusion, μ_o is the free space permeability, M_v is the magnetization per unit volume of the particle, V_p is the volume of each particle, H is the magnetic field, η is the fluid viscosity and a is the particle radius. The simulation results have an average sum of squares of error of 1.12%.

4.4.2 Test for Porous Medium Limits

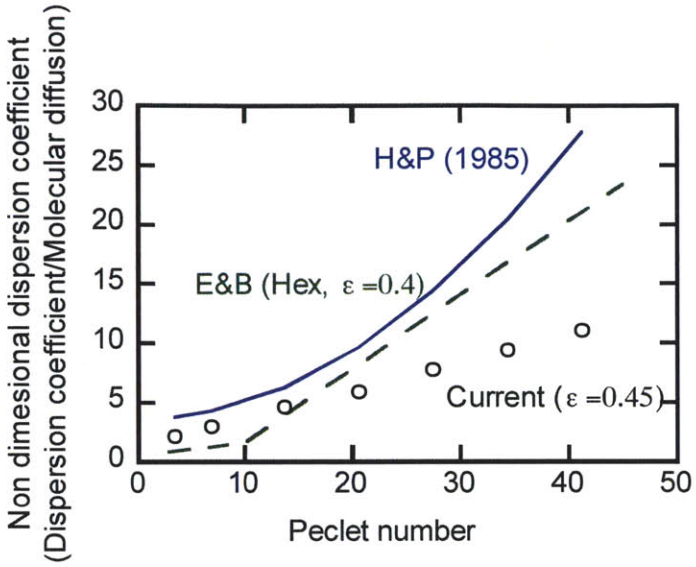

Figure 4-9: Comparison of dispersion in a porous medium with analytical results of Hoagland and Prud'homme and numerical results of Edwards and Brenner

Porous medium predictions are compared with two literature sources, Edwards et. al[7] and Prud'homme and Hoagland[10]. In 1985 Hoagland and Prud'homme's paper[10], work on solute dispersion in a porous medium characterized by a constricted capillary tube possessing a periodically varying circular cross-section (sinusoidal tube) was analyzed and compared with our model. They derived a theoretical expression using methods of moments to predict dispersion as a function of Peclet number, distance between the two paths and tortuosity (Equation 7).

$$\frac{\zeta}{D_{mol}} = \frac{1}{(1+c^2)^3}\left[1 + \frac{15}{2}\varepsilon + \frac{45}{8}\varepsilon^4 + \frac{5}{16}\varepsilon^6\right] + \left(\frac{\bar{U}r_0}{D}\right)^2 \left[\frac{1}{48(1+\varepsilon^2)^3}\right][1 + 3\varepsilon^2 + \frac{3}{8}\varepsilon^4] \qquad (7)$$

Edwards and Brenner[11] numerically determined dispersion coefficients by applying a finite element method to their square, staggered and hexagonal array geometries. As shown in Figure 4-9, the values obtained from our model predictions are similar to the predictions by the models in the two literature sources, especially at low Peclet numbers. The difference in values is attributed to differences in geometries and porosities of our model and those in the two literature models. Our model has a stretched hexagonal packing and a porosity of 0.4 while the Hoagland

and Prud' homme model has a long wavelength sinusoidal tube with an approximate porosity of 0.45 and Edward Brenner used three different geometries (square, hexagonal and staggered arrays) with porosities of 0.4, 0.599 and 0.804 respectively.

Table 4-1: Comparison of dispersion in square array geometries for porosities $\epsilon = 0.599$ and 0.804 with Edwards and Brenner's numerical results

Porosity	**Peclet number**	**Theoretical dispersion coefficient**	**Simulation dispersion coefficient**
$\epsilon = 0.599$	1	0.7095	0.7166
	10	0.8605	0.7590
	100	7.1223	6.2673
	1000	359.37	336.09
$\epsilon = 0.804$	1	0.8357	0.8147
	10	0.9464	0.9396
	100	6.0692	6.1074
	1000	301.76	303.74

To further test the versatility of the methodology employed in dispersion prediction, two different geometries were simulated, square and staggered array configuration as described in Edwards et. al. Table 4-1 shows that our predictions match well with the reported values in the paper. Dispersion decreases with increase in porosity owing to the availability of more space for the solute molecules to move about and hence causing less mixing or dispersion. Additionally, increasing porosity results in lower micro scale velocities that is responsible for the lowering the value of dispersion coefficient.

4.5 Results and Discussions

After confirming the accuracy in the predictions of our model in the absence of magnetic field gradients, we next evaluated the magnetic dispersion coefficients in porous medium. This was done in two steps. First step was to add grains or make the system porous and the second was to add the magnetic field gradient.

4.5.1 Effect of Grains on Dispersion

It can be seen in Figure 4-10 that the presence of grains or making a channel porous results in increase in dispersion of magnetic fluid. These grains reduce the effective volume for the passage of fluid to travel through, thereby increasing the effective micro scale velocity of fluid flowing through the porous medium. Increased velocity and mixing caused by the obstruction offered by the walls of the grains results in enhanced dispersion. It is also observed that the dispersion in a porous medium has a less curved dependence on Peclet number as compared to squared dependence on Peclet number in a non porous medium. This can be explained as follows. Dispersion coefficients depend directly on the velocity profile in the channel. Therefore, the dispersion coefficient in a non porous medium has a curved dependence on velocity while the less curved dependence of dispersion coefficient in a porous medium can be explained by the existence of an average plug flow type velocity profile resulting from multiple channels in a porous medium, each channel having laminar velocity profiles. These results corroborates well with the findings of Edwards et. al[7] and Edisath et. al[5].

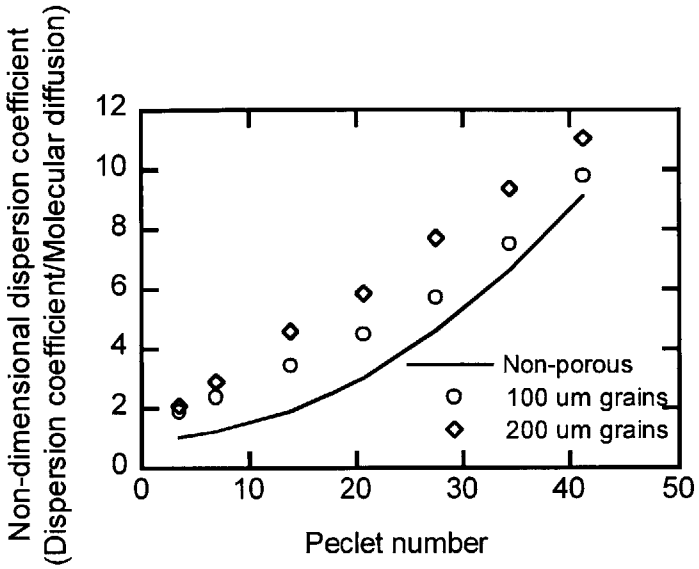

Figure 4-10: Presence of porous medium grains enhances dispersion

4.5.2 Effect of Magnetic Field Gradient on Dispersion

In Figure 4-11, it is seen that presence of magnetic field gradient (parallel to the flow field) in a porous medium of 200-micron sediment grain results in enhanced dispersion. Dispersion's less curved or linear trend in Peclet number is preserved. The enhancement in dispersion can be explained by the additional increase in micro scale velocity due to the additional magnetic flux experienced by the MNPs. This flux results in a magnetophoretic velocity which gets added to the existing velocity field.

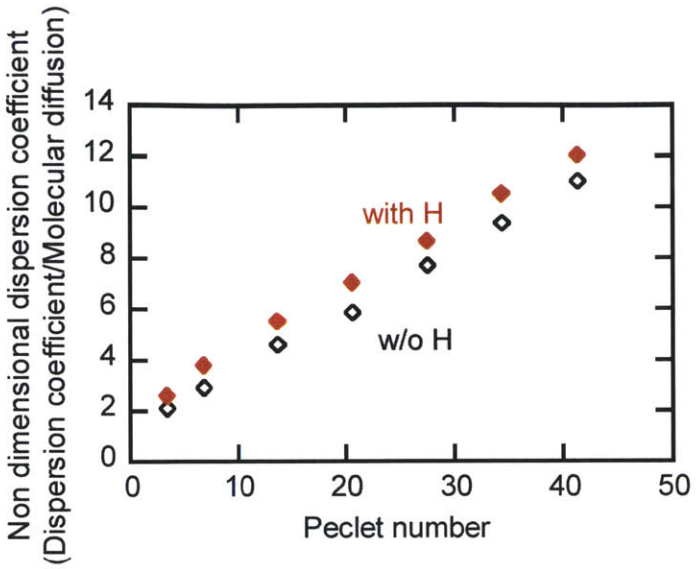

Figure 4-11: Dispersion is enhanced in presence of magnetic field gradient

4.5.3 Predictions of Dispersion for Porous Medium Geometries

In Table 4-2, we show simulation results with and without a magnetic field gradient in a square array porous medium for the two different porosities of 0.599 and 0.804. These porosity values were the same as used by Edwards and Brenner. Enhancement in dispersion due to the magnetic field gradient (Table 4-2) increases with an increase in porosity. For highly porous media, effect of the magnetic field gradient is larger than for low porosity media, resulting in more mixing and higher dispersion value.

Table 4-2: Predictions of combined hydrodynamic and magnetic dispersion in square array geometries for porosities $\epsilon = 0.599$ and /0.804

Porosity	Peclet number	Theoretical dispersion coefficient	Simulation dispersion coefficient	Model predictions in presence of magnetic field gradients
$\epsilon = 0.599$	1	0.7095	0.7166	1.6721
	10	0.8605	0.7590	1.9308
	100	7.1223	6.2673	8.2419
	1000	359.37	336.09	379.03
$\epsilon = 0.804$	1	0.8357	0.8147	3.2150
	10	0.9464	0.9396	3.2997
	100	6.0692	6.1074	7.0304
	1000	301.76	303.74	340.79

4.5.4 Variation of Longitudinal and Lateral Dispersion Coefficient with Orientation

Figure 4-12 shows the effect of magnetic field orientation and velocity on 2D porous medium dispersion coefficients. Longitudinal dispersion coefficient falls linearly while lateral dispersion coefficient rises linearly with increase in the angle between magnetic field and velocity field. Both these dispersion coefficients depend on the morphology of the porous medium and the angle of the magnetic field applied. However, it's difficult to extract a definitive relation in the angle between the two fields as the magnetic dispersion coefficient have different longitudinal and lateral contributions at different angles of magnetic field applied as shown in Figure 4-13.

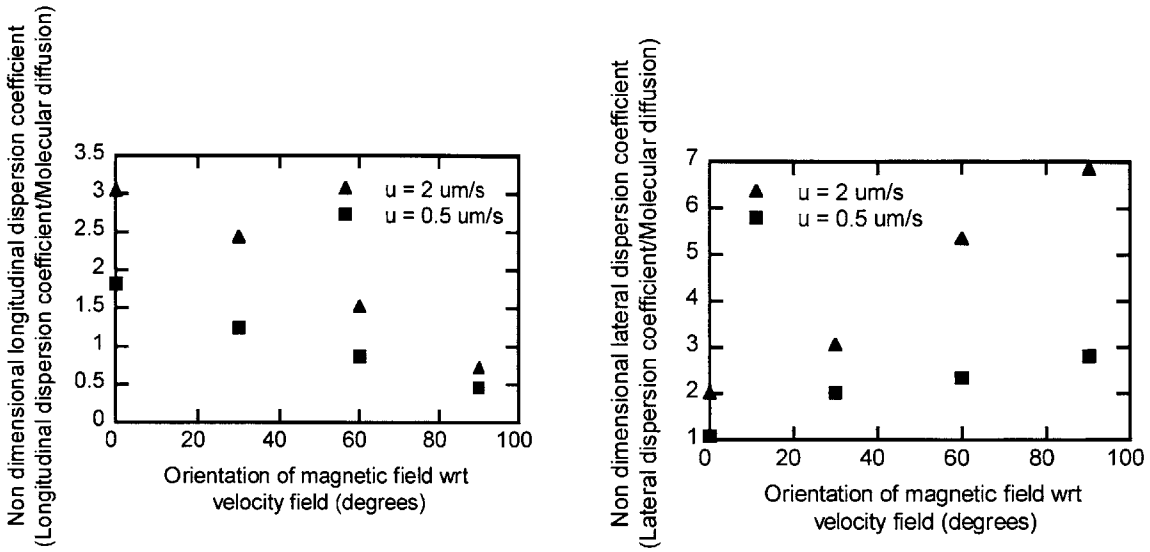

Figure 4-12: Longitudinal dispersion falls (a) and lateral dispersion rises linearly (b) with increasing angle of the magnetic field applied

A schematic illustrating the various contributions to dispersion coefficients is shown in Figure 4-13. In a 2D porous medium, a single velocity field alone will generate two dispersion coefficients, longitudinal and lateral dispersion coefficients. It has been reported that these dispersion coefficients have a somewhat linear dependence on the velocity vector u.[6] Adding additional velocity in the same direction as the original velocity field will result in changes to the same lateral and longitudinal dispersion coefficients. However, adding a new velocity field at an angle to the original velocity field will result in different longitudinal and lateral contributions. These contributions will be dependent on the angle of the field and the morphology of the porous medium.

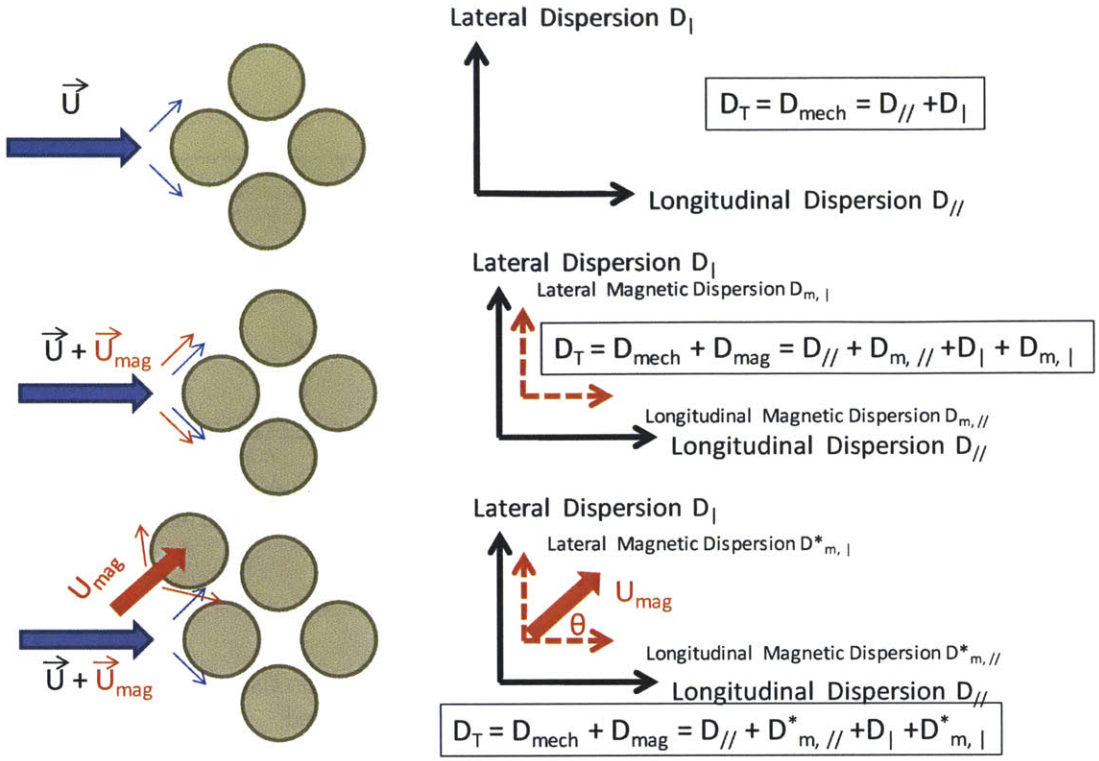

Figure 4-13: Schematic showing the various contributions to dispersion coefficients in a 2D porous medium

4.6 Proposed Phenomenological Model

Magnetic field gradients results in an enhancement of dispersion as illustrated by our simulation results in the previous section. In Taylor dispersion, shear flow increases the dispersion of the species by spreading out the concentration in the direction of the flow. Hydrodynamic dispersion arises from mixing caused by non uniform velocity fields, morphology of the medium, nature of fluid flow (laminar/turbulent) and physical and chemical interactions with the solid surfaces of the medium.[12]

A similar phenomenon of magnetic dispersion can be expected from non uniform magnetic field gradients. MF is expected to move along a gradient modified velocity field (as defined by streamlines) resulting in enhanced mixing of MF and the existing fluid.

Several literature sources have cited a linear dependence of hydrodynamic dispersion coefficient on velocity but most sources[12-13] define it as $D_H = \alpha_h u^n$ where α_h is the hydrodynamic dispersivity and n is in the range of 1 to 1.5. It is observed that both hydrodynamic and magnetic dispersion are caused by similar phenomena, i.e. pressure gradient induced velocity and magnetic field gradient induced magnetophoretic velocity respectively. Based on this observation, we propose a hypothesis that magnetic dispersion will be of the form $D_M = \alpha_M u_{mag}^m$ where α_M is the magnetic dispersivitty and u_{mag} is the magnetophoretic velocity. Magnetophoretic velocity varies with the magnetic field gradient according to[14] $u_{mag} = \frac{\mu_o M_v V_p \nabla H}{6\pi\eta a} = \frac{2M_v a^2 \nabla B}{9\eta}$. Assuming this is correct; we would expect to see a close to linear dependence of magnetic dispersion on magnetophoretic velocity, or magnetization values, and magnetic field strength and orientation. Note, magnetic dispersion is the total dispersion minus the hydrodynamic dispersion and the values of magnetophoretic velocity was obtained by varying magnetization of MNP per unit mass from 33 to 77 emu/gm, a range that can be expected from experimentally synthesized MNP. Magnetic field value used for this model is 1T.

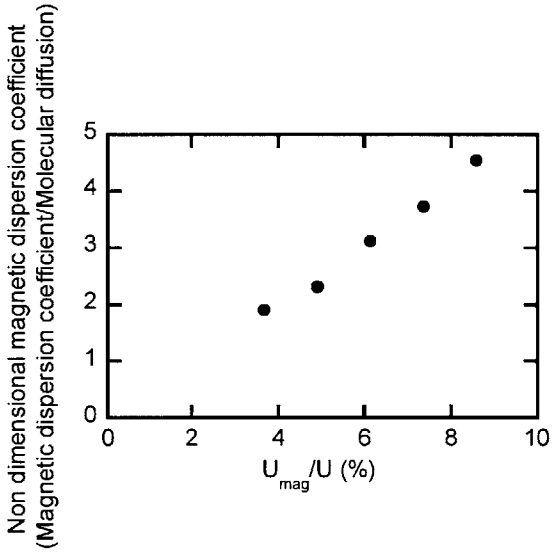

Figure 4-14: Increased magnetophoretic velocity results in increased magnetic dispersion

Figure 4-14 shows a linear trend in magnetic dispersion coefficient as a function of magnetophoretic velocity. The linear trend confirms our hypothesis that dispersion is the result of vector sum of various velocity fields. Depending on the magnetophoretic velocity applied, the effect of magnetic dispersion on the overall dispersion coefficient in a porous media can easily exceed the hydrodynamic dispersion coefficient, making it an important factor to be considered in determining the overall transport of the magnetic fluid.

4.7 Summary

A numerical methodology was proposed for determining effective dispersion coefficients in porous and non porous media whose results compared well with several theoretical limits. An analytical solution to Taylor-Aris dispersion coefficient in presence of an external magnetic field was used to evaluate the dispersion coefficients and compared with the simulation results. A good agreement of the results was found in each case. Some of the key findings of this chapter are that an enhanced dispersion coefficient is observed in presence of grains, external magnetic field gradient enhances dispersion of MNPs; longitudinal magnetic dispersion falls linearly while lateral dispersion rises linearly with the orientation of the magnetic field relative to the velocity field. Magnetic dispersion coefficients in 2D porous medium were also evaluated under varying orientations of magnetic field with respect to the flow field. These coefficients were found to be fairly complex quantities that depend on the porous medium geometry and the orientation of the field applied.

It was also shown that the magnetic dispersion has a linear dependence on magnetophoretic velocity which confirms our hypothesis that both magnetic and hydrodynamic dispersion coefficients can be vector added.

4.8 References

1. Slichter, C. S., Field measurements of the rate of movement of underground waters. *United States Geological Survey Water-Supply and Irrigation Paper* 1905, *140*.

2. Saffman, P. G., A theory of dispersion in a porous medium. *Journal of Fluid Mechanics* 1959, *6* (03), 321-349.

3. Saffman, P. G., Dispersion due to molecular diffusion and macroscopic mixing in flow through a network of capillaries. *Journal of Fluid Mechanics* 1960, *7* (02), 194-208.

4. Koch, D. L.; Brady, J. F., Dispersion in fixed beds. *Journal of Fluid Mechanics* 1985, *154*, 399-427.

5. Eidsath, A.; Carbonell, R. G.; Whitaker, S.; Herrmann, L. R., Dispersion in pulsed systems--III : Comparison between theory and experiments for packed beds. *Chemical Engineering Science* 1983, *38* (11), 1803-1816.

6. Bear, J., *Dynamics of fluids in porous media.* American elsevier publishing company: 1972.

7. Edwards, D. A.; Shapiro, M.; Brenner, H.; Shapira, M., Dispersion of inert solutes in spatially periodic, two-dimensional model porous media. *Transport in Porous Media* 1991, *6* (4), 337-358.

8. Brenner, H., Dispersion Resulting from Flow through Spatially Periodic Porous Media. *Philosophical Transactions of the Royal Society of London. Series A, Mathematical and Physical Sciences* 1980, *297* (1430), 81-133.

9. Aris, R., On the Dispersion of a Solute in a Fluid Flowing through a Tube. *Proceedings of the Royal Society of London. Series A. Mathematical and Physical Sciences* 1956, *235* (1200), 67-77.

10. Hoagland, D. A.; Prud'Homme, R. K., Taylor-aris dispersion arising from flow in a sinusoidal tube. *AIChE Journal* 1985, *31* (2), 236-244.

11. Edwards, D. A.; Shapiro, M.; Brenner, H.; Shapira, M., Dispersion Of Inert Solutes In Spatially Periodic, 2-Dimensional Model Porous-Media. *Transport In Porous Media* 1991, *6* (4), 337-358.

12. Bear, J., *Dynamics of Fluids in Porous Media.*

13. Huang, G.; Huang, Q.; Zhan, H., Evidence of one-dimensional scale-dependent fractional advection-dispersion. *Journal of Contaminant Hydrology* 2006, *85* (1-2), 53.

14. (a) Fateen, S.-E. K. Magnetophoretic Focusing on Submicron Particles Dispersed in a Polymer-Stabilized Magnetic Fluid. MIT, Cambridge, 2002; (b) Gonzalez, L. A. Negative Magnetophoresis of Submicron Species in Magnetic Nanofluids. MIT, Cambridge, 2009.

Chapter 5. Continuous Separation of Magnetic Nanoparticles from an Aqueous Suspension

5.1 Introduction

The treatment of large volumes of effluents with functionalized magnetic nanoparticles and their recovery from the suspension using HGMS techniques has an inherent disadvantage of being non-continuous. Therefore, a number of approaches for continuous separation have been investigated in the literature. For example; Kelland[1] demonstrated continuous separation of particles while subjecting them to an external field. In this work, Kelland shows migration of larger particles (~115nm) from a mixture of particles (size range 11-150nm) in a four channel separator. Given the short residence time in the flow channel, the effective separation is small. Zborowski et al.[2] demonstrated the separation of magnetically labeled cells in a quadrupolar magnetic field while Sharpe et. al.[3] used a similar magnetic quadrupole for continuous magnetophoretic cell clarification. Magnetic quadrupoles have circular magnetic fields (with zero magnetic field in the centre of the quadrupole configuration) that separate particles in annular region of the cylindrical columns placed within the quadrupole. In a more recent work, Chen develops a discrete element model that gives optimized design parameters for a magnetically enhanced continuous centrifugal process suitable for downstream biopharmaceutical processing.[4] This process utilizes the centrifugal force to continuously flow out the sludge of particles separated from the aqueous suspension. Xia et. al. also demonstrates continuous separation of magnetic nanoparticles from flowing biological fluids in a microfluidic channel.[5] To accomplish this a high magnetic field is applied at one side of the channel.

The aim of this work is to develop a simple separation model that can simulate continuous separation of magnetic nanoparticles from an aqueous suspension. A continuum finite element model describing the transport of nanoparticles while assuming an external magnetic field gradient in the flow channel was thus developed in COMSOL. The uniqueness of this model lies in the fact that it explores continuous separation of clusters of nanoparticles in the range of 10-80nm, includes viscosity changes as a function of particle concentrations and is scalable to any length scale of separation channel. The inclusion of viscosity variation provides useful information on regimes where separation fails as it can predict a viscous sludge formation

of particles. Lastly, parametric studies were performed to gain an understanding of the impact of cluster size, magnetic field gradient applied and the flow through the channel on separation efficiency.

5.2 Model Description and Equations

A finite element continuum model was developed to simulate scenarios of continuous separation. A simple flow channel with uniform magnetic field gradient across its height was chosen as the separation unit. This unit has a single inlet for the mixture of water and nanoparticles and two outlets, one for nanoparticles rich stream and one for nanoparticles lean stream. Magnetic nanoparticles migrate to high magnetic field region under the influence of the uniform magnetic field gradient in the channel. As more and more particles migrate to the high magnetic field region, sludge of particles starts to form in this region. Continuous flow of aqueous suspension pushes or carries this sludge out of the channel. Thus, there are two main forces affecting the separation. They are advective force which tries to flow out the particles with the water stream and magnetic force which tries to separate out the particles from the suspension. A careful balance of these two forces is required for continuous separation and flow of separated particles in the channel. A schematic of how continuous separation in a flow channel can be achieved is shown in Figure 5-1.

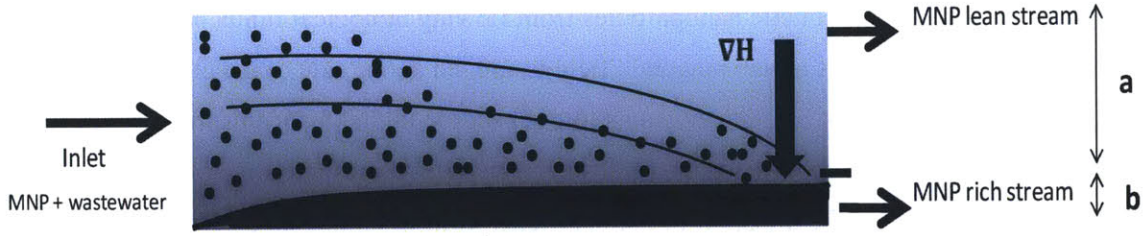

Figure 5-1: Schematic for continuous separation of nanoparticles from an aqueous suspension

Default flow channel dimensions were kept at 1cm x 0.8mm (length by height) unless specified. In the model developed, three equations, magnetostatics equation for simulating

external magnetic field, Navier-stokes equation for the fluid flow and a convective diffusive equation for the concentration profiles were simultaneously solved. The convective diffusive equation was coupled with the fluid flow equation through the viscosity term where viscosity varied as a function of concentration of the particles. In addition, a linear magnetic gradient across the channel (i.e. along the direction of height of the channel) was maintained. Equations and boundary conditions used in the model are given below:

Navier-Stokes equation (Equation 1) and continuity equation (Equation 2) were used to determine the fluid flow through the channel.

$$\rho(u.\nabla)u = \nabla.[\rho + \eta(\nabla u + \nabla u^T)] \quad (1)$$

$$\nabla.u = 0 \quad (2)$$

Here, u is the velocity vector, η is the fluid viscosity and ρ is the density of the medium. Boundary conditions used are as follows, inlet boundary: $U_0 = v_0$, walls of the flow channel: $u_T = 0$ (no slip) and outlet boundary: p_0 (normal stress) = 0

For dilute magnetic nanoparticles, viscosity varies linearly with concentration of particles as shown below[6,7,8]

$$\eta = \eta_0(1 + 2.5\phi) + \eta_r \quad (3)$$

where, η is the viscosity of the suspension, η_0 is the viscosity of the aqueous fluid, ϕ is the volumetric concentration of the particles and η_r is the rotational viscosity of the magnetic nanoparticles that becomes important in the presence of an external magnetic field. Limiting value of the rotational viscosity in presence of strong magnetic field is given as follows[6]

$$\eta_r = \frac{3}{2}\phi \quad (4)$$

A convective diffusive equation (Equation 3) was used to determine the concentration profiles of magnetic fluid in the channel. This equation was modified with an additional term (given in red) that takes into account the presence of external magnetic field.

$$\frac{\partial c}{\partial t} + u.\nabla c = \nabla.(D_{mol}\nabla c) - \nabla(u_{mag}c) \quad (5)$$

$$u_{mag} = \frac{\mu_o M_v V_p \nabla H}{6\pi\eta a} \quad (6)$$

Here, c is the concentration of the magnetic fluid, t is the time, D_{mol} stands for molecular diffusion, μ_0 is the free space permeability, M_v is magnetization per unit volume of the particles, V_p is the volume of each particle, H is the magnetic field, η is the viscosity of the fluid and a is the particle radius. Following boundary conditions were used: inlet boundary: $u\frac{\partial c}{\partial x}|_{in} = u_0\frac{\partial c_0}{\partial x}$, walls of the grains $u\frac{\partial c}{\partial x} + D\frac{\partial^2 c}{\partial x^2}|_{Total\ flux} = 0$, and outlet boundary: $u\frac{\partial c}{\partial x}|_{out} = u\frac{\partial c_0}{\partial x}$ (continuity of flux). To account for clusters, V_p was based on volume of magnetite while particle size a was based on hydrodynamic radius of the entire cluster.

Following equation from the magnetostatics module of COMSOL (Equation 5) was used to determine the magnetic field.

$$\nabla\times(\mu_0^{-1}\nabla\times A - M) = 0; A = A_z e_z \tag{7}$$

Here, A is the magnetic potential, M is the magnetization. For boundary conditions, $H_x = H_0\left(\frac{x}{L}\right)$ and $H_y = H_0\left(\frac{y}{L}\right)$ on the entire geometry and its boundaries, were used.

The solved equations were then used to calculate separation efficiency of the system. Separation efficiency is defined as follows:

$$\text{Efficiency} = \frac{\int_0^b vc_y dy}{\int_0^{a+b} vc_y dy} \tag{8}$$

In other words, separation efficiency equaled the flux exiting from the magnetic nanoparticles rich phase to the total outlet flux exiting the channel. In our simulations, $a = b$, i.e. the two outlets were of same length, therefore a completely efficient separation yielded a separation efficiency of 1 (or 100%) while no separation had a separation efficiency of 0.5 (or 50%).

5.3 Adjustment to Clusters

As noted in chapter 2, the synthesized nanoparticles assembled into clusters of 60-100nm. To account for the clusters in our models, the method of Ditsch[9] describing the properties of fractal aggregates was used.

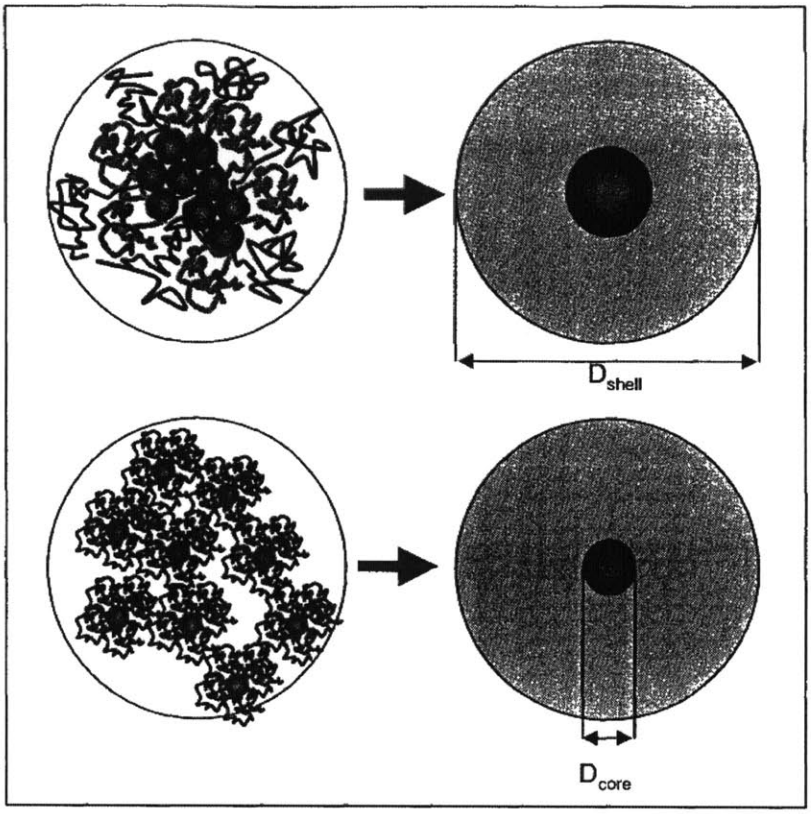

Figure 5-2: Magnetic clusters are modeled as equivalent core-shell particles where the shell diameter equals the cluster diameter and the core diameter equals the diameter of magnetite having the same total magnetite volume as in the cluster (adapted from Ditsch[9])

As illustrated in Figure 5-2, based on the way the magnetite cores are connected to each other in the cluster one can calculate equivalent core and shell diameters. For core to core contact of magnetite, the number of aggregates in the cluster and the equivalent core radius can be calculated as

$$N_{agg} = \left(\frac{R_{shell} - 2R_{G,poly}}{R_c}\right)^{D_f} \tag{9}$$

$$R_{core} = R_c \left(\frac{R_{shell} - 2R_{G,poly}}{R_c}\right)^{\frac{D_f}{3}} \tag{10}$$

For polymer bridging of the magnetite cores, the number of aggregates in the cluster and equivalent core radius can be written as

$$N_{agg} = \left(\frac{R_{shell}}{R_c+2R_{G,poly}}\right)^{D_f} \tag{11}$$

$$R_{core} = R_c\left(\frac{R_{shell}}{R_c+2R_{G,poly}}\right)^{\frac{D_f}{3}} \tag{12}$$

Where, D_f is the fractal dimension of the core, assumed to be 2 to be in this work. Based on the TEM images obtained of the synthesized nanoparticles (as shown in chapter 2), we concluded that cluster was formed with polymer bridging of the magnetite cores. The equivalent core radius for our clusters was determined using Equation 9.

5.4 Results

Viscosity variation as a function of concentration is a unique feature of our model. This allows for both cross sectional viscosity and velocity profiles to vary along the length of the flow channel. Figure 5-3 shows an increase in cross sectional viscosity along the flow channel length. The three cross sectional curves correspond to the beginning, centre and close to the end of the flow channel. Correspondingly, the velocity profile shifts from being laminar to a non linear profile that includes the effects of a viscous sludge formation.

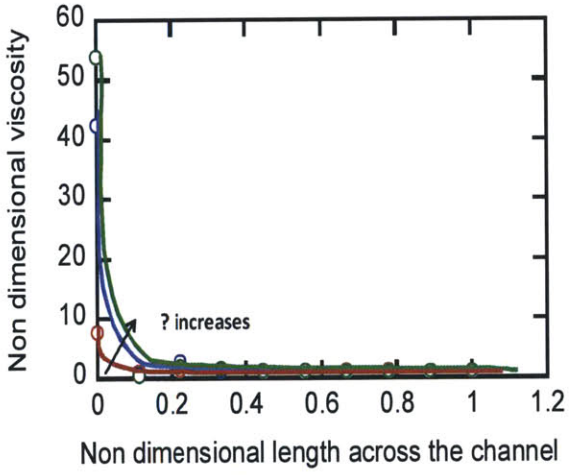

Figure 5-3: Cross sectional viscosity increases along the flow channel length

Figure 5-4 shows the concentration profile of nanoparticles at different cross sections along the flow channel length. The graphs plot non-dimensional concentration and how it varies as a function of non-dimensional length. As seen from the four graphs given in this figure, the length of no nanoparticle concentration region increases as one progresses along the length of the channel indicating migration of nanoparticles to the higher magnetic field region leaving behind larger lengths of channel devoid of particles. Also, the concentration of nanoparticles at the base of channel increases which is consistent with accumulation of migrated nanoparticles.

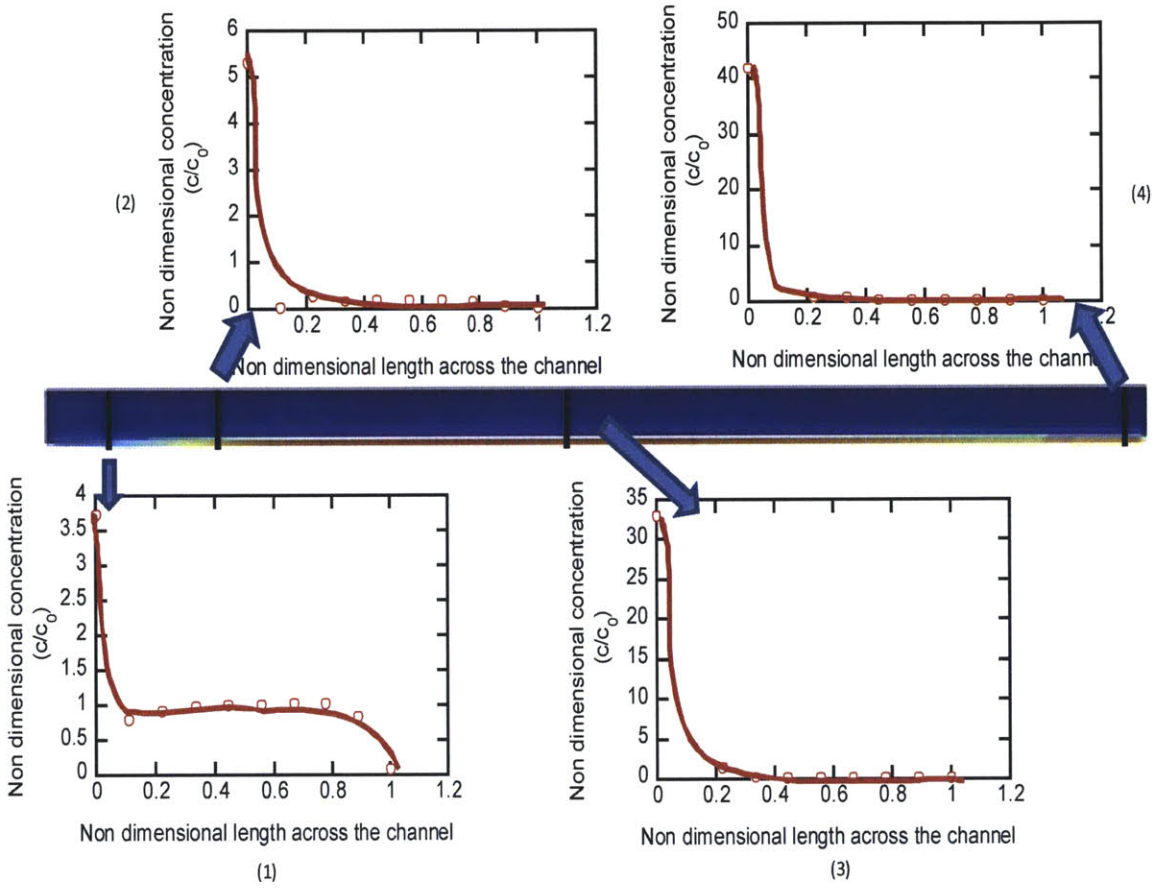

Figure 5-4: Increasing concentration profiles along the length of the flow channel

5.4.1 Variation with Cluster Size

It is observed that separation efficiency increases with the square of particle size (Figure 5-5). Also, 20nm clusters of nanoparticles having the same magnetic volume fraction (~15%) as 10nm magnetite particles, separate out more easily compared to the smaller magnetite particles. This is because the magnetic force on the nanoparticle scales with the square of radii of the magnetic core and this term increases dramatically with increasing the cluster size. Also, though there is some decrease due to increase in drag force (caused by larger size of the cluster), there is a net increase in the magnetic pull term.

In essence, there are two forces acting on the particles in the channel, advective fluid flow force that carries the particles out of the system and that due to a transverse magnetic force that attracts the particles to the region of higher magnetic field strength. It is the tradeoff between these two forces that results in separation and removal of the nanoparticles from the flow channel. To test this hypothesis, the simulation results were plotted against a non dimensional ratio of these two forces ($\alpha = \frac{u_{mag}}{u} = \frac{\mu_0 M_v V_p \nabla H}{6\pi\eta a u}$). As seen in Figure 5-6, an increase in separation efficiency with an increase in α is observed which is in line with our expectation that the larger magnetic force will increase the overall separation effectiveness.

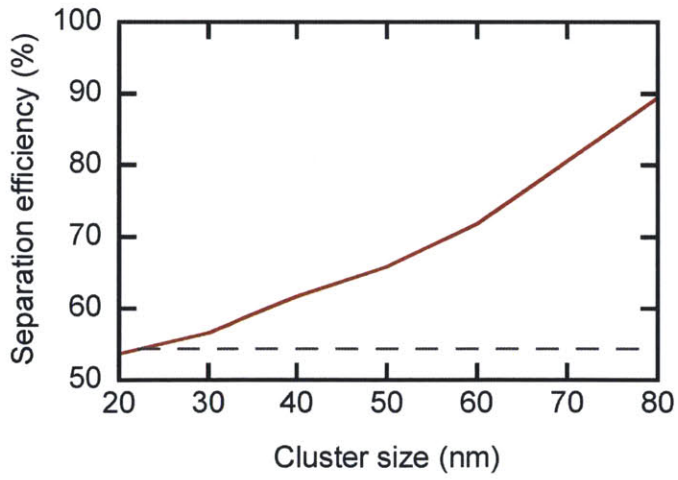

Figure 5-5: Separation efficiency increases dramatically for clusters (red line with markers) as compared to 10 nm magnetite particle (black dashed line).

Simulation parameters: Aspect ratio (L/H) = 12.5, H = 0.8mm, u = 0.1mm/s, B = 20 mT

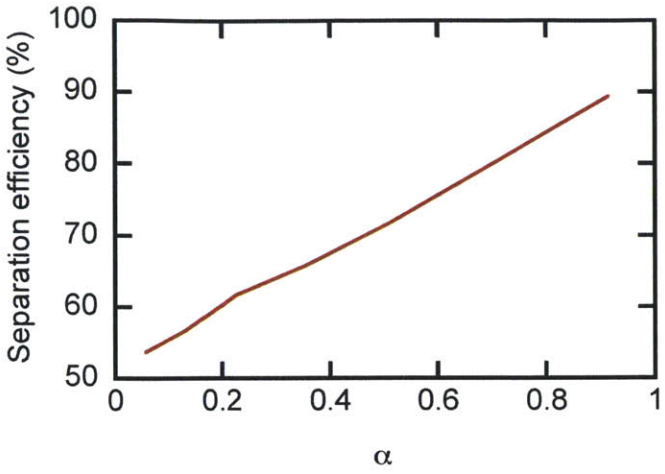

Figure 5-6: Separation efficiency as a function α

5.4.2 Variation with Magnetic Field Gradient

Figure 5-7 shows that complete separation of particles under low magnetic field gradients is possible with the correct design of the channel. It also shows that increasing magnetic force beyond a certain point results in lower efficiency in a continuous sense, as the particles form a sludge that settles to the bottom of the channel which is not carried out of the channel. So, even if separation of particles is achieved, the particles are not continuously removed from the channel which results in lower efficiency. A smaller cluster size of 10nm was chosen to study the trends in separation efficiency as a function of the system parameters. Figure 5-8 shows the particle separation efficiency based on α for different aspect ratios (length x height) of the flow channel. Once again, it is shown that we can manipulate the channel dimensions to optimize separation efficiency in the presence of a low magnetic field gradient.

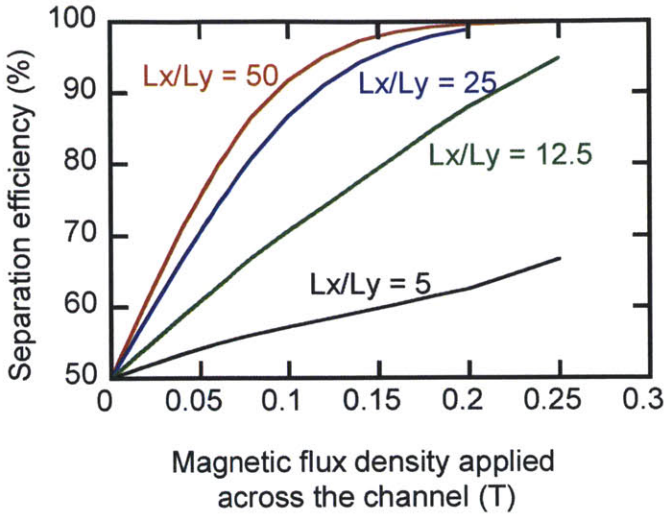

Figure 5-7: Separation efficiency as a function of magnetic field applied across the channel and channel aspect ratio

Simulation parameters: u = 0.1mm/s, a = 10nm magnetite, Lx = 1cm

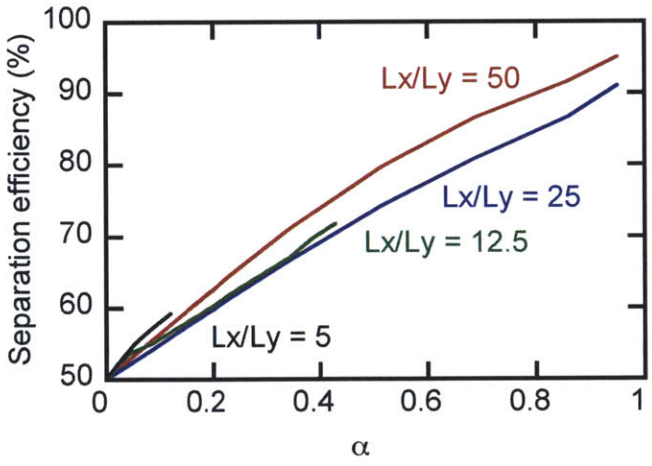

Figure 5-8: Separation efficiency for different channel aspect ratios as a function of α

5.4.3 Variation with Flow

Figure 5-9 shows the increase of advective velocity has a deleterious effect on the separation efficiency. Increasing magnetic force on the nanoparticles though increases the separation of particles from the stream, reduces the overall removal efficiency from the aqueous

stream in a continuous manner. Hence the net separation efficiency reduces with increasing flow as shown in Figure 5-10.

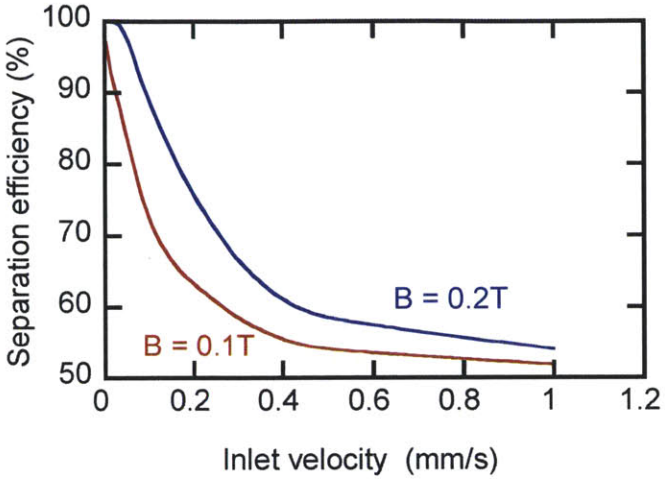

Figure 5-9: Separation efficiency as a function of advective velocity through the channel Simulation parameters: Aspect ratio (L/H) = 12.5, H = 0.8mm, a = 10nm magnetite, umag = 0.01 mm/s

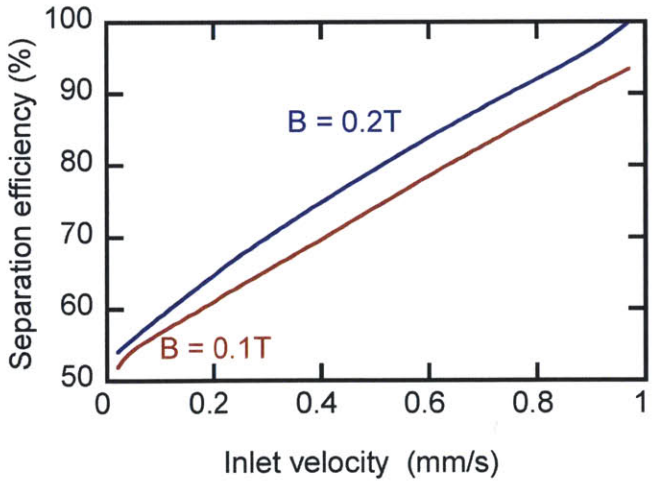

Figure 5-10: Separation efficiency for different magnetic field strengths as a function of α

Thus, these results show us that operating parameters (magnetic field, flow rate) and design parameters (cluster size, channel dimensions) can be manipulated to make complete separation of nanoparticles possible and scalable to any experimental conditions.

5.5 Summary

In this work, continuous separation of nanoparticles using a continuum model was explored. The model has two unique features besides being scalable, one that it includes viscosity variation as a function of concentration of particles and two that it accounts for nanoclusters. It is seen that in such systems, there exists in essence one non-dimensional parameter which determines the separation efficiency. This parameter (α) is denoted as the ratio of magnetic force to drag force or the ratio of magnetophoretic velocity to advective flow velocity. Based on the parametric results, separation efficiency has a squared dependence of particle size, a linear dependence on aspect ratio at low magnetic fields that plateaus off at higher fields and drastically falls with increased advective flow. These simulation results and the individual trends in each parameter provide information on the possible operating regimes for continuous separation.

The results shown here address the trends in different system parameters. It is an important first step in understanding the separation system at hand. In order to use these simulations in industrial scale applications, we need to extend the current models to consider larger clusters (100-150nm), higher flow rates and the magnetic field gradient from either a permanent magnet or magnetized wires. Continuum models become increasingly difficult to solve when we try to extend them to the above mentioned scenarios as their inclusion makes the equation stiff and prone to convergence failure. It is therefore recommended to use particle tracking methods in lieu of continuum models to avoid the convergence problems.

5.6 References

1. Kelland, D. R., Magnetic separation of nanoparticles. *Magnetics, IEEE Transactions on* 1998, *34* (4), 2123-2125.

2. Zborowski, M.; Sun, L.; Moore, L. R.; Stephen Williams, P.; Chalmers, J. J., Continuous cell separation using novel magnetic quadrupole flow sorter. *Journal of Magnetism and Magnetic Materials* 1999, *194* (1-3), 224-230.

3. Sharpe, S. A. Magnetophoretic cell clarification. Massachusetts Institute of Technology, Cambridge, 2004.

4. Chen, F. Magnetically enhanced centrifugation for continuous biopharmaceutical processing. Massachusetts Institute of Technology, Cambridge, 2009.

5. Xia, N.; Hunt, T.; Mayers, B.; Alsberg, E.; Whitesides, G.; Westervelt, R.; Ingber, D., Combined microfluidic-micromagnetic separation of living cells in continuous flow. *Biomedical Microdevices* 2006, *8* (4), 299-308.

6. Raikher, Y. L.; Shliomis, M. I., Limiting viscosity of ferromagnetic suspensions in a strong magnetic field. *Journal of Applied Mechanics and Technical Physics* 1974, *15* (4), 470-475.

7. Odenbach, S.; Thurm, S., Magnetoviscous Effects in Ferrofluids. In *Ferrofluids*, Odenbach, S., Ed. Springer Berlin / Heidelberg: 2003; Vol. 594, pp 185-201.

8. McTague, J. P., Magnetoviscosity of magnetic colloids. *Journal of Chemical Physics* 1969, *51* (1).

9. Ditsch, A. A. P. Purification of recombinant proteins with magnetic nanoclusters. Massachusetts Institute of Technology, Cambridge, 2005.

Chapter 6. Lab-scale Implementation of Mercury Removal

6.1 Introduction

In chapter 2, the adsorption capacities of dithiocarbamate-modified magnetic nanoparticles for heavy metals, in particular for mercury (Hg), lead and manganese ions were investigated. It was observed that these particles have a high capacity for Hg and even in presence of competing ions, such as calcium, magnesium and chloride, these particles displayed binding to Hg. As outlined in chapter 1, these particles can then be captured from suspension using HGMS techniques. This chapter thus brings together two operations, adsorption of Hg on the particles and capture of particles, and considers removal of Hg by using these particles in a semi-continuous manner. The goal of the work presented here was to explore the implementation of the lab scale removal of Hg spiked aqueous solutions in a manner similar to its industrial implementation.

A quantitative analysis of the feasibility of using these particles for Hg spiked aqueous media was performed. Already having looked at adsorption in the previous chapters, this work focuses on the capture of magnetic nanoparticles. The efficiency of removal of magnetic nanoparticles using a HGMS setup along with adsorption of Hg by the particles is discussed in terms of breakthrough curves. The total capacity of the column for capturing particles was calculated by extrapolating the magnetic nanoparticle breakthrough curve data. In addition, the efficiency of stripping off the Hg adsorbed on these particles by thiourea is discussed. This efficiency is crucial in determining the reusability of the magnetic nanoparticles for further heavy metal removal. The relative ease in removing magnetic nanoparticles from the HGMS unit by flushing water through the unit is also demonstrated. Multistage adsorption units will be required to scale up this process, as it uses less adsorbent amount than a single batch process. Sorbent amounts required in two and three stage continuous countercurrent adsorption process for varying binding affinities between the particles and heavy metals and different inlet and outlet ratios of metal concentrations were thus calculated to guide the choice of number of adsorption units to be used in the process scale up.

6.2 Experimental Methods

Two solutions were used in the experiments; one was an effluent mimic or water spiked with mercury nitrate salt ($[Hg^{2+}]$ = 5ppm) and the second was an aqueous solution with 0.3mg/ml of the magnetic nanoparticles or the Hg adsorbents. This solution was maintained at pH = 6.7 by addition of 0.1M HCl and 0.1M NaOH solutions. The concentration of magnetic nanoparticles was chosen such that the number of functional groups present on the particles was 10 times that of the total Hg concentration and would ensure adsorption of Hg species. Fluid from both these beakers were then each pumped at roughly 60ml/min into a static mixer. The mixer brought together the magnetic nanoparticles and contaminated water and allows for complete mixing to take place. This mixing ensured that the majority of Hg species was adsorbed onto magnetic nanoparticles as there are negligible mass transfer limitations offered by the particle suspension. Fluid from the static mixer was then pumped through the HGMS column and the outlet of this column was removed as the treated water. This outlet solution was sampled for Hg and MNP concentrations to determine the net Hg adsorbed and removed by the particles and the efficiency with which the particles were removed from the solution. A schematic for this entire setup is shown in Figure 6-1.

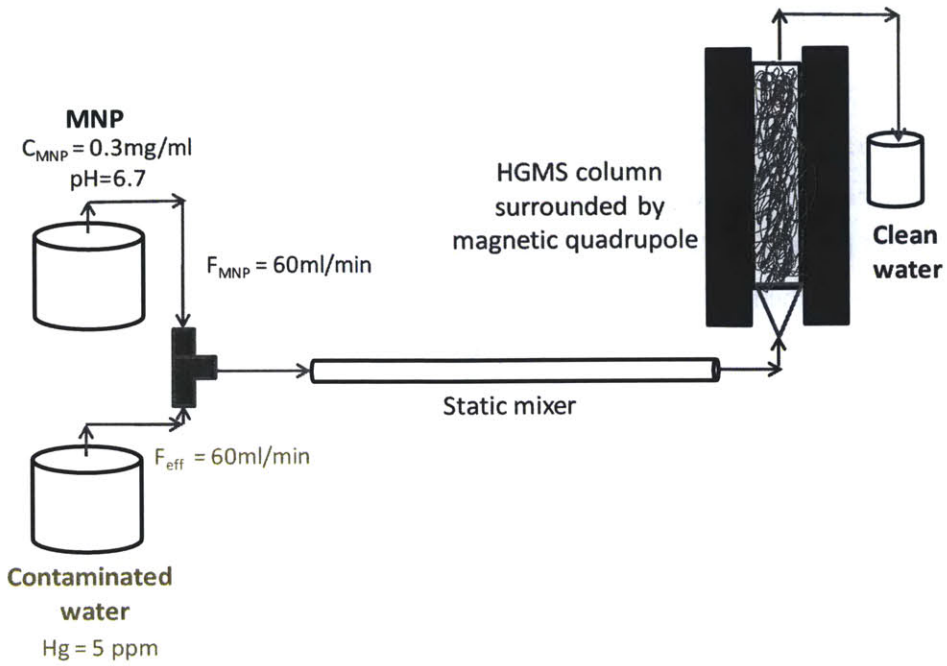

Figure 6-1: Schematic of lab scale implementation of treating Hg contaminated water with magnetic nanoparticles. Contaminated fluid is treated with magnetic nanoparticles in a semi-continuous manner

With the passage of more and more particles, the column wires (magnetized by the external magnet) become completely saturated with captured particles. To continue removal of Hg adsorbed particles, the outlet of the mixer can be then fed into another HGMS unit while Hg can be stripped off the captured particles in the first HGMS unit by using thiourea. Following the contaminant removal from the particles, the regenerated particles can be recovered from the HGMS unit by removing the external magnetic field and flushing water through the column. Thus, by following the steps highlighted above, a semi continuous lab scale removal of Hg was achieved.

The static mixer used in the lab setup was a Stratos tube mixer # 3/16-27 manufactured by Koflo Corporation. An image of the mixer and its helical mixing elements is shown in Figure 6-2. This mixer has an outer diameter of 3/16" and 27 alternating mixing elements. Based on both the flow rates and the fluid properties used, the mixing elements were sufficient for complete mixing of the two fluids in our system.

The HGMS column was built using a serological pipette (25ml by BD Falcon) filled with stainless steel wool. The column was then placed inside a magnetic quadrupole. The stainless steel wool used in an earlier work[1] was measured to be approximately 50 μm in diameter. The magnetic quadrupole consisted of four nickel plated Neobydium permanent magnets (18cm x 1.8cm x 1.8 cm) arranged in cross shaped configuration. The magnets were equidistant from each other and the arrangement had an open region in the center through which the pipette could pass. The pipette was cut to length to fit the height of the column. The steel wool occupied roughly 8% of the total 37.5ml volume of the pipette.

Figure 6-3 illustrates the magnetic field in the core region of the magnetic quadrupole. COMSOL, a multiphysics finite element modeling software package, was used to model the magnetic field in the HGMS column. As seen from the field plots, the field in the core region is circular with a zero magnetic field at the center of the quadrupole configuration or the pipette which was placed in the center of the quadrupole. More details on the magnetic quadrupole can be found in Sharpe.[2] The working principle of the HGMS system is that the stainless steel wool in the pipette gets magnetized by the magnets in the quadrupole and generates strong local magnetic field gradients that are responsible for capturing magnetic nanoparticles. The force with which the particles are attracted to the wires is given as

$$F = \mu_0 M_v V_p \nabla H \tag{1}$$

where μ_0 is the free space permeability, M_v is the magnetization per unit volume of the particle, V_p is the volume of the particle and H is the magnetic field strength.[3]

Net flow rate of 120ml/min in the static mixer and the HGMS column was chosen such that the resultant linear velocity through the HGMS column was 1cm/s, which is typically an optimal velocity through HGMS columns that optimizes productivity.[1]

In all these experiments, dithiocarbamate modified nanoparticles were used to adsorb Hg. Materials used in synthesizing these particles along with the particle synthesis procedure are described in chapter 2. An image of the complete lab setup is shown in Figure 6-4.

Figure 6-2: Static mixer used in the lab scale experiment (Stratos tube mixer # 3/16-27 by Koflo Corporation)

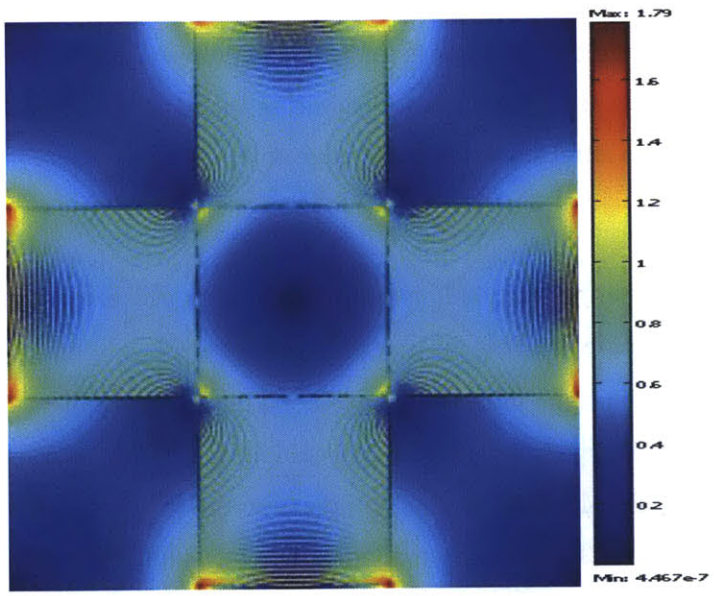

Figure 6-3: Surface plot and contour plots of magnetic field (T) generated by the magnetic quadrupole. Red represents the highest magnetic field regions while blue represents the lowest. As seen, the magnetic fields are circular in the middle of the quadrupole configuration

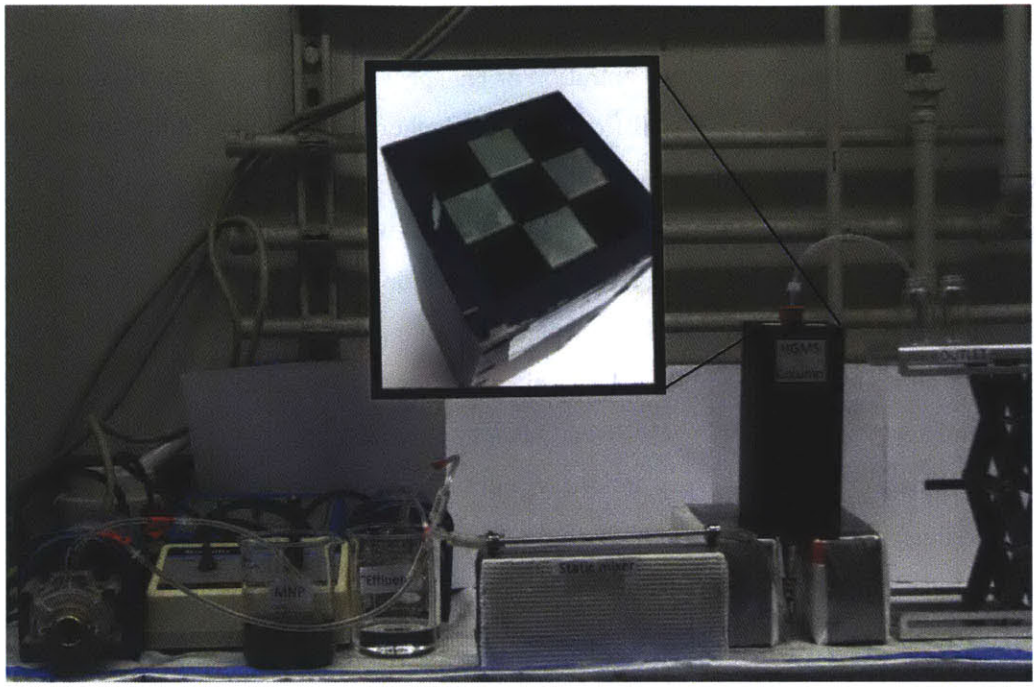

Figure 6-4: Complete lab scale setup for treating Hg spiked water with magnetic nanoparticles

6.3 Breakthrough Curve Analysis

We used chloride ions as a tracer to obtain the residence time in our setup as it is a non-reactive tracer that is not affected by the magnetic field and because it is easy to measure the conductance using a standard conductivity meter.

The results of these experiments are plotted in Figure 6-5. The result shows non-retarded jump in the chloride conductance to its maximum conductance value as soon as it outlets the system. It remains at this value till the end of the experiment. This breakthrough curve confirms that the chloride ions were non reactive to the system and was not retarded by any element of the setup. The lack of significant axial dispersion in the system indicates absence of channeling in the column. One pore volume was 22mL.

It was necessary to determine also whether Hg species were retarded in our setup especially by the steel wool packing in the HGMS column. Water spiked with Hg salt was introduced into the mixer and HGMS column by two beakers and the outlet from the HGMS column was measured for Hg concentration using Inductively Coupled Plasma - Optical

Emission Spectroscopy (ICP-OES). Mercury breakthrough curve obtained is plotted in Figure 6-5. As observed from this figure, concentration of Hg species reaches the initial concentration at approximately one pore volume. It is difficult to say whether the difference in the chloride and Hg breakthrough curves was due to slight retardation of Hg species or the discrete nature of measurements. This was clarified in a different experiment where passage of Hg solutions was followed by a dilute acid wash and the exiting wash solution was measured for Hg concentration. In this experiment, 20ml of dilute acidified water (containing 2 wt% of nitric acid) was passed through the column to remove any free Hg species. Results on four samples obtained from the acid flush and analyzed by ICP-OES showed that very small concentrations (< 0.03ppm) of unbound Hg ions were released. Very small concentrations of unbound Hg obtained from this experiment suggests the difference in breakthrough curves of chloride and Hg is primarily due to the discrete measurements rather than any retardation.

The last set of breakthrough experiments was performed for the mixture of magnetic nanoparticles and Hg spiked water (Figure 6-5). The HGMS outlet was then analyzed for the Hg concentrations and nanoparticle content. The iron content was a direct indicator of concentration of magnetic nanoparticles that were not captured by the HGMS column.

The results for the magnetic nanoparticle and Hg breakthrough curves are shown in Figure 6-5. The empty markers represent the Hg breakthrough without the treatment of magnetic nanoparticles while the filled in markers represent the breakthrough curve for the mixture of magnetic nanoparticles and Hg solution.

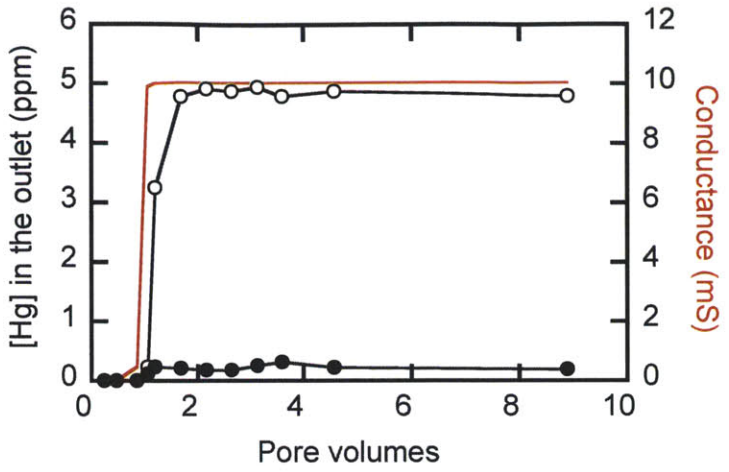

Figure 6-5: Breakthrough analysis for chloride and Hg (Red line represents the chloride ion conductance, empty markers represent the Hg breakthrough without the treatment of magnetic nanoparticles while the filled in markers represent treated system)

The Hg concentration expected in the outlet without any treatment with magnetic nanoparticles is 2.5 ppm (half of initial concentration since this system has half the MNPs containing fluid and half of Hg spiked fluid). With treatment, the Hg concentrations in the outlet were below 0.31ppm. This means that there was a consistent, around 90% removal of Hg from the initial spiked fluid. A 100% removal of Hg was not seen, as there were some residual Hg concentrations in the aqueous stream in equilibrium with the Hg adsorbed on the particles. Based on the binding affinity of Hg and the functional group on the particles, there will always be an equilibrium concentration of Hg in the aqueous stream that makes 100% removal impossible. The iron analysis showed that the iron content in HGMS outlet concentration were below 0.1ppm. The low values indicate more than 99% removal of magnetic nanoparticles by the HGMS column as the initial concentration of particles was 300ppm. Removal of the particles was also evident from the clarity of the outlet fluid samples when compared to the inlet fluid stream.

The total capacity of the HGMS column for captured magnetic nanoparticles was calculated by extrapolating the volume of column filled up during the breakthrough experimental run. It was observed that passing of nine pore volumes resulted in 0.7cm of the column (or 4.1%) to be filled up by the particles. Thus, the total capacity of the column before it is completely

saturated and needs to be replaced was calculated as 220 pore volumes (or 8800ml of mixed fluid). An image showing the partially filled pipette after the breakthrough experiments is given in Figure 6-6. An approximate loading of particles per volume occupied was calculated as 34mg/ml. The loading of particles per column volume can be further improved by increasing the packing density of stainless steel wires in the column (current packing density is 8%) as this increases the net capture zone. Ditsch[1] highlights that beyond an optimal packing density for a given HGMS column, there is incremental change in capture of particles.

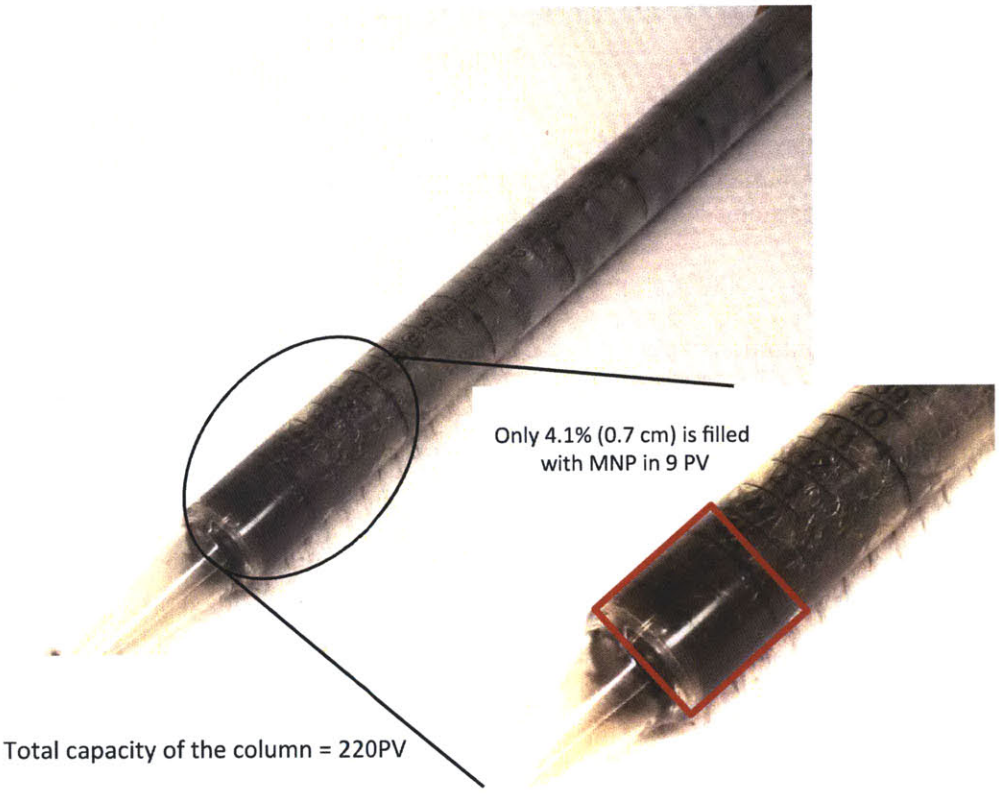

Figure 6-6: Partially filled pipette used as HGMS column on passing nine pore volumes of fluid

6.4 Recovery of Adsorbed Mercury

The partially filled pipette (HGMS column) was then flushed with thiourea to strip off the adsorbed Hg species from the particles. Thiourea was chosen to remove Hg from the particles as it has high stability constants ($\sim 10^{11}$) with mercury.[4] In this experiment, 10 ml of 1M aqueous

thiourea soltuion was flushed through the HGMS column at a flow rate of 1.2 ml/min. Based on the difference between the amount passed through the column and the Hg not removed by the particles, 2.18 μmoles of Hg were present on the particles. The concentration of Hg in the thiourea flush suggests that 2.04 μmoles of Hg were removed by the organic compound solution. In other words, an approximate efficiency of 93% was obtained for recovering Hg by thiourea. Thus, this experiment suggests the possibility of reusing the particles by extracting Hg from the magnetic nanoparticles using the thiourea solution. Spent thiourea solution containing Hg will then need to be disposed off to a landfill. The question then remains whether to use thiourea to extract the adsorbed species, generate a secondary stream of Hg contamination and find suitable disposal means for the spent thiourea or to directly dispose the Hg containing magnetic nanoparticles. Overall economics of both the alternatives will determine the answer to the above question. For now, its suffice to say that particles can be regenerated using thiourea.

The experiment was performed with excess thiourea to demonstrate preferential binding of Hg species to thiourea than dithiocarbamate group. It has been reported that the binding constant of Hg^{2+} ions to thiourea is $10^{11.4}$ while the binding constants of Co^{2+}, Zn^{2+} and Cu^{2+} to propranolol dithiocarbamate are $10^{2.61}$, $10^{2.94}$ and $10^{4.42}$ respectively.[4,5] Extending the results to dithiocarbamate binding and using a higher affinity of Hg^{2+} to the ligand, while keeping in mind the experimental results of chapter 2, we can approximate the binding constant of Hg^{2+} to dithiocarbamate to be around 10^5. This indicates the Hg is likely to bind 10^6 times more to thiourea than the dithiocarbamate ligand.

6.5 Removal of Captured MNPs

In addition to the previous experiments, we investigated the ease with which the captured magnetic nanoparticles were removed from the steel wool matrix in the HGMS column. To conduct this experiment, the steel wool filled pipette was first removed from the magnetic field of the quadrupole. This ensured that the particles were not held by strong magnetic forces. After removal of the external field, water was flushed through the system at a moderate speed of 20ml/min. The outlet collected from two to three minutes of water passage was then evaporated to enable the weight of the magnetic nanoparticles collected to be measured. Based on the initial concentration, volume of magnetic fluid passed through the system and the weight of collected

particles, we estimated the efficiency of recovering captured magnetic nanoparticles. On an average, 96% removal of captured magnetic nanoparticles was obtained. Additionally, a visual inspection of the column showed clear steel wool wires that confirmed efficient removal of particles.

6.6 Continuous Countercurrent Multistage Adsorption Process

Industrial implementation of this technology, if the adsorption is carried out in a batch process, will require a large amount of nano sorbents to treat the high volumes of effluents. A more economical approach applied in separating processes is to use a continuous countercurrent multistage operation instead. Countercurrent operation has the advantage of maintaining a high driving force throughout the process while the multistage adsorption significantly reduces the amount of sorbent required. Mass balances were used to determine the sorbent required for varying number of stages, inlet to outlet concentration ratio and the binding affinity between the adsorbent and the adsorbate. This study provides us information on sorbent required per volume of fluid to be treated for a given chemical system and number of stages.

Mode of operation in a single batch adsorption process and 'n' stage countercurrent adsorption process is shown in Figure 6-7. Based on simple mass balance equation and concentration of contaminant in the inlet and outlet of the liquid stream, we can determine the sorbent loading required to reduce the contaminant concentration. It is seen that having more than two adsorption stages marginally reduces the sorbent required while substantially increasing the capital costs of installing a third unit. The calculations herein were thus restricted to three stages. Mass balance for one stage is given below

$$S(x_f - x_0) = L(y_0 - y_f) \tag{2}$$

Here S is the sorbent amount, L is the volume of liquid to be treated, y_0 and y_f are the initial and final concentrations of contaminant to be adsorbed from the liquid phase while x_0 and x_f are the concentration of contaminant on the sorbent. Assuming equilibrium at each stage, concentration of adsorbed contaminant can be related to the liquid stream concentration by using the Langmuir equation as shown in the equation below.

$$x_j = \frac{K_L y_j}{1+K_L y_j} \tag{3}$$

Here K_L is the Langmuir constant, y_j and x_j are the liquid and sorbent concentrations exiting the j^{th} stage.

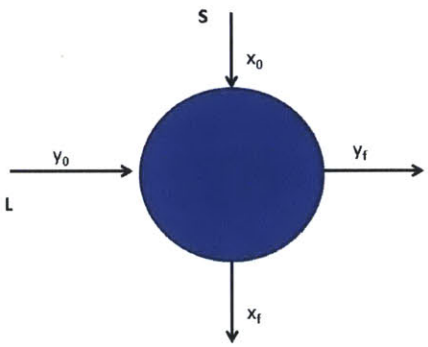

(a)

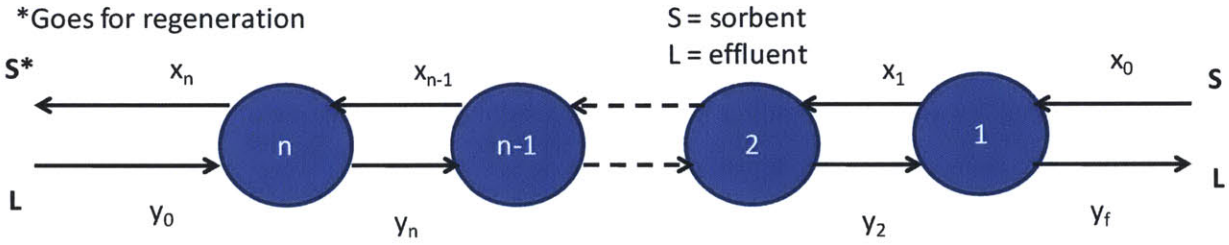

(b)

Figure 6-7: Schematic for (a) batch adsorption process (b) continuous countercurrent multistage adsorption process

In both two stage and three stage operations, similar mass balances can be written over the entire process and individual stages. Intermediate concentrations in the liquid and on sorbent phase are then calculated by equating the slope of the operating line or 'S/L' ratio in each of the mass balance equations obtained for different stages. These intermediate concentrations are used in evaluating the sorbent amount for a particular liquid volume. In case of two stages, following

relation can be used to evaluate the intermediate concentration y_2. With y_2 known, x_1 is evaluated using the above given Langmuir relation. Equation 4 was used to calculate y_2.

$$\frac{y_2 - y_f}{y_i - y_f} = \frac{y_f}{y_2} \frac{1 + K_L y_2}{1 + K_L y_f} \tag{4}$$

For three stage operation, two non-linear equation (Equation 5 and 6) needs to be solved simultaneously to obtain the intermediate concentrations y_2 and y_3. These concentrations can then be used to evaluate the sorbent stream contaminant concentrations using the above given Langmuir relation.

$$\frac{y_2 - y_f}{y_i - y_f} = \frac{y_f}{y_3} \frac{1 + K_L y_3}{1 + K_L y_f} \tag{5}$$

$$\frac{y_2 - y_f}{y_3 - y_f} = \frac{y_f}{y_2} \frac{1 + K_L y_2}{1 + K_L y_f} \tag{6}$$

Results on amount of sorbent required for processing 100 liters of contaminated liquid in one stage, two stage and three stage adsorption process for different $\frac{y_i}{y_f}$ ratios and at a given K_L = 500 (L/g) is shown in Figure 6-8. It is observed that sorbent amount required reduces drastically as we go from one stage to two stages. However there is marginal reduction in sorbent amount as we go from using two stages to three stages. This result highlights that use of two stages shall be sufficient to economically implement our process.

Effect of K_L on sorbent amount required was also studied for both one stage and two stage processes. The results are shown in Figure 6-9 and as expected sorbent amount required decreases as the K_L value increases.

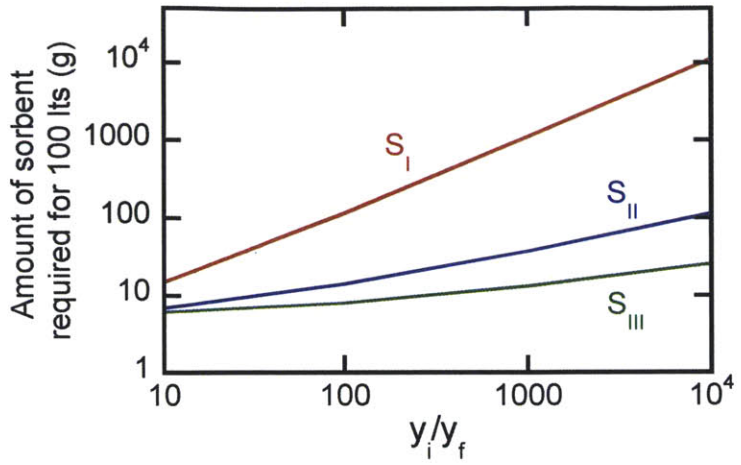

Figure 6-8: Amount of sorbent required in one, two and three stage operation for treating 100 liters of effluent. K_L, the Langmuir affinity constant between sorbate and sorbent is equal to 500

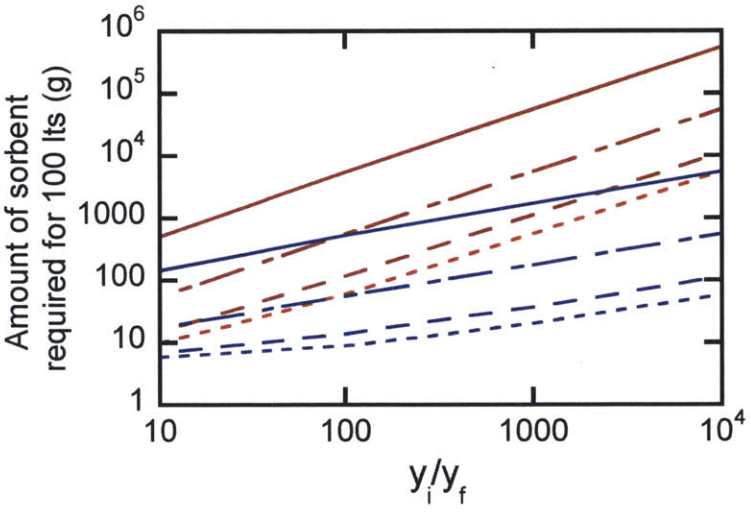

Figure 6-9: Increasing K_L reduces the required sorbent amounts in both one (red lines) and two (blue lines) stage adsorption operation. The four lines (with increasing number of dashes) in each case are for K_L of 10, 100, 500 and1000 L/g respectively

Values of sorbent required in one, two, three and infinite number of stages for different K_L and $\frac{y_i}{y_f}$ ratios in the liquid stream are shown in Table 6-1. Two of the calculated values for both two and three stage operations when compared to the results of Wu and Tseng,[6] who also look at multistage countercurrent adsorption on activated carbon, were found to match exactly. Thus these calculations are valuable guides in determining the sorbent loading for any given system.

Table 6-1: Sorbent amount required and the ratio of sorbent required in one stage to multistage with varying K_L and $\frac{y_i}{y_f}$ values

y_i/y_f	K_L	S_{II}	S_I/S_{II}	S_{III}	S_I/S_{III}	y_i/y_f	K_L	S_{II}	S_I/S_{II}	S_{III}	S_I/S_{III}
10^4	10	5470	100.5	1167	471.3	100	10	523	10.4	236	23.1
	100	550	100.0	119	464.2		100	55	9.9	26	21.1
	500	112	98.0	25	432.6		500	14	8.2	8	14.2
	1000	58	95.6	14	394.8		1000	9	6.7[6]	6	9.4[6]
1000	10	1712	32.1	532	103.2	10	10	143	3.5	95	5.3
	100	174	31.6	55	99.6		100	18	3.1	13	4.3
	500	37	29.7	13	84.4		500	7	2.2	6	2.4
	1000	20	27.5	8	67.7		1000	6	1.7	6	1.8

6.7 Summary

Successful treatment of contaminated water with magnetic nanoparticles in a semi continuous manner was demonstrated through experimental results of this chapter. The conductivity probe used indicated a residence time of 30s that corresponded well with passing one pore volume of fluid through the system. The Hg breakthrough curve was consistent with the chloride breakthrough curve suggesting little to insignificant retardation of ions by the steel wool matrix of HGMS column. The observed small difference in the breakthrough curves of chloride and Hg was attributed to discrete measurements and confirmed through a dilute acid flush experiment. Around 90% Hg was removed using these magnetic nanoparticles from the initial spiked fluid in the bench scale experiments. The experiments on Hg recovery show that 93.4% extraction of adsorbed Hg by thiourea was possible and a careful choice of extracting agent can ensure complete recovery of contaminant from the particle. An efficient removal of Hg frees the

functional groups present on the particles and regenerates them for further reuse. In addition, it was shown that an easy water flushing method was sufficient to recover captured particles (> 96%). The ease of regenerating and recovering particles from the system makes them suitable for further waste water treatment. Scaling the process up to an industrial implementation will require large amounts of sorbent. To economize the use of sorbent, more than one stage of adsorption will be needed. A mass balance was thus performed to determine sorbent amounts for varying number of adsorption stages, adsorption affinities and ratio of inlet to outlet concentrations. These calculated amounts are valuable guides in designing these processes.

Extending the lab-scale studies of treating waste streams to pilot plant or field scale studies for determining the best operating conditions for maximal removal of heavy metals is an important next step in evaluating the feasibility of this technology. The experimental set up tested in the lab was a fairly simple one, having Hg as the only species present with no competing ligands. However, real systems are not limited to one metal species but has a several different competing metals, anions, and pH conditions depending on their industrial source. The presence of multiple species and variability in ionic strengths and pH in turn results in complex metal speciation and adsorption behaviors that can be challenging to study. Thus, this study can be extended to evaluate the effectiveness of using our particles for industry-specific waste streams. In addition, the design of magnetic nanoparticles can be optimized to yield maximal adsorption for the target heavy metals.

6.8 References

1. Ditsch, A. A. P. Purification of recombinant proteins with magnetic nanoclusters. Massachusetts Institute of Technology, Cambridge, 2005.

2. Sharpe, S. A. Magnetophoretic cell clarification. Massachusetts Institute of Technology, Cambridge, 2004.

3. Gerber, R.; Birss, R. R., *High gradient magnetic separation*. Research studies press: London, UK, 1983.

4. Ravichandran, M., Interactions between mercury and dissolved organic matter--a review. *Chemosphere* 2004, *55* (3), 319-331.

5. Gölcü, A., Transition Metal Complexes of Propranolol Dithiocarbamate: Synthesis, Characterization, Analytical Properties and Biological Activity. *Transition Metal Chemistry* 2006, *31* (3), 405-412.

6. Wu, F.-C.; Tseng, R.-L., Liquid-solid phase countercurrent multi-stage adsorption process for using the Langmuir equation. *Journal of Hazardous Materials* 2008, *155* (3), 449-458.

Chapter 7. Concluding Discussion

7.1 Summary of Research

Currently the most common technique for treating effluents or remediating contaminated sites uses activated carbon to adsorb the contaminants.[1,2,3] This process suffers from disadvantages such as high costs (detailed cost comparison can be found in the Capstone paper), mass transfer limitation and risk of not recovering the carbon back from the contaminated sites. As an alternative to existing remediation techniques, especially adsorption on activated carbon, we propose using functionalized magnetic nanoparticles (MNPs) to adsorb the contaminants of interest. Nanotechnology though in its infancy, has become popular in recent times as the small size and larger surface area to volume ratio of nanoparticles makes the nanoparticles more reactive than larger one and easier to deploy.[4,5,6] Their superiority to activated carbon lies in the fact that they offer high surface area to volume ratio by being small and without introducing mass transfer limitations common to porous structures as it has all the surface area outside the particle. Secondly, under the external magnetic field gradients, complete removal of the particles from its medium of application is possible. Unlike activated carbon which is left behind in the environment, we can now isolate the contaminant rich adsorbents. These versatile magnetic nanoparticles can be applied to both treat effluents and sediment matrices. The biggest advantage of this process is that we are reducing the net volume of disposal waste by concentrating the contaminants from a large dilute volume to a small concentrated volume.

The aim of this work was to investigate the feasibility of applying magnetic nanoparticles for treating effluents. In particular, this thesis explored various aspects of the process starting with the synthesis of the particles. Chemical co-precipitation technique was used in a four-step process to generate dithiocarbamate-modified magnetic nanoparticles. The dithiocarbamate functional group was chosen as it was widely reported to have high affinities for heavy metals and in particular for mercury.[7,8,9,10] Details of this synthesis can be found in Chapter 2. These particles were then used for determining their adsorption capacity for mercury under different conditions of pH, salt concentrations and presence of other metal salts such as those of calcium and magnesium. Differences in equilibrium adsorption curves were attributed to differences presence of mercury species that had varying "softness" character and the relative concentrations under different experimental conditions. The varying softness character was responsible for the

difference in binding affinities of different mercury species. In addition, mercury adsorption experiments in the presence of calcium ions and calcium and magnesium ions were performed. Amount of mercury adsorbed decreased with increasing competition from calcium and magnesium ions. These particles were also used for adsorbing lead and manganese ions. The experiments showed a lower adsorption capacity (both on mass and mole basis) for lead compared to mercury and manganese compared to lead. The trend of adsorption capacity is in good agreement with the prediction from HSAB theory.[11]

A theoretical study to determine binding constants of the dithiocarbamate functional group on these particles to the mercury species was evaluated using Gaussian (Chapter 3).[12] Adsorption curves using these binding constants were then used for comparison with experimental data. Predictions using binding constants for the hydroxide-mercury species were in good agreement with experimental data however the results for chloro-mercury species were not consistent In addition, it was seen that different methods predict differently for the solvation models. Thus the choice of method to be used in Gaussian models is an important one and needs to be optimized for the system at hand. These models are therefore limited to providing information on relative mapping of species in terms of binding rather than actual values of binding constants.

In chapters 4, transport properties through porous (representing sediment like structures) and non-porous (representing effluents) media were studied. Results in this chapter confirm an enhanced dispersion in presence of magnetic field in both kinds of media considered. Magnetic dispersion coefficients in 2D porous medium were also evaluated under varying orientations of magnetic field with respect to the flow field. These coefficients were found to be fairly complex quantities that depend on the porous medium geometry and the orientation of the field applied. It was also shown that the magnetic dispersion has a linear dependence on magnetophoretic velocity which confirms our hypothesis that both magnetic and hydrodynamic dispersion coefficients can be vector added.

A finite element model for continuous separation of magnetic nanoparticles from an aqueous suspension was developed in COMSOL. The model provides information on separation efficiency as a function of different system parameters. In order to use these simulations in industrial scale applications, it was recommended to extend the developed models to consider larger clusters (100-150nm), higher flow rates and the magnetic field gradient from either a

permanent magnet or magnetized wires. It was suggested to use particle tracking methods in lieu of continuum models to avoid the convergence problems.

Lastly a bench scale run for treating wastewater with these particles was discussed in Chapter 7. Apart from adsorption this process uses a well studied HGMS system. Breakthrough analysis of mercury and particles through the complete lab setup system was discussed. It was demonstrated these particles could reduce the mercury concentrations by 90% and were almost completely captured (99.99%) by the HGMS system. The experiments on Hg recovery show that 93.4% extraction of adsorbed Hg by thiourea was possible and that an easy water flushing method was sufficient to recover captured particles (> 96%). The ease of regenerating and recovering particles from the system makes them suitable for further waste water treatment. A mass balance was also performed to determine sorbent amounts required for varying number of adsorption stages, adsorption affinities and ratio of inlet to outlet concentrations.

7.2 Future Directions

Extending the lab-scale studies of treating waste streams to pilot plant or field scale studies for determining the best operating conditions for optimal removal of contaminants are an important next step in evaluating the feasibility of this technology. System tested in the lab was a fairly simple one with no competing ligands. In various real systems, there will be the presence of different anions and different pH conditions. Depending on the contaminated site or the waste stream to be treated, there will be a fairly complex metal speciation present. Each system is thus unique and will need to be studied individually to understand the impact of metal speciation on metal removal, amount of particles required for the cleanup, equilibrium adsorption capacity of the particles, implementing recovery of particles etc.

As explained in Chapter 2, dithiocarbamate functional group was chosen for its high affinity towards mercury. Depending on the class of target contaminants, we can optimize the design of these particles by exploring different chemistries for the functional group on the magnetic nanoparticles. In addition to this, we can also optimize the existing structure of magnetic nanoparticles in terms of magnetite content and the functional group content for optimal target contaminant removal.

Determining the toxicity of these particles with and without the contaminant adsorbed onto it is an essential next step in implementation of this technology.[13] This is important as it determines the efficiency of recovering magnetic nanoparticles and the time invested to recover almost all of the particles.

Lastly, an economic analysis of this technology needs to be performed to compare it to the existing technologies for environmental applications.

7.3 References

1. Padak, B.; Wilcox, J., Understanding mercury binding on activated carbon. *Carbon* 2009, *47* (12), 2855-2864.

2. Rivera-Utrilla, J.; Sánchez-Polo, M.; Gómez-Serrano, V.; Álvarez, P. M.; Alvim-Ferraz, M. C. M.; Dias, J. M., Activated carbon modifications to enhance its water treatment applications. An overview. *Journal of Hazardous Materials* 2011, *187* (1-3), 1-23.

3. Wang, J.; Deng, B.; Wang, X.; Zheng, J., Adsorption of Aqueous Hg(II) by Sulfur-Impregnated Activated Carbon. *Environmental Engineering Science* 2009, *26* (12), 1693-1699.

4. Agency, U. S. E. P., Nanotechnology for site remediation fact sheet. 2009.

5. Dionysiou, D. D., Environmental applications and implications of nanotechnology and nanomaterials. *J. Environ. Eng.-ASCE* 2004, *130* (7), 723-724.

6. Mauter, M. S.; Elimelech, M., Environmental Applications of Carbon-Based Nanomaterials. *Environmental Science & Technology* 2008, *42* (16), 5843-5859.

7. Say, R.; Birlik, E.; Erdemgil, Z.; Denizli, A.; Ersöz, A., Removal of mercury species with dithiocarbamate-anchored polymer/organosmectite composites. *Journal of Hazardous Materials* 2008, *150* (3), 560-564.

8. Denizli, A.; Kesenci, K.; Arica, Y.; Piskin, E., Dithiocarbamate-incorporated monosize polystyrene microspheres for selective removal of mercury ions. *Reactive and Functional Polymers* 2000, *44* (3), 235-243.

9. McClain, A.; Hsieh, Y.-L., Synthesis of polystyrene-supported dithiocarbamates and their complexation with metal ions. *Journal of Applied Polymer Science* 2004, *92* (1), 218-225.

10. Venkatesan, K.; Srinivasan, T.; Vasudeva Rao, P., Removal of complexed mercury by dithiocarbamate grafted on mesoporous silica. *Journal of Radioanalytical and Nuclear Chemistry* 2003, *256* (2), 213-218.

11. Pearson, R. G., Hard and soft acids and bases, HSAB, part II: Underlying theories. *Journal of Chemical Education* 1968, *45* (10), 643-null.

12. Frisch, M. J. e. a. *Gaussian 03; Gaussian, Inc.* , Wallingford, CT, 2003.

13. Goho, A. M. Testing the Toxicity of Nanomaterials *Technology review* [Online], 2008.

Chapter 8. Capstone Paper: Commercialization of Magnetic Nanoparticles for Industrial Wastewater Treatment

8.1 Introduction

8.1.1 Water and Wastewater Treatment Chemicals Market

In 2012, global sales of water and wastewater treatment chemicals was just under $24 billion with North America (US and Canada) accounting for 8.5% or $2.03 billion of this global market.[1] It is a highly matured and fragmented market but it continues to grow at a stable low growth rate of 3.6%. The main reason for this steady growth is that water is an integral part of all processes in almost all of industries in the world that requires being treated both before its use in industrial processes and when the effluents are reused or discharged. Several industries including petrochemicals and oil and gas industry emphasize chemical treatment of effluents, process water and raw water to abide by the regulatory requirements and to ensure smooth functioning of their processes. In addition, there are several factors that necessitate the need for wastewater treatment chemicals and drive its steady growth. They include:

1. Environmental laws and regulations that sets stringent wastewater standards for various industries in order to minimize the impact of effluent discharge on the environment
2. East Asia especially China rapidly expanding its power, wastewater and water infrastructure which adds tremendously to the growing market. By 2020, chemical purchases by China for its coal fired boiler will be at 300% of the US volume
3. Increased emphasis on water recycling and water management that requires water to be treated and reused
4. Chemical treatment proven as a cost effective treatment as compared to advanced technologies like reverse osmosis, UV technology etc
5. Demand for high quality water in power and nuclear plants. In addition, certain applications in the electronics, healthcare and automotive industries also require pure water

Several market research companies like Frost & Sullivan[1-2] and McILVAINE[3] project steady growth of this market and expect the North American market to grow to $2.79 billion by the end of 2018. Not all segments of this market will experience equal growth rather their growth rate will vary on basis of the end industry consumption. Despite the overall enthusiasm around this industry, there are several restraints that could negatively impact the market size and growth. These include:

1. Companies streamlining their water treatment costs as these costs are viewed as overheads in times of economic downturn
2. Increased competition from suppliers in China and India create pricing pressures and lower profit margins
3. Regulatory restrictions on use of certain chemicals limit the product offering of chemical companies
4. Emergence of alternative technologies and the green chemicals that increases competition

8.1.2 Objective of this Chapter

This chapter aims to critically examine the commercialization prospects of magnetic nanoparticle technology for wastewater treatment especially for industrial applications and heavy metal removal. The North America water and wastewater chemicals treatment market is analyzed in great details to understand the current state and future trends. A deep dive in the competitive landscape of this market is carried out followed by a description of new and innovative players in this field. Cost comparison of the magnetic nanoparticle technology with existing players is carried out to determine its economic viability. Though the technology is still at an early stage of development, a roadmap of strategies for successful commercialization of this technology is highlighted based on its unique value proposition. The chapter concludes with the implications for nanoparticles as chemical treatment agent and it's potential as a disruptive technology in North America water and wastewater markets.

8.2 Water and Wastewater Treatment Chemicals Market Definition

Water treatment in the industrial sector can be divided into three major types of water and wastewater treatment processes (Figure 8-1): raw water treatment, process water treatment and industrial wastewater treatment. As the name suggest, raw water treatment refers to primary water treatment where impurities are removed by both physical and chemical separation methods. Chemicals like aluminum sulfate and ferric chloride are used as coagulants or flocculants to remove dissolved organic and inorganic compounds. Activated carbon can be sometimes used to remove specific impurities. In case of process water treatment, chemicals are added to reduce scaling, corrosion, bio fouling and foaming and making it reusable for process operations. In case of effluent wastewater treatment, chemical and biological treatment is carried out to remove heavy metals like mercury, arsenic and lead, metal oxides, color and odor. A combination of chemicals, biocides and activated carbon is used for this type of treatment. From here on, this chapter's discussions will focus on industrial wastewater treatment and chemical treatments. It will, for the purposes of this discussion, not focus on physical treatment or biological treatment.

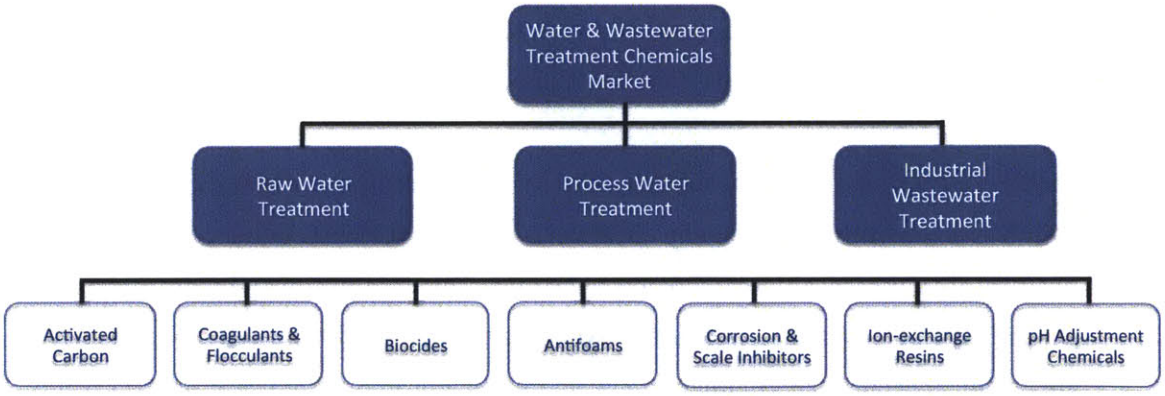

Figure 8-1: Categories within Water and Wastewater Treatment Chemicals Markets

8.3 Industrial Water and Wastewater Treatment Chemicals Market Analysis

8.3.1 Different Wastewater Treatment Chemicals /Technologies

There are seven major types of treatment chemicals that are used for industrial wastewater (Figure 8-1) that are described below. Details on entire value chain in this market are given in the next section.

1. **Activated Carbon:** This is typically produced from carbonaceous material like coal, wood etc. It is highly porous in nature and treats water by adsorbing all the contaminants from it. It is available in three different forms (different physical structures); granular, pelletized and powdered.
2. **Coagulants & Flocculants:** Chemicals used to neutralize the charge in colloidal impurities and help in the floc formation. They are two main types: organic coagulants based on water soluble polymers like polyamine and poly acrylamide and inorganic coagulants based on chloride and sulfate salts of iron and aluminum like ferric chloride and aluminum sulfate. Similar to coagulants, flocculants prevent the formation of floc in water that contains suspended solids. They are three main types of flocculants – cationic, anionic and polyampholyte. Cationic flocculants are based on nitrogen, anionic flocculants are based on carboxylate ions and polyampholyte flocculants have both positive and negative charges.
3. **Biocides:** These are chemical substances or microorganisms that can kill or render harmless any harmful organism by chemical or biological means. Some commonly used biocides are chlorine, chlorine dioxide and ozone. There are two main kinds of biocides depending on the nature of chemicals: oxidizing and non-oxidizing. Oxidizing biocides are chemical agents that kill microorganism by creating an oxidized environment while non-oxidizing biocides are chemical agents that do not create an oxidizing environment.
4. **Antifoam:** Antifoam or defoamer agents are chemical additives that reduce the formation of foams in industrial process liquids. These are generally added as foams can reduce the equipment capacity, increasing the duration of the process and hence the operating costs involved. There are two major types of antifoam agents available in the markets: silicon

and non-silicon based antifoam agents. Silicon based antifoam agents have a silica-based backbone and are often heavy-duty agents compared to non-silicon based.

5. **Corrosion & Scale Inhibitors:** Corrosion inhibitors are chemicals that prevent the conversion of a metal into a soluble compound. They themselves adsorb the metallic surfaces to prevent other compounds corroding the metal surface. Scale inhibitors are chemicals that inhibit scale formation. Soluble solids become insoluble as temperature rises and deposit as scales on surfaces. Scale cause operational inefficiencies, making it important to add these chemicals.
6. **Ion-exchange Resins:** These are insoluble granular substances that have acidic and basic radicals in their molecular structure that can exchange ions with the surrounding medium. They can be categorized based on porosity (gel type or macro porous type) or number of functional radicals presents (mono functional and poly functional).
7. **pH Adjustment Chemicals:** As the name suggests these are chemicals that adjust the pH of the water stream so that it can reused as process water.

Key Insight: Activated carbon, ion–exchange resins and coagulants and flocculants are the most commonly used chemicals in the industrial wastewater treatment, especially for removal of heavy metals and will be considered as competitive chemicals for further analysis after the market analysis discussion.

8.3.2 Financials

The North American market has total 2012 revenue of $2.03B and with 2,395.5 M lbs. of chemicals being sold, the average price of the chemicals come to $0.85/lb.[1] Not much in itself and would require any competing technology to be comparable in cost if not cheaper than this average price. To understand the dominant industrial wastewater treatment chemical, we will look at the breakdown of total revenue and corresponding market shares of each chemical type (Figure 8-2).

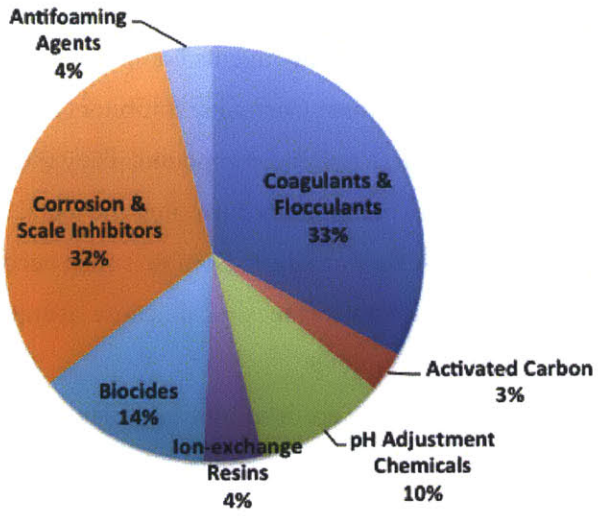

Figure 8-2: Revenue breakdown for each chemical type in North America's Water and Wastewater Treatment Chemicals Market (2012)

As seen from the above figure, we can see that Coagulants and Flocculants is the largest chemical treatment segment (33%) followed closely by Corrosion & Scale Inhibitors (32%). Out of these categories, activated carbon and ion exchange resins specifically apply to heavy metal ion removal. In other words, approximately 7% of $2.03B or $ 143M is spent on heavy metal removal in North America's water and wastewater Treatment Chemicals Market. However, Coagulants & Flocculants are also used to remove heavy metal ions, which extend the potential market to be as high as 40% of $2.03B or $ 812M.

Key Insight: Market size (size of our pie) for heavy metal removal/treatment is in the range of $150M and $810M. As a technology provider/chemical manufacturer in this fragmented market, our hope is to capture a high fraction of the current market size (~$150-810M) but even with a 15%, a very optimistic number given the number of players, market share capture we can aim for is in the range of $23 - $122M, which in itself is not enough. New applications like use in treating shale gas water recovery are important to make commercializing this technology worth the investment.[4]

8.3.3 Value Chain and Distribution Channel Analysis

As mentioned in the introduction, this market is highly fragmented with an extensive value chain comprising of chemical manufacturers, formulators, distributors service providers and end users (Figure 8-3). Following is a list of major players in each stage of the value chain.

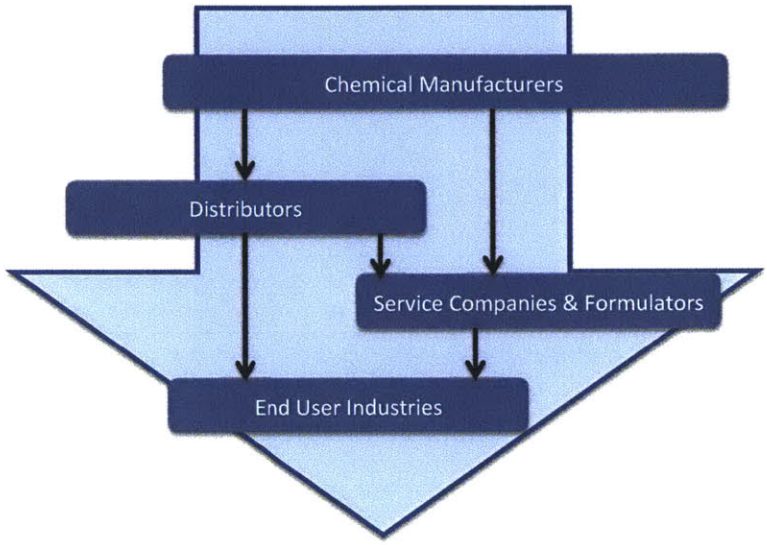

Figure 8-3: Value Chain in the Water and Wastewater Treatment Chemicals Market

Chemical Manufacturers:

a) Kemira Oyj
b) SNF Floerger
c) Ciba Specialty Chemicals
d) Dow Chemicals Company
e) Rhodia
f) Calgon Carbon Corporation
g) BWA Water Additives
h) Norit Americas Inc.
i) Rohm & Haas Company
j) BASF Corporation

Distributors:

a) Univar

b) Brenntag
c) Altivia

Leading Service Companies & Formulators:

a) Ashland Water Technologies
b) Siemens
c) Nalco Company
d) GE Water Solutions
e) ChemTreat, Inc.
f) Ecolab
g) Buckman

End Users:

a) Petrochemical & Chemicals
b) Power Generation
c) Food & Beverage
d) Pulp & Paper

At each stage of the value chain, there are lots of participants ranging from global to regional players providing products as well as services. In terms of distribution channels, manufacturers sell directly to service companies who then sell it to end customers. Sometimes the service companies formulate or reformulate their own product to sell to the end customers that further adds to increasing competition. Distributors play a smaller role, as majority of sales occur through service companies. Companies like GE Water Solutions and Nalco Company have tried to vertically integrate as a way to streamline costs and operate more efficiently in this fragmented and almost commoditized market. So far, majority of mergers & acquisitions have been horizontal in nature and rarely across the different stages of value chain.

Key Insight: Given the complex nature of the value chain, it would make sense leveraging distributors and leading service companies' well-established relationship with the end customers to sell our magnetic nanoparticle technology. Secondly, establishing our technology in this

fragmented market will be difficult to achieve unless and until we come up with a superior solution that is cost competitive.

8.3.4 Market Trends

Overall the market is experiencing a low to moderate growth.[1] This weak yet stable growth can be attributed to slow recovery in certain industry sectors since the economic crisis. However like several other industries, this market too is fast evolving to be a global market with an increased emphasis on the Asian customers. There are three main trends in the industrial wastewater treatment chemicals market in line with globalization: increased mergers & acquisition activity, commoditization of products leading to focus on services and increased competition necessitating innovative products. These trends are described below.

One of the challenges of being in this business is that the matured nature of this market results in lower profit margins and growth potential. The larger players squeeze the profits of the smaller niche players leading to an increased consolidation in this business sector. In addition, the fragmented nature adds to the increased competitiveness of this industry and subsequently lowers profits

Commoditization of treatment chemicals is resulting in moving away from the chemical product itself and focusing on services to increase company revenue and profitability

Increased competition from Asian companies necessitates US manufacturers to emphasize on productivity, new technologies and service offerings. All this makes the introduction of innovative products and application necessary to remain in business. That being said, the chemicals will continue to dominate the treatment landscape due to its cost effectiveness.

Key Insight: Low cost is key here as both commoditization and competition lowers profit margin. Given razor thin margins, entering this market might not be a good idea unless we have a superior technology that is cheap.

8.3.5 Porter's Five Forces Framework

Porter's five forces analysis is a framework[5] for industry or market analysis and business strategy development that helps determine the competitiveness of an industry and therefore its

attractiveness. A highly competitive market would be unattractive as it would eventually lead to small profits or even price wars while an attractive market is one where there is less competition and a higher probability of entering this market and capture high profits. The five forces are

1. Threat of New Entrants,
2. Threat of Substitutes,
3. Intensity of Rivalry,
4. Bargaining Power of Customers and
5. Bargaining Power of Suppliers

The first three forces are external to a company but within the microenvironment of the market while the last two relate to power within a company's internal supply chain. Each of these forces reduces the overall profitability of a company.

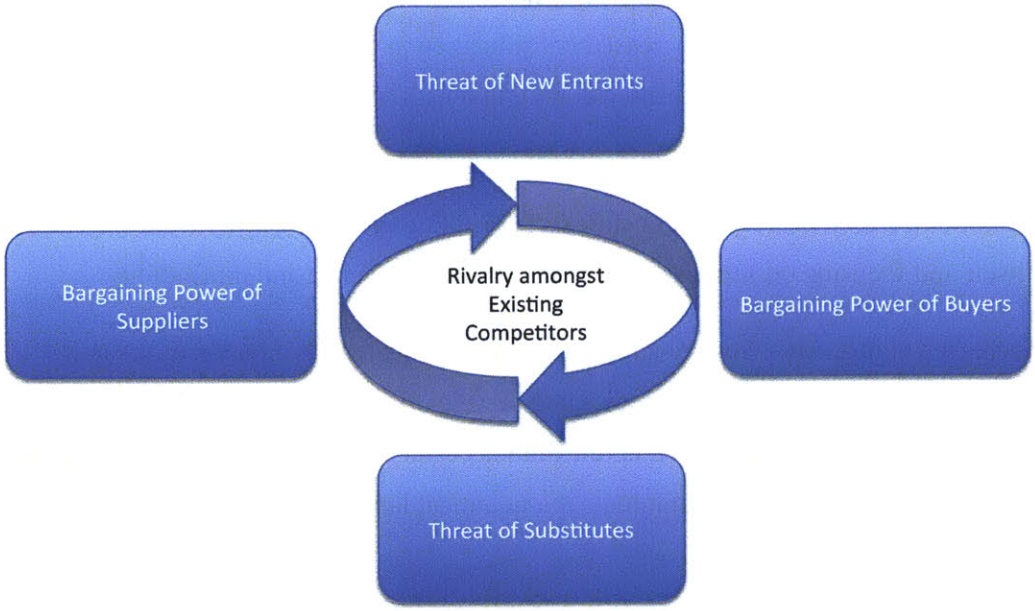

Figure 8-4: Porter's Five Forces Framework

In case of industrial wastewater market (Figure 8-4), the threat of new entrants is low. This is because of its matured nature and the specialized and differentiated products offered by each of the regional and global player. Environment concerns of excessive use of chemicals increase the threat of substitutes. Any substitute technology looking to reduce or eliminate use of certain chemicals as well as drive users to non-chemical technologies will find it easier to enter

this market. The threat from substitutes is therefore medium to high. Competitive rivalry has increased tremendously as all players in the distribution chain, be it manufacturers, service providers or formulators are concentrating on providing bundled solutions of chemicals and services to retain customers at favorable price points. The high intensity of competitive rivalry further adds to the commoditization of chemicals making it a less favorable market. Fragmented supplier base along with low cost imports from Asian countries greatly increase the bargaining power of customers who now demand high quality product and services at lower prices. On the other hand, bargaining power of suppliers is greatly reduced due to increased customer power, weakened economy and decreased differentiation of chemicals.

Key Insight: This is an unattractive market because of the low profits. Also, this is an easy market to enter but difficult to sustain long-term presence. There is a high probability of being acquired or being integrated with existing big players. Thus, to enter this market, there is a need for innovative alternative technologies that can transform the current chemical treatment paradigm.

8.4 Need for Innovation: New Technologies

Chemicals play a vital role in industrial waste water treatment and cannot be completely eliminated as treatment agents but with increasingly strict regulations, competition and extensive use of recycled water, there is a need and growing importance of 'greener' alternative technologies like membrane technologies, newer treatment substrates and nanotechnologies. US EPA considers all of these technologies cleaner but the only barrier to a widespread adoption is the higher expense. However, it is expected that through product learning, the cost of these technologies will reduce substantially making it a viable substitute for existing chemicals. In this section, we would like to highlight and compare some of the new technologies for removal of heavy metals from aqueous media. The focus here will be on technologies that have potential to be commercialized for heavy metal removal or in other words, pose a threat to the developed magnetic nanoparticle nanotechnology.[6]

Microbial Bio-adsorbents: High-affinity microbial bio-adsorbents for heavy metal removal for the removal of heavy metals such as Cd, Hg, and Pb has been developed by a team

of researchers at University of California, Riverside. However based on the industry research our understanding that this innovation is still confined in the exploratory research phase and little has been done to include it in industry use. The two main reasons for it not being scaled up are that the research is still to be proven at a larger scale and low economic viability of using this technology.[7]

Peat: A simple, effective, economical way to remove heavy metals is to capture dissolved heavy metals using peat. This technology too has only been tested in lab scale and is yet to be commercialized. Similar to microbial adsorbents, this technology is still in infancy and should not pose a problem in the next few years.

Membrane Processes: Reverse osmosis and nanofiltration technologies have been shown to be effective for heavy metal removal and are the most promising technologies to be included in wastewater management. Several water management based service firms like CDM Smith and Modern Water are including membrane processes as part of their water management solution. However, this technology still does not address the problem entirely and there remains a quest for a more innovative technology for removal of Selenium, Strontium, Mercury etc.

Nanotechnologies: There are two nanotechnology-based companies NanoChem, Inc. and Pars Environmental, Inc. that are producing nano chemicals for industrial wastewater treatment.[8] NanoChem, Inc. utilizes polyaspartate compounds to inhibit scale and corrosion. On the other hand, Pars use two unique technologies, electrocoagulation and Nano-Fe^{TM} to remove heavy metals from wastewater and groundwater and soil remediation. Both these companies though operating in the same space as magnetic nanoparticle technology are not directly competing with it. There is a risk of not including them as competitors as they could develop a competing technology and "frog leap" our innovation.

Magnetic Nanoparticle Technology: Magnetic nanoparticles act as sorbents of heavy metals that can be removed from application media by using an external magnet or magnetic field. This technology is highly efficient in adsorbing heavy metals, particularly mercury under a variety of medium conditions. It is a promising technology that could be tailored to target hard to remove metal ions like Selenium, Strontium etc. More importantly, it has been demonstrated in lab that this technology can remove more than 90% of mercury.

In summary based on our research, we believe that apart from membrane processes and nanotechnologies, there are no other solutions that could compete with existing technologies of activated carbon and ion exchange resins for heavy metal removal from industrial effluents. The ultimate goal of all water management and treatment is finding **cost effective technologies that can reliable meet effluent standards on a continuous basis.**[9] We will therefore compare our magnetic nanoparticle based technology with the market's existing and new technologies to see its competitive advantage. Before we do that, the cost associated with using the magnetic nanoparticle based technology is discussed.

8.4.1 Comparison of Magnetic Nanoparticle Based Technology Costs with Existing Technologies

Wastewater treatment is a cost center for all companies in the industries described above and bears this cost with little to no impact on revenue prospects. Therefore the market trend is to consolidate and minimize this cost involved in meeting the government guidelines of waste treatment and disposal. Any technology that improves the efficiency of treatment at a lower cost will drastically change the existing paradigm and can easily gain market share. Based on our market analysis, the only way forward for the magnetic nanoparticle technology is to demonstrate its cost effectiveness. This discussion in essence tells us the commercialization prospects of this technology. In this section, the cost components of using a magnetic nanoparticle based technology from the perspective of an end user will be discussed. In addition, rough estimates of cost numbers for the end user are highlighted.

The overall cost incurred in the technology can be thought to have two major components: capital costs and operating costs. Capital costs include equipment costs such as static mixers and HGMS columns plus any additional pipeline of routing the effluent through the new treatment facility. In addition, cost of land (additionally required to set this facility up) and / or financial leverage should be included for a better estimate. In case of operating costs, there are the MNP costs (comprising of chemicals plus synthesis), utilities, labor and final waste disposal. An overall cost structure would also include R&D costs and/or licensing costs (depends if this technology is being utilized in-house or is licensed).

Comparing on basis of capital costs, magnetic nanoparticle technology might be thought to have slightly higher costs associated with the expensive magnetic devices require. While use

of other equipment such as static mixers, pipelines are fairly commonplace and can be thought not to add to costs. Based on METSO estimates HGMS columns would only cost around $500,000 for a throughput of 450,000 L/hr.[10] That is a daily cost of $0.05 assuming that the machine is operating all 24 hours. Capital costs of buying a METSO HGMS column though expensive as an initial investment will reduce to a small number once amortized. There might be high interest payments associated with this purchase but given the profile of end industry users, I doubt if leveraging to purchase this equipment would lead to any financial concerns or differences amongst technologies. Also, one can use simpler assembly of magnets in lieu of a HGMS column, which could substantially remove any financial differences amongst technologies.

Now, compared to existing technologies of activated carbon and ion exchange the cost of operating this technology would be of the same order of magnitude as there will be a higher raw material costs but no costs associated with carbon regeneration, additional resin batches that involves operating and maintenance. Costs around utilities and labor will roughly be the same. The big difference would lie in the cost of "raw material" or treating agent and we can see from Table 1 and Table 2 that the estimated cost of MNP is 1-1.5x higher than these technologies. Another source of cost advantage could come from reduced final waste disposal/carbon regeneration costs as less final volume of waste is produced. This is a rough guide on costs as several assumptions and approximations were taken into account. Currently, there are probably one or two sellers of nanomaterials but none for wastewater treatment. This creates a unique opening for a company that has a viable technology and low costs.

Table 1: Cost of synthesizing 1 gram of magnetic nanoparticle (Lab and Large Scale Estimates)

MNP Costs	
Chemicals	
Fe (II) chloride	$ 0.53
FE (III) chloride	$ 1.31
NaOH (28 wt. %)	$ 5.07
TMAOH (0.33M)	$ 5.88
GPTMS	$ 2.05
DMSO	$ 7.44
Ethanol	$ 0.63
Acetone	$ 0.63
CS2	$ 1.94
Lupasol (* assuming the most expensive cost item)	$ 5.88
Total Cost	$ 31.35
Cost of chemicals/gm of MNP produced	$ 0.70
Synthesis Costs	
Utilities	$ 5.00
Labor	$ 30.00
Total Cost	$ 35.00
Costof synthesis/gm of MNP produced	$ 0.78
Cost/gm of MNP produced	$ 1.47

(a) Lab Scale Estimates

MNP Costs	
Chemicals	
Fe (II) chloride	$ 0.002
FE (III) chloride	$ 0.005
NaOH (28 wt. %)	$ 0.015
TMAOH (0.33M)	$ 0.003
GPTMS	$ 2.05
DMSO	$ 0.020
Ethanol	$ 0.100
Acetone	$ 0.125
CS2	$ 0.008
Lupasol (* assuming the most expensive cost item)	$ 1.500
Total Cost	$ 3.83
Cost of chemicals/gm of MNP produced	$ 0.09
Synthesis Costs	
Utilities	$ 5.00
Labor	$ 30.00
Total Cost	$ 35.00
Costof synthesis/gm of MNP produced	$ 0.78
Cost/gm of MNP produced	$ 0.86

(b) Large Scale Estimates

Assumptions:

1. Costs of lab purchases were used in calculating lab estimates[11] while costs of purchasing chemicals from Alibaba.com were used in calculating the large scale estimates
2. Three man hours at $10 per hour was used as an approximation for labor costs
3. Utilities for two day synthesis were approximated at $5 based off approximate utility consumption costs
4. Total chemical raw material and synthesis costs were divided by the total amount of magnetic nanoparticle produced
5. For activated carbon cost calculation, activated carbon bought online was assumed to be functionalized with the same functional groups [12]
6. For ion-exchange resins, cost of comparable resins that can target same equivalent moles of heavy metals was taken as basis for comparison[13]

Table 2: Treating agent costs of comparable technologies (Lab and Large Scale Estimates)

Activated Carbon Costs			**Ion-Exchange Resins**	
Buy it online (Alibaba)				
Activated Carbon	$	0.90	Buy it online (Dow Chemicals)	
Functionalizing Costs	$	0.41		
			Amberlite IRC478	0.5125
			(~ # of functional groups; 60% moisture capacity)	
Cost/gm of activated carbon	$	1.31	**Cost/gm of ion exchange resins**	$ 0.51

(a) Lab Scale Estimates

Activated Carbon Costs			**Ion-Exchange Resins**	
Buy it online (Alibaba)				
Activated Carbon	$	0.90	Buy it online (Dow Chemicals)	
Functionalizing Costs	$	0.08		
			Amberlite IRC478	0.5125
			(~ # of functional groups; 60% moisture capacity)	
Cost/gm of activated carbon	$	0.98	**Cost/gm of ion exchange resins**	$ 0.51

(b) Large Scale Estimates

It can be seen that the cost of magnetic nanoparticle technology is higher than competing technologies (even with large scale estimates the costs are very high). However, there is a potential to reduce this costs substantially when produced in bulk (based on large scale production estimates but this usually requires a minimum order of 25 metric tons for each of these chemicals). One can play with the assumptions of costs of utilities and labor but the costs continues to be higher than $0.50/gm of MNP synthesized.

Reduced final waste disposal costs: There is a potential cost saving associated with reduced secondary waste disposal. Instead of several kilograms of ion exchange resins, we now have grams of magnetic nanoparticles that has the same heavy metal removal efficacy. One estimate of potential cost saving is that for every kilogram reduction in weight of final waste disposal (typically to landfills), one could save $0.03-$0.10.[14] All this can be compared on per volume of wastewater treated but more information is required before such an analysis can be undertaken.

The economic analysis of various technologies suggest that in addition to the green image, there is promising dollar benefits of magnetic nanoparticle technology. Overall this technology needs to reduce its cost of production and the overall waste substantially to be considered as a viable replacement of existing technologies

8.4.2 Comparison of Existing and New Technologies for Heavy Metal Removal

Magnetic Nanoparticle Technology's Value Proposition: Based on Table 3, we can see that magnetic nanoparticle technology has the potential to be successful if costs are reduced before its commercialized. Its superior technology effectiveness and much reduced waste volume have benefits of a greener image. Additional benefits of this technology are listed below:

1. Highly effective with high affinities for heavy metals
2. Simple design and raw materials
3. Operating simplicity
4. Easy to incorporate in existing treatment facilities
5. Does not require additional floor space
6. Passive technology and reduces overall energy needs

7. Overall reduced waste volume that can have additional costs savings in reduced waste disposal costs

A lot depends on the impact of these benefits in monetary terms, which leads us to the question that **is commercialization even possible yet?**

The answer to that question is **not yet** as the cost of particles is not low enough to be considered as an alternative to use of existing chemicals. The two immediate steps that need to be addressed to commercialize this opportunity are to scale the experiments up and to test the viability of this technology with real world complexities and to test for cost reduction. This technology would not be worth introducing in the market if its not cost competitive now or in near future. Given that this technology though promising is still in infancy, instead of a business plan, we will highlight some of key steps to be taken to get on track for commercialization.

Table 3: Comparison of existing technologies and magnetic nanoparticle based technology (based off industry research)

Technology	**Economic Viability**		**Technology Effectiveness**		**Additional Comments**
	Installation Costs	O&M Costs	Efficiency	Broad applicability	
Activated Carbon	Low	High	Med	Med	Spent carbon can be regenerated and reused to make the process greener
Ion-exchange Resins	Med	High	High	High	Siemens Wastewater Ion Exchange Services can rapidly respond to stricter guidelines of reducing contaminants to ppt levels
Membrane Processes (Reverse Osmosis, Nanofiltration)	Med	High	High	High	Highly effective technologies but suffers from higher O&M costs due to membrane fouling, pretreatment etc
Nanotechnologies	Low	Med	High	Med	Existing nanotechnologies do not focus on heavy metal removal from wastewater effluents. Technology is yet to be proven at industrial scale
Magnetic Nanoparticle based Technology	Med	High	High	Medium	Could be a disruptive game changer if technology is efficient at scaled up operations

8.5 Roadmap to Successful Commercialization

The key to a successful commercialization strategy is to have a vision on steps to be taken and milestones where the vision and strategy is reevaluated. Focusing your efforts earlier on allows you to target niche markets and to this end, we will start off by restating the opportunity, our product offering followed by technology development plan, business model, financial, marketing, operating and organizational plans.[15]

8.5.1 Opportunity

Each year, industries in North America more than spend $ 150M (up to $ 810M) on heavy metal removal from industrial wastewater to meet the EPA guidelines. Magnetic nanoparticle technology has the potential to reduce costs involved in this process while maintaining high efficiency. Thus it addresses an unmet need of removing toxic metals from wastewater in a highly effective manner. The greatest advantage of magnetic nanoparticle technology lies in its super specificity and green nature.

8.5.2 Product Offering

The product will be magnetic nanoparticles that can adsorb target heavy metals where the chemistry of particles will be optimized depending on the application (i.e. adsorb Strontium or Lead ions). In addition to the particles, service will be provided to suggest how this technology can be incorporated in the overall treatment process.

8.5.3 Development Plan

Following steps will need to be taken to take this lab idea and build a company around it.

1. Patent protection and company incorporation
2. Fund raising for product testing
3. Product development: extending lab scale work to pilot plant studies
    i. Real system: more competing inorganic and organic ligands, metals, different pHs, ionic strengths
    ii. Optimal design of the particles
    iii. Chemistry of the ligands
    iv. Toxicity of the particles
4. Fund raising for further commercialization

5. Partnership & sales channel development
6. Facility selection and large scale manufacturing
7. Staffing
8. Optimizing overall supply chain
9. Market & sell products

8.5.4 Business Model

A potential business plan for this technology could be to collaborate with existing distributors and leading service formulators to continue research & development for real test systems. The early funds obtained from research grants and partnership can go towards validating the technology platform. Once the credibility is established and expertise developed, we could leverage this for better contract terms with these parties. These technology partners would help us in navigating through the fragmented and matured industry and securing end users of our technology In case we choose not to work with these parties, we can think of licensing out our technology i.e. MNP synthesis and overall process to a third party to sell the product in the market. It is too early to say which model will be appropriate and for now it makes sense to focus on proving the technology.

8.5.5 Financial Plan

Step 1. Apply to research grants, funding from government agencies etc. for getting funds to further develop the technology. As explained in the development strategy, it is essential in order to get this work moving that the technology be proven at a larger more complex scale.

Step 2: The next step could be to secure funding from potential technology and distribution partners who are looking to innovate their existing product offerings to end user industries. This could be a win-win situation for both parties. For us, it provides money, access to real systems to test our product and a guaranteed business through distribution relationship. For the partner, in exchange of money and access to real systems, they could have first rights to technology, innovative and green offering for the clients and reduced costs. An alternative to step 2^{16} could be to secure funding from Angel investors which is typically done in three series, that is

1. • Series A funding of $3 to $5 million (after transferring the technology from the academic institution where it was developed, and identifying areas for R&D)[17]
2. • Series B funding of $15 to $20 million (after securing partnerships and collaborations and initiating internal development of drug candidates)
3. • Series C funding of $20 to $50 million, which is usually the last round before exit

We would have to demonstrate technology feasibility in step 1 before applying to step 2. Raising capital often requires giving away a percentage of your company that might be worth considering if the company reaches step 2.

Exit Strategy: One potential exit strategy is to get acquired by one of the major manufacturing companies highlighted in highlighted in section 8.3. Given the recent market trend of consolidation, the company could be sold at a good price once it has been established n the marketplace.

8.5.6 Marketing Plan

1. Target "Heavy Metal" removal market: To establish a commercial presence, it is important to focus on a sub market, gain market share and then move towards horizontal product lines like targeting other contaminants etc. Within this sub market, it might make sense to further focus on a particular industry (Petrochemicals and Chemicals for example) to gain traction. It is key for any startup to have a prioritization plan where they target easier to achieve goals earlier on. It is also important to realize that due to industrial wastewater market being matured and having a complex value chain system, an indirect sales strategy would be ideal. That is partnering with wastewater treatment solution providers (distributors and leading service companies) rather than selling to end user industries directly.

2. Positioning & Advertising: Magnetic nanoparticle technology will be positioned on three main benefits: (a) Green image (b) Lower price (reduced waste disposal costs/cost of treating agents) and (c) Simplicity (easy to incorporate in existing systems and operate). Lower price assumes that we are able to go down the cost of learning and reduce the production costs.

8.5.7 Operating Plan

Once the technology is proven, the company should incorporate some guiding principles in their operations. It will be successful both in short in long term if they continually reduce

production costs i.e. remain cost competitive while maintaining superior quality. This requires establishing and maintaining strong relationship with raw material suppliers. A dedicated sales team that could sell to and develop long term relationships with various players in this fragmented industry would be key to our company's revenue generation. Providing post sales technical support would be a key to building brand equity and distinguishing the company.

8.5.8 Organizational Structure

Small team having technical, management and financial skills is essential to get the company off the ground. Technical skills are essential in the first year of experimentation and product development while management and financial skills will be essential to get the seed funding, work effectively towards the company goals and build tie-ups with potential partners. A former PhDCEP from MIT might be an ideal fit for this organization with their combined technical and business skills. Adding an industry expert on the team after the technology platform has been proven might also be a good idea to build a network within the industry and avoid poor judgments as the operations ramp up.

8.6 Conclusions and Implications for Magnetic Nanoparticles in Wastewater Treatment

Based on market analysis, industrial wastewater treatment chemicals market (specifically for heavy metal removal sub segment) is an unattractive market because of lower market size (which is around $150-$810M) and lower profit margins. Like industrial manufacturing industries, the matured and fragmented nature of this market makes it highly cost competitive. However there are increased and stricter regulations and environmental concerns against use of chemicals coupled with steady low growth in the market calls for either innovations in existing chemicals or new technologies to replace existing ones. There are few emerging technologies like membrane processes and nanotechnologies that hold promise of lowering the overall costs of wastewater treatment. Cost comparison of the magnetic nanoparticle technology to these technologies suggests that there is some commercialization prospect for this technology but is not completely ready for it. Two immediate steps to be taken are to prove the efficacy of technology for real world systems and to reduce overall production costs. Once the technology

efficacy and economic viability is proven, adopting the roadmap of strategies discussed above could lead to successful commercialization of magnetic nanoparticle technology.

8.7 References

1. Sullivan, F., North American Industrial Water Treatment Chemicals Markets **May 2012**.

2. Sullivan, F. *North American Industrial Water Treatment Chemicals Markets* August 2007.

3. Report, M. C. M. *Water and Wastewater Treatment Chemicals World Markets*; June 2010.

4. Sullivan, F. *Analysis of the Wastewater Treatment Equipment Market in the North America Shale Gas Industry*

Long-term supply of natural gas and high water consumption will stimulate growth; May 2012.

5. Porter's Five Forces Model. http://www.businessballs.com/portersfiveforcesofcompetition.htm.

6. *Oilgae Report: New Technologies in Heavy Metals Removal from Wastewater*

7. Chen, W., Mehra, Rajesh , Mulchandani, Ashok *Final Report: Development of Novel Bioadsorbents for Heavy Metal Removal.*

8. (a) NanoChem Inc. http://www.nanochemsolutions.com/; (b) Pars Environmental Inc. http://www.parsenviro.com/.

9. CDM SMITH. http://cdmsmith.com/.

10. Ditsch, A. Purification of Recombinant Proteins with Magnetic Nanoclusters. MIT, 2005.

11. Sigma Aldrich Commercial Website. http://www.sigmaaldrich.com/united-states.html.

12. Alibaba Commercial Website. http://www.alibaba.com/product-gs/533149478/price_of_activated_carbon_malaysia.html?s=.

13. (a) Dow Chemical Commercial Website. http://www.dow.com/products/product/amberlite-irc748/; (b) Fisher Scientific Commecial Website. http://www.fishersci.com/ecomm/servlet/itemdetail?productId=2405953&storeId=10652&langId=-1.

14. Mineral Processing Waste Treatment and Disposal Costs: Low Cost Analysis http://www.epa.gov/wastes/hazard/tsd/ldr/mine/aprappc.pdf.

15. Metal Removal Technologies: A Business Plan. http://demingstartup.net/wp-content/uploads/mrt-business-plan.pdf.

16. Pocurull, B. O. Mechanistic Modeling of Increased Oxygen Transport Using Functionalized Magnetic Fluids in Bioreactors. MIT, Cambridge, 2007.

17. Fleming, J. J. *"Platform versus Product Strategies" presentation at the MIT Sloan School of Management as part of course 15.363, Strategic Decision Making for the Life Sciences*; April 2007.

Appendix

Appendix 1: Aris Taylor Dispersion with an External Magnetic Force

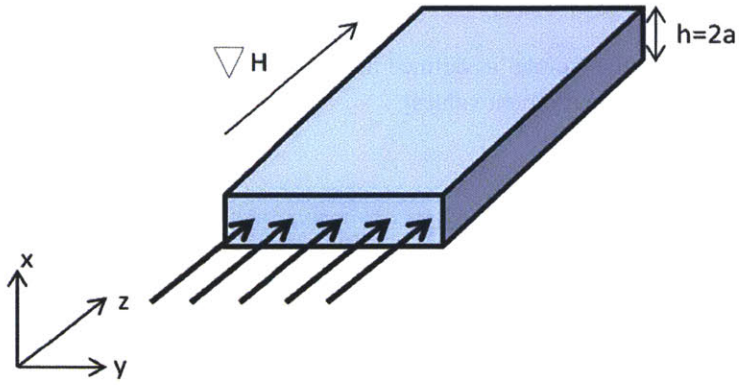

Governing advective diffusive equation for flow through a rectangular channel without any external magnetic field:

$$\frac{\partial c}{\partial t} + U_{avg}\chi(x)\left(\frac{\partial c}{\partial z}\right) = D\left(\frac{\partial^2 c}{\partial x^2} + \frac{\partial^2 c}{\partial z^2}\right)$$

Where $\chi(x) = (\frac{3}{2} - \frac{3}{2}x^2)$

In presence of a magnetic field, the equation is modified with an additional magnetic flux term

$$\frac{\partial c}{\partial t} + U_{avg}\chi(x)\left(\frac{\partial c}{\partial z}\right) = D\left(\frac{\partial^2 c}{\partial x^2} + \frac{\partial^2 c}{\partial z^2}\right) - \frac{\partial}{\partial z}(cu_{mag})$$

Now, $\frac{\partial}{\partial z}(cu_{mag}) = u_{mag}\frac{\partial c}{\partial z} + \frac{\partial u_{mag}}{\partial z}c$ [Deen]

Assuming u_{mag} = scalar and ignoring the "$\frac{\partial u_{mag}}{\partial z}c$" term for simplification

$$\frac{\partial c}{\partial t} + U_{avg}\chi(x)\left(\frac{\partial c}{\partial z}\right) = D\left(\frac{\partial^2 c}{\partial x^2} + \frac{\partial^2 c}{\partial z^2}\right) - u_{mag}\frac{\partial c}{\partial z}$$

Or,

$$\frac{\partial c}{\partial t} + [U_{avg}\chi(x) + u_{mag}]\left(\frac{\partial c}{\partial z}\right) = D\left(\frac{\partial^2 c}{\partial x^2} + \frac{\partial^2 c}{\partial z^2}\right) \quad (1)$$

Assumptions:

- Ignore y dependence of velocity

- Flow is laminar and fully developed
-

Boundary conditions:

$D\frac{\partial c}{\partial x} = 0$ at x = +/-a

$c = 0$ @ z = +/- ∞

[It is necessary to assume that the 'solute' as defined in Taylor Aris dispersion is confined in a finite length of channel to result in finite moment values]

Initial conditions:

At t=0, $c = \frac{1}{a^2}, -\frac{a}{2} \leq x \leq \frac{a}{2}$ $else$ 0

Changing the frame of reference with the assumption that the origin moves with the mean speed of the flow i.e. $U_{avg} + u_{mag}$, the governing equation is made dimensionless by using the following new variables

$$\zeta = \frac{z - (U_{avg} + u_{mag})t}{a}$$

$$\eta = \frac{x}{a}$$

$$C = a^2 c$$

$$\tau = \frac{Dt}{a^2}$$

Dimensionless form of the governing equations and the boundary/initial conditions

$$\frac{\partial C}{\partial \tau} + \frac{\{U_{avg} + u_{mag}\}a}{D}[\chi(\eta) - 1]\left(\frac{\partial C}{\partial \zeta}\right) = D\left(\frac{\partial^2 C}{\partial \eta^2} + \frac{\partial^2 C}{\partial \zeta^2}\right)$$

Where, $\chi(x) = \left(\frac{3}{2} - \frac{3}{2}\eta^2\right)$

Simplifying the equation leads to

$$\frac{\partial C}{\partial \tau} + \frac{\{U_{avg} + u_{mag}\}a}{D}[\{(\frac{1}{2} - \frac{3}{2}\eta^2)\}]\left(\frac{\partial C}{\partial \zeta}\right) = D\left(\frac{\partial^2 C}{\partial \eta^2} + \frac{\partial^2 C}{\partial \zeta^2}\right)$$

$$\frac{\partial C}{\partial \tau} + Pe[\{(\frac{1}{2} - \frac{3}{2}\eta^2)\}]\left(\frac{\partial C}{\partial \zeta}\right) = D\left(\frac{\partial^2 C}{\partial \eta^2} + \frac{\partial^2 C}{\partial \zeta^2}\right)$$

Where, $Pe = \frac{\{U_{avg} + u_{mag}\}a}{D}$

$\frac{\partial C}{\partial \eta} = 0$ @ η = +/- 1

C=0 @ ζ= +/- ∞

At $\tau = 0$, $C = 1 - \frac{1}{2} \leq \eta \leq \frac{1}{2}$ *else* 0

[Using "Moment" analysis as described in Aris 1953, 1956*/Deen]

k^{th} Moment of C on a filament parallel to the ζaxis

$$\mu_k(\eta, \tau) = \int_{-\infty}^{\infty} \zeta^k C(\eta, \zeta, \tau) d\zeta$$

The overall moment over the cross section is

$$\overline{\mu_k} = \frac{\int_{-1}^{1} \mu_k d\eta}{\int_{-1}^{1} d\eta} = \frac{1}{2} \int_{-1}^{1} \mu_k d\eta$$

Based on the initial conditions, the initial values for the initial moment μ_0 and $\overline{\mu_0}(0)$ are

$$\mu_0(\eta, 0) = \int_{-\infty}^{\infty} \zeta^0 C(\eta, \zeta, \tau) d\zeta = \int_{-\frac{1}{2}}^{\frac{1}{2}} d\zeta = 1$$

$$\overline{\mu_0} = \frac{1}{2} \int_{-\frac{1}{2}}^{\frac{1}{2}} 1.\, d\eta = \frac{1}{2}$$

Dimensionless form of governing equation

$$\frac{\partial C}{\partial \tau} + Pe\{f\chi(\eta) + (1-f)\}\left(\frac{\partial C}{\partial \zeta}\right) = D\left(\frac{\partial^2 C}{\partial \eta^2} + \frac{\partial^2 C}{\partial \zeta^2}\right)$$

Dimensionless form of equation in terms of moments is given as

$$\int_{-\infty}^{\infty} \zeta^k \frac{\partial C}{\partial \tau} d\zeta + Pef \int_{-\infty}^{\infty} \chi(\eta) \zeta^k \frac{\partial C}{\partial \zeta} d\zeta + Pe(1-f) \int_{-\infty}^{\infty} \zeta^k \frac{\partial C}{\partial \zeta} d\zeta = D\left[\int_{-\infty}^{\infty} \zeta^k \frac{\partial^2 C}{\partial \eta^2} d\zeta + \int_{-\infty}^{\infty} \zeta^k \frac{\partial^2 C}{\partial \zeta^2} d\zeta\right]$$

Or,

$$\frac{\partial \mu_k}{\partial \tau} + Pe(\chi(\eta))k.\mu_{k-1} = k(k-1)\mu_{k-2} + \frac{\partial^2 \mu_k}{\partial \eta^2} \qquad (2)$$

Boundary conditions in terms of moments:

At η =+/-1;

$$\int_{-\infty}^{\infty} \zeta^k \frac{\partial C}{\partial \eta} d\zeta = 0$$

Or,

$$\frac{\partial \mu_k}{\partial \eta} = 0$$

Initial conditions in terms of moments:

$$\int_{-\infty}^{\infty} \zeta^k C d\zeta = \mu_0 = 1$$

Normalizing each term by integrating over η from -1 to 1 and dividing $\int_{-1}^{1} d\eta$ to get average $\overline{\mu_k}$

$$\frac{\partial \overline{\mu_k}}{\partial \tau} + \frac{kPe}{2} \int_{-1}^{1} \chi'(\eta) \mu_{k-1} d\eta = k(k-1)\overline{\mu_{k-2}} + 0$$

$$\frac{\partial \overline{\mu_k}}{\partial \tau} + \frac{kPe}{2} \int_{-1}^{1} \chi'(\eta) \mu_{k-1} d\eta = k(k-1)\overline{\mu_{k-2}} \quad (3)$$

Note that the last term is zero because of the no flux boundary conditions.

For k = 0;

$$\frac{\partial \overline{\mu_0}}{\partial \tau} = 0$$

i.e. from initial conditions

$$\overline{\mu_0} = constant = \frac{1}{2}$$

Non normalized moment equation reduces to

$$\frac{\partial \mu_0}{\partial \tau} = \frac{\partial^2 \mu_0}{\partial \eta^2}$$

With the boundary conditions (@ η =+/-1)

$$\frac{\partial \mu_0}{\partial \eta} = 0$$

And initial condition ($for\ -\frac{1}{2} \leq \eta \leq \frac{1}{2}$)

$$\mu_0 = 1$$

Else

$$\mu_0 = 0$$

μ_0 is symmetric and can be solved over the region η

FFT method is used for solving for μ_0

$$\mu_0 = \sum_{n=0}^{\infty} \phi_n(\eta) g_n(\tau)$$

Where,

$$\phi_0(\eta) = 1, \phi_n(\eta) = \sqrt{2} cosn\pi\eta$$

$$g_n(\tau) = \int_0^1 \phi_n(\eta)\mu_0 d\eta$$

Transforming the non normalized moment equation (equation 2) yields

$$\frac{dg_n}{d\tau} = -(n\pi)^2 g_n$$

Or,

$$g_n(\tau) = g_n(0)\exp(-(n\pi)^2\tau)$$

Transforming initial conditions results in $g_0(0) = \frac{1}{2}$ and $g_n(0) = \int_0^1 \sqrt{2}\ \cos(n\pi\eta)\,\mu_0 d\eta = \frac{\sqrt{2}}{n\pi}\sin\left(\frac{n\pi}{2}\right)$

Thus,

$$\mu_0 = \frac{1}{2} + \sum_1^{\infty} \frac{2}{n\pi}\sin\left(\frac{n\pi}{2}\right)\cos(n\pi\eta)e^{-(n\pi)^2\tau}$$

For k = 1;

$$\frac{\partial\overline{\mu_1}}{\partial\tau} + \frac{Pe}{2}\int_{-1}^{1} \chi'(\eta)\mu_0 d\eta = 0$$

Substitute for $\chi'(\eta)\ and\ \mu_0$ and simplifying

$$\frac{\partial\overline{\mu_1}}{\partial\tau} + \frac{Pe}{2}\int_{-1}^{1}\left(\left(\frac{1}{2} - \frac{3}{2}\eta^2\right)\right)\left(\frac{1}{2} + \sum_{n=1}^{\infty}\frac{2}{n\pi}\sin\left(\frac{n\pi}{2}\right)\cos(n\pi\eta)e^{-(n\pi)^2\tau}\, d\eta\right) = 0$$

$$\frac{\partial\overline{\mu_1}}{\partial\tau} + \frac{Pe}{2}\left[\int_{-1}^{1}(1-3\eta^2)\frac{1}{2}\left(\frac{1}{2}\right)d\eta + \int_{-1}^{1}\frac{1}{2}(1-3\eta^2)\sum_{1}^{\infty}\frac{2}{n\pi}\sin\left(\frac{n\pi}{2}\right)\cos(n\pi\eta)e^{-(n\pi)^2\tau}\, d\eta\right] = 0$$

Solving for 'second term'

$$\frac{Pe}{2}\int_{-1}^{1}(1-3\eta^2)\frac{1}{2}\left(\frac{f}{2}\right)d\eta = \frac{Pef}{8}(\eta-\eta^3)_{-1}^{1} = 0$$

Solving for 'third term'

$$\frac{Pe}{2}\int_{-1}^{1}\frac{f}{2}(1-3\eta^2)\sum_{1}^{\infty}\frac{2}{n\pi}\sin\left(\frac{n\pi}{2}\right)\cos(n\pi\eta)e^{-(n\pi)^2\tau}\,d\eta$$

$$= \frac{Pe}{2}\frac{f}{2}\sum_{1}^{\infty}\frac{2}{n\pi}\sin\left(\frac{n\pi}{2}\right)e^{-(n\pi)^2\tau}\cos(n\pi\eta)\int_{-1}^{1}(1-3\eta^2)\cos(n\pi\eta)\,d\eta$$

$$= -\frac{Pe}{2}f\sum_{1}^{\infty}\frac{6}{(n\pi)^3}\sin\left(\frac{n\pi}{2}\right)e^{-(n\pi)^2\tau}\cos(n\pi)$$

Using $\int_{-1}^{1}(1-3\eta^2)\cos(n\pi\eta)\,d\eta = -\frac{12\cos(n\pi)}{(n\pi)^2}$

Substituting the terms in the averaged moment's equation

$$\frac{\partial\overline{\mu_1}}{\partial\tau} - \frac{Pe}{2}\sum_{1}^{\infty}\frac{6}{(n\pi)^3}\sin\left(\frac{n\pi}{2}\right)e^{-(n\pi)^2\tau}\cos(n\pi) = 0$$

Integrating yields,

$$\overline{\mu_1} = -\frac{Pe}{2}f\left(\sum_{n=1}^{\infty}\frac{6\cos(n\pi)}{(n\pi)^5}\sin\left(\frac{n\pi}{2}\right)\{e^{-(n\pi)^2\tau}-1\}\right)$$

Now, using equation (2)

$$\frac{\partial\mu_1}{\partial\tau} = \frac{\partial^2\mu_1}{\partial\eta^2} - Pe\chi'(\eta).\mu_0$$

For long times, i.e. τ is large

$$\frac{\partial\mu_1}{\partial\tau} \to 0$$

$$\frac{\partial^2\mu_1}{\partial\eta^2} - Pe\chi'(\eta).\mu_0 = 0$$

$$\frac{\partial^2\mu_1}{\partial\eta^2} = \frac{Pe}{2}.\left(\left(\frac{1}{2}-\frac{3}{2}\eta^2\right)\right)$$

Integrating it yields

$$\frac{\partial \mu_1}{\partial \eta} = \frac{Pe}{2}\left((\eta - \eta^3)\frac{1}{2}\right) + A$$

Where A is constant of integration

Applying boundary condition of $\frac{\partial \mu_1}{\partial \eta} = 0$ @η =1

$$A = 0$$

$$\frac{\partial \mu_1}{\partial \eta} = \frac{Pe}{2}\left(\frac{(\eta - \eta^3)}{2}\right)$$

Integrating once again

$$\mu_1 = \frac{Pe}{2}\left(\left(\frac{\eta^2}{2} - \frac{\eta^4}{4}\right).\frac{1}{2}\right) + B$$

Where B is constant of integration

Using $\frac{1}{2}\int_{-1}^{1} \mu_1 \, d\eta = \overline{\mu_{1\infty}}$ $(\tau \to \infty)$

$$\frac{1}{2}\int_{-1}^{1}\left(\frac{Pe}{2}\left(\left(\frac{\eta^2}{2} - \frac{\eta^4}{4}\right).\frac{1}{2}\right) + B\right)d\eta = \overline{\mu_{1\infty}}$$

$$\frac{Pe}{2}\left(\left(\frac{\eta^3}{6} - \frac{\eta^5}{20}\right).\frac{1}{2}\right) + B\eta = 2\overline{\mu_{1\infty}}$$

$$\frac{7Pe}{120} + 2B = 2\overline{\mu_{1\infty}}$$

$$B = \overline{\mu_{1\infty}} - \frac{7}{240}Pe$$

$$\mu_1 = \frac{Pe}{2}\left(\left(\frac{\eta^2}{2} - \frac{\eta^4}{4}\right).\frac{1}{2}\right) + \overline{\mu_{1\infty}} - \frac{7}{240}Pe$$

For k=2

$$\frac{\partial \overline{\mu_2}}{\partial \tau} = 2\overline{\mu_0} - Pe\int_{-1}^{1}\left(\left(\frac{1}{2} - \frac{3}{2}\eta^2\right)\right)\mu_1 d\eta$$

Consider along long time scales

$$\frac{\partial \overline{\mu_2}}{\partial \tau} = 2\overline{\mu_0} - Pe\int_{-1}^{1}\left(\left(\frac{1}{2} - \frac{3}{2}\eta^2\right)\right)\mu_1 d\eta$$

$$2\left(\frac{1}{2}\right) - Pe\int_{-1}^{1}\left(\left(\frac{1}{2}-\frac{3}{2}\eta^2\right)\right)\left(\frac{Pe}{2}\left(\left(\frac{\eta^2}{2}-\frac{\eta^4}{4}\right).\frac{1}{2}\right)+\overline{\mu_{1\infty}}-\frac{7}{240}Pe\right)d\eta = \frac{\partial\overline{\mu_2}}{\partial\tau}$$

Assuming $\overline{\mu_{1\infty}} \to 0$ ('Solute' is confined to a finite length in the channel at large times)

$$Pe\int_{-1}^{1}\left(\left(\frac{1}{2}-\frac{3}{2}\eta^2\right)\right)\left(\frac{Pe}{2}\left(\frac{\eta^2}{2}-\frac{\eta^4}{4}\right).\frac{1}{2}+\overline{\mu_{1\infty}}-\frac{7}{240}Pe\right)d\eta = 1-\frac{\partial\overline{\mu_2}}{\partial\tau}$$

Simplifying LHS:

First term:

$$\frac{Pe^2f^2}{16}\int_{-1}^{1}(1-3\eta^2)\left(\eta^2-\frac{\eta^4}{2}\right)d\eta$$

$$=\frac{Pe^2}{16}\int_{-1}^{1}\left(\eta^2-\frac{\eta^4}{2}-3\eta^4+\frac{3}{2}\eta^6\right)d\eta=\frac{Pe^2}{16}\left[\frac{\eta^3}{3}-\frac{7}{10}\eta^5+\frac{3}{14}\eta^7\right]_{-1}^{1}=-\frac{2}{105}Pe^2$$

Second term:

$$-\int_{-1}^{1}(1-3\eta^2)\frac{7}{2.240}Pe^2=\frac{7}{240}Pe^2f[(\eta-\eta^3)]_{-1}^{1}=0$$

Substituting the terms in the second moment equation yields

$$1-\frac{\partial\overline{\mu_2}}{\partial\tau}=-\frac{2}{105}Pe^2$$

Or,

$$\frac{\partial\overline{\mu_2}}{\partial\tau}=1+\frac{2}{105}Pe^2$$

Therefore,

From Deen (p. 400, equation 9.7-10)

$$\frac{Disp}{D}=\lim_{\tau\to\infty}\frac{\overline{\mu_2}}{2\overline{\mu_0}\tau}$$

$$\frac{Disp}{D}=\lim_{\tau\to\infty}\frac{\left(1-\frac{2}{105}Pe^2\right)\tau+\overline{\mu_2}(\tau=0)}{2\overline{\mu_0}\tau}$$

Therefore,

$$\frac{Disp}{D}=1+\frac{2}{105}Pe^2$$

Where, $Pe = \frac{\{U_{avg}+u_{mag}\}a}{D}$

For dispersion of solute without any external magnetic field gradient i.e. $u_{mag} = 0, or\ Pe = \frac{U_{avg}a}{D}$, the above expression simplifies to

$$\frac{Disp}{D} = 1 + Pe^2(\frac{2}{105})$$

This is the Taylor Aris dispersion limit